DISSERTATION

Development and application of fluorescent protein-based probes to determine protein targeting to mitochondria

Submitted by

Mag.ª Pharm. Jeta Ramadani-Muja

for the Academic Degree of Doctor of Philosophy
(PhD)

at the Medical University of Graz
Gottfried Schatz Research Center for Cell Signaling, Metabolism and Aging

Under the supervision of
Assoz. Prof. Priv.-Doz. Mag. Pharm. Dr. rer. nat. Roland Malli

2020

Declaration

I hereby declare that this thesis is my own original work and that I have fully acknowledged by name all of those individuals and organizations that have contributed to the research for this thesis. Due acknowledgement has been made in the text to all other material used. Throughout this thesis and in all related publications I followed the “Standards of Good Scientific Practice and Ombuds Committee at the Medical University of Graz“.

26.11.2020

Disclosures

Part of this thesis has been published in:

Ramadani-Muja, J., et al., Visualization of Sirtuin 4 Distribution between Mitochondria and the Nucleus, Based on Bimolecular Fluorescence Self-Complementation. Cells, 2019

Co-authors who contributed to the publication:

Benjamin Gottschalk[1], Katharina Pfeil[2], Sandra Burgstaller[1], Thomas Rauter[1], Helmut Bischof[1], Markus Waldeck-Weiermair[1], Heiko Bugger[2], Wolfgang F[1]. Graier and Roland Malli[1]

During my PhD studies I also contributed to the following publications:

- Burgstaller, S; Bischof, H; Gensch, T; Stryeck, S; Gottschalk, B; Ramadani-Muja, J; Eroglu, E; Rost, R; Balfanz, S; Baumann, A; Waldeck-Weiermair, M; Hay, JC; Madl, T; Graier, WF; Malli, R; pH-Lemon, a Fluorescent Protein-Based pH Reporter for Acidic Compartments; ACS Sens. 2019

- Waldeck-Weiermair, M; Gottschalk, B; Madreiter-Sokolowski, CT; Ramadani-Muja, J; Ziomek, G; Klec, C; Burgstaller, S; Bischof, H; Depaoli, MR; Eroglu, E; Malli, R; Graier, WF; Development and Application of Sub-Mitochondrial Targeted Ca2 + Biosensors; Front Cell Neurosci. 2019

- Bischof, H; Burgstaller, S; Waldeck-Weiermair, M; Rauter, T; Schinagl, M; Ramadani-Muja, J; Graier, WF; Malli, R; Live-Cell Imaging of Physiologically Relevant Metal Ions Using Genetically Encoded FRET-Based Probes; Cells. 2019

- Depaoli, MR; Bischof, H; Eroglu, E; Burgstaller, S; Ramadani-Muja, J; Rauter, T; Schinagl, M; Waldeck-Weiermair, M; Hay, JC; Graier, WF; Malli, R; Live cell imaging of signaling and metabolic activities; Pharmacol Ther. 2019

- Madreiter-Sokolowski, CT; Ramadani-Muja, J; Ziomek, G; Burgstaller, S; Bischof, H; Koshenov, Z; Gottschalk, B; Malli, R; Graier, WF; Tracking mitochondria's intra- and inter-organelle signaling; FEBS J. 2019;

- Eroglu, E; Charoensin, S; Bischof, H; Ramadani, J; Gottschalk, B; Depaoli, MR; Waldeck-Weiermair, M; Graier, WF; Malli, R; Genetic biosensors for imaging nitric oxide in single cells; Free Radic Biol Med. 2018

- Eroglu, E; Rost, R; Bischof, H; Blass, S; Schreilechner, A; Gottschalk, B; Depaoli, MR; Klec, C; Charoensin, S; Madreiter-Sokolowski, CT; Ramadani, J; Waldeck-Weiermair, M; Graier, WF; Malli, R; Application of Genetically Encoded Fluorescent Nitric Oxide (NO•) Probes, the geNOps, for Real-time Imaging of NO• Signals in Single Cells; J Vis Exp. 2017

I confirm that all co-authors have agreed to use their data in my thesis. I have obtained permission from *Cells* to reproduce figures published in Ramadani-Muja et al (1) . *Cells* is an international peer-reviewed open access journal and published monthly online by MDPI, which allows the reuse of published data in a PhD thesis at any time after publication (please visit the journal website for rights and permission statements:

https://creativecommons.org/licenses/by/4.0/
https://creativecommons.org/licenses/by/4.0/legalcode

[1] Gottfried Schatz Research Center, Division of Molecular Biology and Biochemistry, Medical University of Graz, Neue Stiftingtalstraße 6/6, 8010 Graz, Austria

[2] Division of Cardiology, Medical University of Graz, 8010 Graz, Austria

Dedication

To my beloved ones.

“The important thing is to not stop questioning, curiosity has its own reasons for existing.”
— Albert Einstein

Acknowledgements

As a PhD student I received funding by the Medical University of Graz through the PhD program Molecular Medicine (MOLMED) and from the Austrian Science Fund (FWF to Roland Malli).

Einstein once said, there are only two ways to live your life. One is as though nothing is a miracle. The other is as though everything is a miracle. This is the way I lived my PhD and therefore this time has been a truly life-changing experience for me. I received great support from many people during my PhD-studies, whom I would like to mention here:

I want to thank my supervisor and mentor, **Prof. Roland Malli** for the great support, advice and patient guidance he has provided throughout my time as a PhD-student. When I was exploring new ideas I benefited a lot from his inputs. The door to his office was always open for me whenever I had issues about my research. His way of accompanying me through the PhD time allowed this thesis to be my own work, but steered me in the direction whenever he thought I needed it.

Besides my advisor, I would also like to thank the head of the Gottfried Schatz Research Center **Prof. Wolfgang Graier**, who is part of my PhD thesis committee and gave me the opportunity to join his team and makes it possible to successfully conduct this research. His positive contributions to my research inspired me and gave me confidence.

I would also like to thank the other members of my PhD thesis committee, **Prof. Seth Hallström** and **Prof. Rainer Schindl**, who also contributed to this work with their valuable and insightful comments.

My sincere thanks also goes to my colleagues and friends **Markus Waldeck-Weiermair**, **Christiane Klec**, **Sandra Burgstaller**, **Thomas Rauter**, **Maria R. Depaoli**, **Benjamin Gottschalk**, **Sandra Blass**, **Helmut Bischof**, **Sonja Barth**, **Anna Schreilechner** and **Rene Rost** for their great support and the thrilling discussions.

The greatest thanks, however I want to express my parents, **Florin** and **Lirije Ramadani**, my husband **Gjin Muja**, my sister **Argjenta Veseli** and my brother **Platin Ramadani**. This memorable time would not have been possible without your great support. You expected nothing less than excellence from me and encouraged me in all of my pursuits.

Table of Contents

Declaration 2
Disclosures 3
Dedication 5
Acknowledgements 6
Abbreviations 10
Zusammenfassung 12
Abstract 13
Preface 14
1. Introduction 15
1.1. Mitochondrial architecture 16
1.1.1. The outer mitochondrial membrane (OMM) 18
1.1.2. The inner mitochondrial membrane (IMM) 19
1.1.3. The intermembrane space (IMS) 20
1.1.4. The mitochondrial matrix (MM) 21
1.2. The mitochondrial protein import 22
1.2.1. TOM complex: the hotspot of recognition and initial precursor protein targeting at the OMM 22
1.2.2. Import of mitochondrial precursor proteins through the IMM at the TIM complex 24
1.2.3. Mitochondrial protein import into the mitochondrial matrix 25
1.2.4. Overview of the import machinery pathways of mitochondrial proteins targeted to the IMM, IMS and OMM 26
1.3. The mitochondrial protein import as a regulatory hub for physiological and pathophysiological conditions 27
1.3.1. Mitochondrial unfolded protein response (mtUPR) 28
1.3.2. Mitochondrial comprised import response (mitoCPR) 29
1.3.3. Signaling mitochondrial stress via peptide efflux 29
2. Hypothesis and Aims 30
3. Material and Methods 32
3.1. Chemicals and buffer solutions 32
3.2. Generation of the FP-based constructs 33
3.3. Cell culture and cells 35
3.4. Transfection 36
3.5. Mitochondrial Staining 36
3.6. Submitochondrial Localization of Sirt4-sfGFP and 2mt-sfGFP 37
3.7. Structural design and construction of the FP-based probes 37
3.8. Fluorescence Imaging 38

3.8.1. Confocal Imaging 38
3.8.2. Structural illumination microscopy (SIM)....39
3.9. Mitochondrial morphology assessment....39
3.10. Data analysis and statistical analysis 39
4. Results 41
4.1. 2mt-sfGFP, a fast maturing GFP-variant fused to a mitochondrial targeting sequence locates to the mitochondrial matrix....41
4.2. 2mt-sfGFP is suitable for the qualitative and quantitative determination of mitochondrial targeting efficiency 43
4.3. Cancer cells import high amounts of 2mt-sfGFP into mitochondria very efficiently .46
4.4. Only a strong overload of the mitochondrial protein import machinery triggers an accumulation of 2mt-sfGFP in the cytosol 48
4.5. Depolarization of mitochondria leads to severe mistargeting, independently of the expression of 2mt-sfGFP 52
4.6. Depolarization of the mitochondrial membrane potential instantly affects the targeting of 2mt-sfGFP into mitochondria 54
4.7. seCFP-OMP25, a cyan FP-variant targeted to the outer mitochondrial membrane shows no mistargeting upon depolarization of mitochondria 57
4.8. Application of the mitochondrial protein import analysis approach to Sirtuin4, a mitochondrial sirtuin isoform 60
4.9. Sirt4-sfGFP is less efficiently targeted and imported into mitochondria of HeLa cells compared to 2mt-sfGFP....61
4.10. INS-1 cells also target and import Sirt4-sfGFP with a lower efficiency to mitochondria, compared to 2mt-sfGFP....63
4.11. Sirt4-sfGFP is equally distributed between the nucleus and the cytosol in HeLa and INS-1 cells 65
4.12. Fusion of four different mitochondrial targeting sequences to sfGFP lead to accumulation of the probe in the nucleus upon mitochondrial mistargeting 67
4.13. The n4mt-sfGFP as well as Sirt4-sfGFP locates to the outer mitochondrial membrane 70
4.14. Applying super-resolution microscopy confirmed the localization of Sirt4-sfGFP to the outer mitochondrial membrane....72
4.15. Expression of Sirt4-sfGFP induced mitochondrial swelling....74
4.16. Fusion of slower maturing FPs to Sirt4 improve the targeting efficiency to mitochondria 76
4.17. Import of Sirt4 into the mitochondrial matrix visualized by the self-complementing split-FP variant of sfCherry2....78
4.18. mito-STAR, a tripartite self-complementing FP-based probe enables the visualization of the distribution of Sirt4 between mitochondria and the nucleus in living cells 81
4.19. mito-STAR does not induce mitochondrial swelling in HeLa cells 85
4.20. mito-STAR is suitable for the visualization of mitochondrial stress induced by oligomycin-A and antimycin-A1 87

4.21. Development of mito-PRIMA, a dimerization-dependent FP based sensor to visualize defects in mitochondrial protein uptake with no need for optical resolution 88

4.22. mito-PRIMA lights up upon impaired mitochondrial protein import induced by depolarization of the mitochondrial membrane potential 91

4.23. Stimulation of transcription triggered an overload of the mitochondrial protein import machinery in cancer cells 93

4.24. mito-PRIMA is suitable for the online visualization of impairments in the protein uptake machinery of mitochondria 95

4.25. Combining online recordings of mito-PRIMA with 2mt-sfGFP emphasizes the high capacity of cancer cell mitochondria to import proteins efficiently 97

5. Discussion 101

5.1. Visualization of the activity and efficiency of protein targeting to mitochondria using 2mt-sfGFP 101

5.2. Investigating the subcellular distribution of mitochondrial Sirtuin4 using a construct, based on bimolecular fluorescence self-complementation 103

5.3. Dimerization-dependent FP based sensors to assess impairments in the mitochondrial protein import machinery with no need for optical resolution 105

5.4. Application of the novel mitochondrial protein import sensors in the field of neuroscience 106

6. References 107

Abbreviations

Acronym	Term
µ	micro (10-6)
2mt-sfGFP	2 x mitochondrial targeting sequence-super folder green fluorescent protein
ABC	ATP-binding cassette
ADP/ATP	Adenosine diphosphate/ adenosine triphosphate
ATF_5	activating transcription factor 5
ATFS-1	activating transcription factor associated with stress-1
ATP	adenosine triphosphate
ATPase	adenosine triphosphatase
B-NLS	monomer B nuclear localization sequence
BSA	bovine serum albumin
Ca^{2+}	calcium
ClpP	caseinolytic protease proteolytic subunit
DMEM	Dulbecco's modified Eagle's medium
DNA	desoxyribonucleic acid
FCS	fetal calf serum
Fe-S	iron sulfur
GA-NLS	monomer A nuclear localization sequence
Hsp60	heat shock protein 60
IBM	inner boundry membrane
IMM	inner mitochondrial membrane
IMP	inner membrane peptidase
IMS	inner membrane space
iMTS	internal mitochondrial targeting sequence
INS-1	insulinoma cell line
ITS	internal targeting sequence
MC	mitochondrial cristae
MIA	mitochondrial intermembrane space assembly

MIM	machinery of the inner membrane
mitoCPR	mitochondrial comprised import response
mito-PRIMA	mitochondrial protein import analyzer
mito-STAR	mitochondrial sirtuin4 tripartite abundance reporter
MM	mitochondrial matrix
MPI	mitochondrial protein import
mPOS	mitochondrial precursor over accumulation stress
MPP	mitochondrial processing peptidase
mtDNA	mitochondrial desoxyribonucleic acid
mtHsp70	mitochondrial heat shock protein 70
MTS	mitochondrial targeting sequence
mtUPR	mitochondrial unfolded protein response
OMM	outer mitochondrial membrane
Oxa1	oxidase assembly translocase 1
PAM	presequence translocase associated motor
SAB	sorting and assembly machinery
seCFP	super enhanced cyan fluorescent protein
seCFP-OMP25	super enhanced cyan fluorescent protein outer membrane protein 25
sfCherry2	super folder Cherry2
$sfCherry2_{11}$	super folder Cherry2 eleventh beta strand
$sfCherry2_{1-10}$	super folder Cherry2 first to tenth beta strand
sfGFP	super folder green fluorescent protein
Srit4	sirtuin 4
TCA	tricarboxylic acid
TIM	translocase of the inner mitochondrial membrane
TOM	translocase of the outer mitochondrial membrane
UPRam	unfolded protein response activated by mistargeted proteins
VDAC	voltage-dependent anion channel

Zusammenfassung

Fast alle Proteine der Mitochondrien werden im Erbgut des Zellkerns kodiert, weshalb diese Proteine nach bzw. schon während ihrer Bildung im Zytosol in die Mitochondrien importiert werden müssen. Daher ist ein effizienter Proteinimport in die Mitochondrien essentiell für die vielen wichtigen Funktionen dieser Zellorganellen. Die Fähigkeit der Mitochondrien, Proteine zu importieren, kann jedoch eingeschränkt sein, wodurch es zu einer Akkumulation dieser Proteine im Zytosol oder Kern kommen kann. Die Erfassung des mitochondrialen Proteinimports (MPI) und seiner Defekte kann sowohl zellulären Stress als auch Fitness anzeigen. In dieser Arbeit werden hochauflösenden Sensoren, welche auf der Basis von fluoreszierendem Protein (FP) aufgebaut sind, zur Visualisierung des MPI und seiner Defekte entwickelt, charakterisiert und angewandt. Die Anwendung der ersten Klasse von MPI-Sensoren, bei denen FPs mit verschiedenen mitochondrialen Targeting-Sequenzen (MTS) fusioniert wurden, ergab, dass Krebszellen konstant und sehr effizient sehr hohe Mengen von Proteinen mit optimiertem MTS in die Mitochondrien importieren können. Zusätzlich deuten unsere Daten auf einen kotranslationalen Import solcher Proteine in Mitochondrien hin, der die hohe Kapazität von Mitochondrien zur Aufnahme von kernkodierten Proteinen erklären könnte. Dieser Ansatz erwies sich auch als geeignet, um die Bedeutung des Membranpotentials der Inneren Mitochondrien-Membran für den Proteinimport zu erforschen. Bei Depolarisation der Mitochondrien kam es akut zu fehllokalisierten Proteinen außerhalb der Organellen. In einem weiteren Versuch entwickelten wir neuartige zwei- und dreiteilige Sensoren, bei denen Split-FP-Technologien (scSplit-FP) und dimerisierungsabhängige FP-Technologien (ddFP) zur Anwendung kamen. Die auf dem scSplit-FP-Ansatz basierende Generierung des **mito**chondrial **S**irtuin4-**T**ripartite-**A**bundance-**R**eporter (Mito-STAR) ermöglicht die quantitative Untersuchung der subzellulären Verteilung von Sirtuin 4 (Sirt4), einem mitochondrialen Matrixprotein, das Signalwege und Zellstoffwechseländerungen bei bestimmten Zellstressarten auslöst. Unsere Daten zeigten, dass Sirt4 bei Zellstress verstärkt auch im Zytosol und Zellkern von Krebszellen vorkommen kann. Mithilfe der ddFP-Technologie haben wir eine weitere Klasse von FP-basierten Sensoren für die Untersuchung von MPI entwickelt. Diese sogenannten **Mito**chondrial **Pr**otein **Im**port **A**nalyzer (Mito-PRIMA). ermöglichen die Erkennung von Störungen in der MPI-Maschinerie, indem dabei ein Fluoreszenzsignal durch FP Dimerisierung erzeugt wird. Die Nutzung von Mito-PRIMA ergab, dass die Stimulierung der Transkription eine Überlastung der MPI-Maschinerie in Krebszellen auslösen kann. Insgesamt unterstreichen die in dieser Arbeit vorgestellten Ergebnisse, dass die neuentwickelten Sensoren und Protokolle genaue Untersuchungen des Proteinimportes in Mitochondrien ermöglichen, wodurch Defekte und deren Ursachen dieses wichtigen zellulären Vorgangs bei unterschiedlichen Erkrankungen besser erforscht werden können.

Abstract

Almost all mitochondrial proteins are encoded by nuclear genes, meaning that all of these proteins have to be imported into mitochondria. Therefore all mitochondrial functions rely on an efficient protein import into the organelle. However, the capability of mitochondria to import proteins can be exceeded, leading to an accumulation, hence mistargeting of nuclear encoded mitochondrial proteins in the cytosol and/or nucleus. Thus, the detection of the targeting efficiency of mitochondrial proteins can act as a sensor of mitochondrial fitness or mitochondrial stress, respectively. Here, we introduce the engineering and application of novel fluorescent protein (FP) based probes, protocols and image analysis for the visualization of the MPI and its defects in single cells under various conditions.

Applying the first class of MPI-sensors, where we fused FPs to different mitochondrial targeting sequences (MTS), revealed that cancer cells constantly and very efficiently import very high amounts of proteins with optimized MTS to mitochondria. Additionally our data emphasize a cotranslational import of proteins into mitochondria that might explain the high capacity of mitochondria to take up nuclear-encoded proteins. This approach proved also suitable for the detection of defects in MPI, due to depolarization of mitochondria resulting in an instant accumulation of mitochondria-targeted proteins within the cytosol and nucleus.

In an additional attempt we developed novel bi- and tripartite sensors, applying self-complementation split-FP (scSplit-FP) and dimerization-dependent FP (ddFP) technologies. Generation of **mito**chondrial **S**irtuin4 **T**ripartite **A**bundance **R**eporter (mito-STAR), based on scSplit-FP approach allows the quantitative investigation of sirtuin 4 (sirt4), a mitochondrial matrix protein considered to be involved in cellular stress responses. Our data indicate that sirt4 may contribute to the mitochondrial unfolded protein response by its accumulation within the cytosol and nucleus upon cell stress.

By applying the ddFP-technology, we developed an additional class of FP-based probes to study the efficiency and activity of MPI. We named these probes **mito**chondrial **Pr**otein **Im**port **A**nalyzers (mito-PRIMA). The mito-PRIMAs are dually targeted bipartite probes that allow the detection of impairments in the MPI machinery by generating fluorescence within the nucleus, when the MPI is defect. Exploiting mito-PRIMA revealed that stimulation of transcription can trigger an overload of the MPI machinery in cancer cells.

Altogether, the findings presented in this work emphasize that the novel fluorescent MPI-sensors are suitable to gain mechanistic insights into MPI, its defects and mitochondrial-to-nucleus signaling as well as mitochondrial stress responses under various cellular conditions.

Preface

Since the beginning of my PhD I have the honor to deal with a research area, which was pioneered by Gottfried Schatz, namely the mitochondrial protein import (MPI).

Gottfried Schatz, not only demonstrated in the early sixties that mitochondria contain their own DNA (2), he also deciphered the mechanisms by which mitochondrial proteins are synthesized (3). Because only a very small fraction of mitochondrial proteins are encoded in the mitochondrial genome, his attention turned to those proteins, which are encoded by the nuclear genome and hence have to be imported into the organelle. Nuclear encoded mitochondrial proteins harbor a so called mitochondrial targeting sequences (MTS) (4). These MTS are responsible to direct nuclear encoded mitochondrial proteins to the organelle and make it possible that these proteins are imported into mitochondria (5). Scientists put a lot of effort and came up with various tricks to explore and discover the essential parameters, which guarantee a functioning MPI and to identify the key players of the MPI machinery.

1. Introduction

Mitochondria, classically considered as the powerhouse of the cell, contribute as metabolic highly active organelles to far more than bioenergetics. To guarantee a functioning mitochondrial network within a cell and hence being able to fulfill the various duties in the cell, mitochondria have to exhibit a functioning mitochondrial protein import (MPI) machinery, since more than 99% of all mitochondrial proteins are nuclear encoded and have to be directed and imported into the organelle (6) (7) (8). The maintenance of the mitochondrial protein homeostasis is essential for cell viability (9). Therefore all mitochondrial functions rely on an intact and efficient import of nuclear encoded proteins into the organelle. For many years two main mitochondrial import pathways have been described (10), which were responsible to direct proteins into the mitochondrial inner membrane and the lumen of mitochondria, the mitochondrial matrix. During the last years, more and more research has been done in this regard, leading to the identification of various new players in the MPI (11). This novel mechanistic insights deliver the findings of new pathways and the discovery of new import mechanism into the outer mitochondrial membrane and the intermembrane space. Nowadays, the versatile composition of mitochondrial import machineries and mechanisms include at least four main MPI pathways, which facilitate the import and sorting of nuclear encoded mitochondrial proteins (12).

The reason, why the MPI machinery comprises more different import pathways is probably due to the fact, that mitochondria possess a characteristic architecture (13) . Mitochondria consist of at least four sub-compartments, namely the outer mitochondrial membrane (OMM), the intermembrane space (IMS), the inner mitochondrial membrane (IMM) and the mitochondrial matrix (MM). The many nuclear encoded mitochondrial proteins, are translated as presequences on cytosolic ribosomes and have to be directed to one of the compartments afterwards.

An intact MPI machinery, consisting of the different pathways for each submitochondrial compartment, is necessary to control mitochondrial biogenesis, dynamics and function under physiological and pathophysiological conditions (14) (15).

As mitochondria play an essential role in cell viability, cells established a nuclear response when mitochondrial functions such as the mitochondrial protein import face defects (16). Therefore, the import machinery of mitochondria is not only essential for the survival of the cell but can additionally act as a regulatory hub in metabolism, stress and disease in the frame of the retrograde signaling (17). However, an effort is needed to answer questions related to MPI in terms of cellular and mitochondrial stress.

1.1. Mitochondrial architecture

The diversity of various functions, which mitochondria participate in, such as intermediary metabolism, oxidative phosphorylation, synthesis of Fe-S clusters, heme and certain phospholipids are tightly linked to the organelles structure (18).

Light microscopy makes the visualization of mitochondria already possible, however an electron microscope or super-resolution microscopy is required to reveal their detailed internal ultrastructure. Mitochondria are build up of two membranes, namely the outer mitochondrial membrane (OMM) and the inner mitochondrial membrane (IMM) (19). In addition to that, mitochondria also harbor an intermembrane space (IMS), which is located between the OMM and the IMM. The innermost part of mitochondria consists of the lumen of mitochondria, the mitochondrial matrix. Frey and Mannella claim that the cristal membrane and inter-cristal space represent additional sub-compartments (20).

Both membranes, the OMM and the IMM have distinct functions and different protein and lipid compositions (21). A complex and very specific translocation machinery escort more than 1000 proteins selectively to those compartments (17). The OMM functions as a barrier to the cytosol. The outer membrane of mitochondria depicts a porous, meaning freely traversed membrane, which can be passed by ions and small uncharged molecules. The voltage-dependent anion channel (VDAC), is such a pore-forming unit, enabling these kind of passages (22). Also, the VDAC happens to be one of the most abundant proteins of the OMM (23) (24). The voltage-dependent pore operates not only as an gatekeeper, it also functions as a mediator between mitochondria and the rest of the cell, by controlling the entry and exit of mitochondrial metabolites (25). The transport of molecules between the cytosol and mitochondria through the outer membrane of mitochondria might be rather unspecific (24). In contrast to that, the inner mitochondrial membrane (IMM), however seems to represent a tight filter under normal physiological conditions (24). Whereas the OMM, due to its porosity harbors no membrane potential, the inner membrane, acting as a tight diffusion barrier to all ions and molecules, shows a membrane potential of about -180 mV (negative inside), possibly because of specific membrane transport proteins, channels and exchangers, which are all selective for particular ions and molecules (26).

In contrast to the OMM, which shields mitochondria from the rest of the cell and represent one compartment, the IMM by forming invaginations, the cristae junctions, is classified into two structurally and functionally distinct domains. The IMM can be subdivided into in the cristae membrane (CM) and the inner boundary membrane (IBM) (27). These two sub-compartments of the inner membrane of mitochondria outline the localization of proteins for electron transport chain subunits and ATPase, and also for proteins of the import machinery of the IMM.

Interestingly, also components of the mitochondrial Ca^{2+} uniporter machinery are differently distributed among the IMM sub-membranes (28).

The OMM and the IMM act not only as two independent mitochondrial membranes, facilitating a huge amount of various pathways and tasks. Hackenbrock proposed the model of both membranes being in close contact, based on transmission electron micrographs (19). The IBM, which is also tightly attached to the outer membrane of mitochondria may be responsible for the translocation of proteins coming from the cytosol into the lumen of mitochondria, the MM. Phospholipids are probably also transported through the contact spots between the OMM and the IBM (13). The physical connection between the outer membrane and the inner membrane of mitochondria, proposed by Hackenbrock is essential for a number of mitochondrial processes (29) , such as metabolite exchange (30) and the mitochondrial protein import (31).

The space between the outer membrane of mitochondria and the IBM, the so called IMS, represents a mediator area for interactions between the OMM and the IMM (32). This specialized region is the location of many physiological and pathophysiological processes, such as the import of mitochondrial proteins coming from the cytosol (33) or apoptosis, the programmed cell death (34).

The invaginations formed by the inner membrane of mitochondria and the IBM, the cristae, which were first seen by electron microscopy in plastic-embedded mitochondria and tissue can penetrate deeply into the matrix (35) (36). Generally crista invaginations form tubular or lamellar shapes and can even exceed into the matrix space (35). In post-mitotic heart or liver cells mitochondria, however, the crista junctions depict circular structures of around 25 nm diameter (37) (38). The structural maintenance of cristae junctions is essential, since a recent studies show the correlation between the shape of cristae and the oxidative phosphorylation activity, having an impact on cellular metabolism (39).

1.1.1. The outer mitochondrial membrane (OMM)

The outer mitochondrial membrane (OMM) serves as a barrier between mitochondria and the cytoplasm (26). Generally the OMM represents a membrane, where ions and small, uncharged molecules can pass through porins, such as the voltage-dependent anion channel VDAC (22). Proteins and any larger molecules however, cannot freely traverse the OMM. Therefore the OMM harbors special multi-subunits, which are responsible for the highly specific detection and translocation of nuclear encoded mitochondrial precursor proteins (40). Three protein complexes form up the protein import machinery of the outer membrane of mitochondria.

One of them is the translocase of the outer membrane (TOM) and depicts with its various subunits the main entry gate for mitochondrial proteins encoded in the nucleus (41). The main subunits, forming the TOM complex, namely the TOM20, TOM22 and TOM70 show cytosolic domains, which are known to interact with their cytosolic domains with nuclear encoded mitochondrial preproteins (42). There are two different classes of mitochondrial precursor proteins, which can be recognized by the subunits of the TOM complex. The TOM20 and TOM22 is responsible for the detection of preproteins harboring a MTS on the N-terminus (40). Proteins, which have an internal targeting sequence (ITS) are usually recognized by the TOM70 (42).

The TOM complex depicts a holo-complex, including at least seven subcomponents with receptor proteins, which recognize and bind the precursor proteins targeted to mitochondria (43). The pore of the TOM complex is made up of TOM40 (44). Moreover, the pore-forming TOM-complex acts as a passageway for the unfolded polypeptide chains across the outer membrane (42) (43). This passage of nascent peptides through the protein-conducting channel TOM40 is assisted by three small TOM proteins, the TOM5, TOM6 and TOM7, whereby TOM5 guides the insertion of precursor proteins into the TOM40 channel (45) and the other two small TOM proteins take part in the stability of the TOM complex itself (46).

The second protein complex on the outer membrane of mitochondria is the TOB/SAM complex (47). This complex works separated from the TOM, by sorting and assembling mitochondrial precursor proteins, that cannot be correctly integrated at mitochondrial membranes by the TOM complex alone and are hence transferred from the TOM to the SAM complex (47).

The mitochondrial import (MIM) complex is the third complex of the outer membrane of mitochondria. This complex is responsible for the insertion and import of precursor proteins, which contain single- and multi-spanning transmembrane helices, into the OMM (48) (49).

1.1.2. The inner mitochondrial membrane (IMM)

The inner mitochondrial membrane (IMM) contains also several translocases and subunits, which are specific for various classes of proteins and enable the further transport and insertion of mitochondrial proteins, once they are passing the TOM complex. So far, five subunits of the TIM machinery are identified at a molecular level (50) (51) (52).

Two classes of translocases, the TIM23 complex and the TIM22 complex for the TIM complex (53) (54). These two TIM complexes, namely the TIM23 and TIM22 cooperate with the TOM complex during the import of nuclear encoded mitochondrial precursor proteins.

Further subunits of the TIM23 complex represent the TIM17 and TIM44, which also play and essential role in the import of mitochondrial precursor proteins. The TIM23 protein acts as a presequences receptor for precursor polypeptides in the IMS, whereas together with the TIM17, these two TIM subunits form a protein-conducting channel across the inner membrane of mitochondria (55) (56).

The TIM22 complex, which is responsible for the import of another class of mitochondrial proteins interacts with three small TIM proteins, namely the TIM9, TIM10 and TIM12 (53) (56) (57).

Additionally, the IMM hosts another complex, which is essential for the MPI machinery, namely the oxidase assembly (OXA) translocase or OXA1 complex. This complex is needed for the insertion of mitochondrial proteins, which have faced the lumen of mitochondria into the inner membrane (58). Proteins, which are inserted by the OXA1 into the IMM have already passed the TOM and TIM complex machinery (59).

The inner membrane peptidase (IMP), located on the outer surface of the IMM, cleaves the targeting signal off for some intermembrane space proteins, making the release of the mature protein into the IMS possible (60).

Also, essential for the efficient import of mitochondrial proteins and located at the IMM is the Mgr2, functioning as a lateral gatekeeper for mitochondrial precursor proteins which are sorted into the inner membranes lipid phase (61).

One characteristic of the inner membrane of mitochondria is the formation of invaginations, known as cristae (19) (27). These cristae are the main spot of the oxidative phosphorylation systems, containing the respiratory complex I to IV and the F_1 F_0 – ATP synthase for ATP (62) (63).

1.1.3. The intermembrane space (IMS)

The intermembrane space of mitochondria, the IMS is located between the outer and inner membrane of mitochondria (36). The IMS, as a space separating the two mitochondrial membranes harbors an aqueous environment (64). Therefore a number of subunits of the TIM complex and mitochondrial chaperones are guiding hydrophobic polypeptides or peptides with hydrophobic regions during the import through the TOM and TIM channel and the IMS, so that these proteins do not aggregate or misfold (64).

The complex of the TIM23 machinery, which contains amongst others the TIM9-TIM10 complex is mainly located in the mitochondrial IMS. This specific complex is responsible for the completion of import and translocation of hydrophobic membrane proteins across the outer membrane and through the TOM and TIM pore (65). Meaning, that these proteins act as sort of chaperones of the intermembrane space for insoluble mitochondrial proteins encoded by the nucleus (54). In addition to the TIM9-TIM10 complex, which mainly sits in the IMS, the TIM12 is also structurally related to the IMS (57) . This is necessary to support the TIM22 for carrier translocations (53).

The TOM complex also harbors intermembrane-space domains, such as the TOM22, facing the aqueous milieu of the IMS with its C-terminal terminus (66). Thereby TOM22 facilitates the transfer of nascent polypeptides from the TOM complex to the translocases of the IMM, the TIM machinery (67).

The IMS is a sub-compartment of mitochondria where newly synthesized or matured proteins get disulfide bonds and can be released afterwards in the IMS (68). The formation of disulfide bonds is essential for many proteins to fold and assemble correctly and to gain a specific stability, activity and function in the respective compartment (33). Mitochondria have an own relay system to fulfill this functions, namely the mitochondrial intermembrane space import and assembly protein (MIA), which represents also a translocase of mitochondria (69). One essential partner of the MIA complex in the frame of the disulfide relay system is the sulfhydryl oxidase GFER (70). The GFER is also a central enzyme occurring in the complete architecture of the IMS of mitochondria (70).

1.1.4. The mitochondrial matrix (MM)

The innermost compartment of mitochondria represents the lumen of mitochondria, the mitochondrial matrix (MM) (71). The MM is surrounded by an impermeable membrane, the inner membrane of mitochondria, the IMM.

One of the first times, describing the MM was in isolated rat liver mitochondria, by chemical fixation and subsequent high-resolution electron microscopy (72). The MM harbors the complete mitochondrial genome, still encoding only around 1% of all mitochondrial proteins (4) (73).

However, a huge number of various mitochondrial proteins and enzymes is located in the MM, such as molecules, which are involved in iron-sulfur cluster assembly (74) (75) or also enzymes of the tricarboxylic acid (TCA) cycle (76). Due to the fact, that mitochondria possess their own genetic information they also harbor their own transcriptional and translational systems. This means that mitochondria also contain their own ribosomes, referred to as mitoribosomes, which are localized to the MM (77).

Another essential protein for the MPI, also located to the MM, is the ATP-driven presequences translocase-associated motor (PAM). The PAM forms a huge protein complex, amongst others with the TIM-machinery, referred to as TIM-PAM complex (67). The core of the PAM protein complex is formed by the mitochondrial heat shop protein 70, namely the mtHsp70 (78). The lumen of mitochondria offers a spot for the complex of the MPI machinery, meaning that the PAM complex not only interacts with the TIM machinery and the mitochondrial heat shock protein 70 (mtHsp70), but there is also an additional matrix protein, namely the co-chaperone Mge1, which functions as a nucleotide exchange factor for the mtHsp70 (67). To sum it up, the PAM complex consists of three essential subunits, namely the mtHsp70, the TIM44 protein and the nucleotide exchange factor Mge1, which are important for the translocation and completion of the presequences carrying proteins into the lumen of mitochondria.

In addition to the mentioned PAM-complex in the MM, another essential enzyme is located to the lumen of mitochondria. The mitochondrial processing peptidase (MPP) catalyzes a crucial step in the completion of the import of the polypeptide translocation (79). This crucial step is the cleavage of the N-terminal targeting sequence, which every mitochondrial matrix protein contains (80).

There is a number of other matrix peptidases for further protein processing, which reside in the MM and are necessary for protein stabilization (81) (82).

1.2. The mitochondrial protein import

Taking the endosymbiotic theory into consideration, mitochondria emerge from a host cell, which enclosed a proteobacterium and kept it as an endosymbiont (83) (84). Most of the genes were carried over from the prokaryotic genome into the eukaryotes host cell nucleus during evolution, meaning that almost all mitochondrial proteins are synthesized in the cytosol and have to be somehow imported into mitochondria (85) (86).

How does the cell manage to target nuclear encoded mitochondrial protein to mitochondria? To ensure the transport of mitochondrial protein, which are encoded in the nucleus and afterwards translated on cytosolic ribosomes into mitochondria these specific proteins carry an information making the successful targeting possible (4). This information lies within the polypeptide itself. The so called mitochondrial targeting sequence (MTS) harbors the information for a nuclear encoded protein to be efficiently transported and afterwards imported into mitochondria (5). Targeting signals for mitochondria can be located on the N-terminus of a protein, namely a classic MTS (41) or they can spread out over the protein, referred to as internal targeting signal (ITS). For the initial precursor protein targeting mitochondria distinguish between two different pathways.

1.2.1. TOM complex: the hotspot of recognition and initial precursor protein targeting at the OMM

The first step in the import of mitochondrial proteins is the recognition of targeting signals of mitochondrial proteins, which are translated on cytosolic ribosomes. This recognition of targeting signals takes places at the outer membrane of mitochondria. There are two pathways, which are responsible for the recognition and initial precursor protein targeting to mitochondria (87).

The first pathway captures mitochondrial pre-proteins with a typical MTS. The MTS of these kind of pre-proteins depicts some characteristic features. For an efficient import into mitochondria the length, structure and charge of the MTS is essential. The MTSs exist as cleavable extensions, depicting a lengths of about 10 to 30 amino acid residues (range of approximately 10-80 residues) (88). Containing these specific amino acids, a classic MTS locates at the amino-terminus of a precursor protein (41). Usually MTSs represent amphiphilic helices (89). MTS make up the majority of mitochondrial targeting sequences, referred to presequences (90). Different mitochondrial proteins harbor no presequences with amino-acid

sequence identity, but they do share the above mentioned characteristic physicochemical properties, such as hydroxylated and hydrophobic residues, positively charged regions and the potential to form amphiphilic alpha helices (91) (92).

The first interaction spot between the presequences of a mitochondrial protein and the import machinery of mitochondria is the cytosolic domain of the TOM20 (93). The structure and composition of the TOM20, with its physicochemical properties guarantees the successful recognition of the presequences. Based on NMR structure analysis of Abe et al (94) it became clear that the TOM20 depicts a hydrophobic binding pocket, where e. g. the presequence extension of the aldehyde dehydrogenase can bind through its amphiphilic alpha helix (94).

After the recognition of the presequences on the TOM20, the precursor protein is further transported to the general import pore complex of the TOM machinery, formed by the TOM 22, the small subunit TOM5 and the TOM40, building up the pore of the TOM complex. The positively charged MTS is bound to the TOM22 via its negatively charged cytosolic domain on the surface of mitochondria (95). The intermembrane space domain of the TOM22 enables the further transport through the channel-forming TOM40 protein (96).

The second pathway for the first interaction between precursor proteins and mitochondria occurs also at the TOM complex, but in addition to the TOM20 and TOM22 specifically at the TOM70 and TOM37 subunits, making up the TOM70-TOM37 subcomplex (97) (98). Usually the TOM70 recognizes and binds precursor proteins with ITS, which contain more hydrophobic regions (97). Backes et al. even propose a model of TOM70 and targeting sequences interaction, referred to as stepping stone model (99). They present the existence of internal MTS (iMTS), which mimic the features of classic N-terminal MTS, but in contract to those iMTS are scattered over the whole precursor protein and are recognized in a stepping mode by the TOM70. Bakes et al. think that this stepping stone model occurring at the TOM70 increase the efficiency of mitochondrial proteins in to the lumen of mitochondria (99).

Generally, there is no strict separation between the both pathways, meaning that some proteins are recognized and bound by both TOM subcomplexes, the TOM20-TOM22 and the TOM70-TOM37 (87).

1.2.2. Import of mitochondrial precursor proteins through the IMM at the TIM complex

The translocase complex machinery of the OMM transfers the preproteins through the outer membrane and the IMS. Electrophoretic effects, which evolve through the membrane potential across the IMM and which is negative on the matrix side, are responsible for the further transport of the polypeptide (100).

To transfer and mediate the precursor protein from the OMM and the IMM to the next spot of the mitochondrial import pathway, the inner membrane of mitochondria, the TOM complex collaborates with the TIM machinery. Two subunits of the TIM machinery are the main cooperation partners of the TOM complex, namely the TIM23 and the TIM22 (53) (54). These both subunits, similarly like in the case of the case of the TOM20 and TOM70 are responsible for different classes of targeting signals for mitochondria. The TIM23 facilitates the import of classical N-terminal MTS (101). The TIM22 however mediates the import of mitochondrial proteins, which do not harbor a classic MTS, such it is the case for members of the mitochondrial carrier family, e. g. ADP/ATP carrier or other hydrophobic membrane proteins with ITS (53) (57). Usually, proteins which are imported through the TIM22 pathway are inserted via the Oxa1 machinery into the inner membrane of mitochondria, after facing the MM.

For the translocation of precursor proteins not only across the inner membrane, but also into the matrix a membrane potential is required (51). ATP enables the completion of the protein translocation across the mitochondrial membranes (102).

The TIM23 captures N-terminal MTS and together with the TIM17 which form a channel conducting pore transports the precursor protein through the IMM to the lumen of mitochondria (101).

1.2.3. Mitochondrial protein import into the mitochondrial matrix

Precursor proteins harboring a classical positively charged N-terminal matrix targeting signal face the lumen of mitochondria after being transported through the TIM23 presequence pathway. The TIM44, which is an essential part of the TIM23 complex, plays a crucial role in the import of mitochondrial precursor proteins into the MM (103). It links the mtHsp70 together with its co-chaperone Mge1, forming the motor for the further translocation of the precursor into the lumen, namely the PAM complex (104). MtHsp70 couples the precursor polypeptide chain and is tightly bound to the unfolded protein via its peptide-binding domain (104).

Until today it is not known how exactly the mechanism of the import motor including the TIM23 complex subunits and the mtHsp70 proceeds. However, two models can be taken into consideration. The first model, the trapping model proposes that the preproteins by tightly being bound to the mtHsp70, cannot backslide through the import channel. The Brownian motion enables the inward movement of the polypeptide and afterwards another mtHsp70 can bind the peptide and ensure its stepwise import into the matrix (12). In the second model, the pulling model the PAM complex comes more into play. By generating an inward-directed force the mtHsp70 pulls the precursor polypeptide into the matrix (105) (106).

Once the precursor polypeptide passes the PAM complex machinery the mitochondrial processing peptidase MPP becomes active. The amino-terminal presequence is selectively removed by the MPP (53). The MPP cleaves the amino-terminal targeting extensions of both, inner-membrane targeted and matrix-targeted precursor proteins (79). The catalytic removal of the targeting sequences by the MPP is not necessarily required for the translocation of the precursor protein through the membranes, but can also happen during or after the import of the polypeptide chain through the TIM23 machinery.

Some hydrophobic targeting sequences or ITS have to be cleaved twice. Once by the MPP and then additionally by the inner-membrane peptides (IMP), if the mitochondrial protein is destined for the IMM (107).

1.2.4. Overview of the import machinery pathways of mitochondrial proteins targeted to the IMM, IMS and OMM

In addition to the previously described classical presequence pathway and the carrier pathway to the IMM, which are responsible for the import of about 60% of all mitochondrial proteins to the inner membrane and matrix (81) three other mitochondrial protein import pathways exist, namely that one targeting mitochondrial proteins to the IMS and the outer membrane of mitochondria.

Proteins, destined for the IMS depict some specific features. Meaning that those kind of proteins harbor cysteine rich motifs, which ensure capturing of the protein in the IMS (33) (108).

The import pathway of mitochondrial protein destined for the outer membrane, the so called β-barrel pathway targets precursor β-barrel proteins to the OMM by inserting those into the membrane through the sorting and assembly machinery, the SAM (47). The TOM complex and small TIM chaperones facilitate this import pathway (109).

In addition to the β-barrel pathway, another import pathway is exploited by a number of mitochondrial proteins destined for the OMM, which harbor helical transmembrane segments. Those proteins are targeted to the OMM with the assistance of the MIM complex (48).

For the efficient import and insertion of precursor proteins with transmembrane segments intended for the OMM, these kind of proteins carry also N-terminal targeting sequences, serving as signal-anchor peptides (49). Additionally they can occur as multispanning outer membrane proteins.

1.3. The mitochondrial protein import as a regulatory hub for physiological and pathophysiological conditions

Due to the fact, that almost all mitochondrial proteins are synthesized outside of mitochondria the import of those proteins into the organelle is inevitable. Therefore all mitochondrial functions depend on a successful and efficient protein import into the organelle.

Mitochondria have to fulfill a variety of functions and multiple tasks such as ATP production (110) , synthesis of iron-sulfur cluster and heme (111) , involvement in metabolic pathways including amino acids and lipids (112) and play a crucial role in the immune response (113) and cellular signaling in programmed cell death (114) . Taking these aspects into consideration it becomes clear, that the mitochondrial protein homeostasis have to be a fine-tuned process.

More and more studies come up with indications that the protein import of mitochondria underlies regulations at multiple levels, which are linked to metabolism, stress and pathogenesis of diseases (115) (116) (117). Therefore the activity and efficiency of the mitochondrial protein import (MPI) can act as a sensor of mitochondrial stress or mitochondrial fitness.

Many conditions occurring in the cell can lead to mitochondrial stress, such as the accumulation of mistargeted proteins in the cytosol, reduced activity of the respiratory chain, accumulation of misfolded proteins in the matrix or formation of high levels of reactive oxygen species (116).

Mitochondria react to any kind of mitochondrial stress, mostly via a precise a strict regulated communication with the nucleus, since the nucleus provides mitochondria with proteins and ensures the organelles survival (16). This signaling coming from the nucleus to mitochondria, the so called anterograde regulation includes the tight nuclear control over mitochondria. The consequences of that are influence on mitochondrial activity impact on mitochondrial biogenesis to meet cellular needs (16) . During the last years many studies came up describing the different mitochondrial stress responses in the frame of the retrograde signaling, meaning how mitochondria react upon mitochondrial stress and responses to the nucleus (118) (119) (120).

1.3.1. Mitochondrial unfolded protein response (mtUPR)

The mitochondrial unfolded protein response, the mtUPR, is a signaling pathway occurring under certain conditions of mitochondrial stress. Activation of the mtUPR triggers an adaptive transcriptional response in the frame of the mitochondrial-to-nuclear communication, the so called retrograde signaling pathway (121) . The mtUPR aims to promote mitochondrial recovery and metabolic adaptions to restore mitochondrial proteostasis (121) (122). Transcriptional response programs enable a proper completion of the mtUPR.

The first observations of induction of mtUPR were seen in cultured mammalian cells, when Martinus et al. and Zhao et al. discovered that depletion of mitochondrial DNA (mtDNA) or overexpression of a specific mitochondrially targeted protein variant, which misfolds in the MM activated the transcription of specific chaperones (123) and proteases (124). Furthermore, Yoneda et al. demonstrated that inhibition of the protein synthesis of mitochondria also triggers mtUPR (125). Not only interference in protein homeostasis activates mtUPR, also impairments in the metabolic pathways of mitochondria lead to transcriptional rearrangements in the nucleus (125) (126) (127).

These transcriptional adaptions in the course of mtUPR include induction of;

- mitochondrial chaperons Hsp69 and mtHsp70 (123)
- genes that promote mitochondrial biogenesis and function (128)
- genes involved in the mitochondrial fission for the improvement of mitochondrial biogenesis (129)
- various metabolic adaptions, such as induction of glycolysis genes to promote mitochondrial recovery (118)

Also the induction of specific transcription factors are associated with the activation of mtUPR, such as the ATFS-1, discovered via a genetic screen in *C. elegans* by Nargund et al in 2012 (118). Mitochondrial stress conditions, which hence trigger mtUPR cause a reduction in the mitochondrial import efficiency of the ATFS-1. As a consequence the transcription factor ATFS-1 resides in the cytosol. Due to an additional targeting information for the nucleus, which is embedded in the protein the fraction of ATFS-1, which is not imported into mitochondria anymore and remains in the cytosol is transported to the nucleus. Once being present in the nucleus, ATFS-1 initiates a transcriptional response, thus allowing cells to sense and monitor mitochondrial function and homeostasis (118) (116) (130). The mammalian analogue to the ATFS-1, discovered by Fiorese et al. in 2016 represents the transcription factor ATF5 (131).

Mitochondria exploit their import machinery by equipping the nuclear encoded proteins with dual targeting informations to act as sensor of mitochondrial stress.

1.3.2. Mitochondrial comprised import response (mitoCPR)

Another mitochondrial stress response is the mitochondrial comprised import response (mitoCPR). This response program includes the unfolded protein response activated by mistargeting of proteins (UPRam) and the mitochondrial precursor over-accumulation stress (mPOS) (113) (10) (132) . These pathways lead to the accumulation of mitochondrial targeted proteins outside of the organelle, since their import into mitochondria failed due to conditions of mitochondrial stress (133). Consequently mitochondria react to that in a way which involves the attenuation of cytosolic synthesis of proteins and also the initiation of a degradation program for the mistargeted proteins to counteract the protein homeostasis perturbations (132).

Again, also these stress response pathways demonstrate the capacity of mitochondria to report their functional status via fine-tuned regulation of checkpoints of the MPI.

1.3.3. Signaling mitochondrial stress via peptide efflux

Another mechanism by which mitochondria possibly communicate with the nucleus is exploiting peptides to sense the status (134). Yeast mitochondria contain specific transport proteins, such as the ATP-binding cassette (ABC) protein Mdl1, which was discovered by Young et al. depicting an intracellular peptide transporter and being located in the inner membrane of mitochondria. The assumption came up, that these peptides may cross the OMM and are transported to the nucleus, where they serve as messengers.

2010 Haynes et al demonstrated in mitochondria isolated from *C. elegans* the contribution of the peptide efflux of mitochondria in the mitochondrial stress response (119). This kind of stress response does not only require ABC transporter, such as the HAF-1 in the case of the *C. elegans*, but also mitochondrial matrix proteases. Especially the matrix localized protease of *C. elegans*, the ClpP, which seems to be responsible for the generation of the peptides (135).

All these pathways and signaling processes mentioned in this chapter demonstrate the importance of an intact mitochondrial protein import machinery, not only to ensure the supply of mitochondria with proteins, but also for efficient stress responses, which are necessary to counteract the damage and restore the function and vitality of mitochondria in conditions of mitochondrial stress.

2. Hypothesis and Aims

Until today, only few high resolution methods are currently available that allow the detection of the activity and efficiency of the mitochondrial protein import (MPI) in living cells. Due to the lack of appropriate tools for the assessment of the activity and efficiency of the MPI, we set our self the aim to overcome these limitations and restrictions by developing and establishing novel fluorescent protein based tools, imaging protocols and image analysis to visualize MPIand its defects on the level of individual cells and cell populations

According to this, the specific aims of this study are:

I. Design, development and application of single FP-based MPI sensors:

a. 2mt-sfGFP: fluorescent protein fused to mitochondrial targeting sequence
b. determine the efficiency of the MPI in cancer cells as an endpoint readout and overtime
    - therefore we aimed to stress the MPI of HeLa cells by turning on the proteinbiosynthesis and determine the protein import capacity by exploiting 2mt-sfGFP
    - and accordingly we wanted to block the MPI completely by depolarizing mitochondria and evaluate the suitability of 2mt-sfGFP as an indicator of defects in the MPI machinery

II. Expand the 2mt-sfGFP by exploiting the self-complementation Split-FP and applying it to a nuclear encoded mitochondrial protein, the Sirt4:

a. Sirt4-sfGFP: quantitative analysis of the subcellular distribution of Sirt4
b. 2mt-sfCherry$2_{1\text{-}10}$ + Sirt4-sfCherry2_{11}: confirmation of the localisation of Sirt4 to the mitochondrial matrix
c. mito-STAR: self-complementation Split-FP based mitochondrial Sirtuin4 sensor to study the distribution of Sirt4 between the mitochondria and the nucleus in living cells
d. Sirt4-eGFP, Sirt4-mCherry: Fusion of Sirt4 to slower maturing FPs to improve the targeting efficiency

III. **Besides the development of single FP-based sensors, where a certain optical resolution for the analysis is required we aimed to come up with constructs where no optical resolution is necessary. This kind of probes should be valuable to capture the MPI activity in a whole cell population in a high throughput manner. The read-out of this class of FP-based sensor should act as a direct indicator of import perturbations and protein import defects in the mitochondrial protein uptake machinery. Accordingly we developed:**

a. the mito-PRIMAs: MPI-sensors based on the dimerization dependent fluorescent protein (ddFP) technology

3. Material and Methods

The detailed exposition and comments of the performed experiments in the chapter of Material and Methods of this study were published similarly in Ramadani-Muja et al., 2019 (1).

3.1. Chemicals and buffer solutions

Materials used for the cell culture were purchased from Greiner Bio-One (Kremsmünster, Austria). Chemically competent 10-beta *Escherichia coli (E. coli)* and restriction enzymes were obtained from New England Biolabs (New England, GB.). Following compounds were used and obtained from following companies or suppliers: Oligomycin-A: Sigma Aldrich (Vienna, Austria); Antimycin-A1: Sigma Aldrich (Vienna, Austria). Suberanilohydroxamic acid (SAHA) was a gift from Markus Wallner, Devision of Cardiology, Medical University of Graz, Austria. Agar−Agar Kobe I, D-Glucose, $CaCl_2$, HEPES, $MgCl_2$, KCl, NaCl, NaOH, Trypton/Pepton, extract were purchased from Carl Roth (Graz, Austria). GoTag® was obtained from Promega (Mannheim, Germany) and the purchase of the fetal calf serum (FCS) was done over lifetechnologies (Vienna, Austria). MitoTracker™ Green FM and MitoTracker™ Red FM were purchased from Fisher Scientific (Vienna, Austria). VWR International (Vienna, Austria) was the supplier of the Agarose. 2-deoxy-D-glucose (2-DG) was purchased from Sigma Aldrich (Vienna, Austria).

Cells were stored in HEPES-bufferes solution (storage buffer) prior to fluorescence microscopy experiments. The storage buffer contains 138 mM NaCl, 5 mM KCl, 2 mM $CaCl_2$, 1 mM $MgCl_2$, 10 mM HEPES, 2.6 mM $NaHCO_3$, 0.44 mM KH_2PO_4, 0.34 mM Na_2HPO_4, 10 mM D-glucose, 0.1% vitamins, 0.2% essential amino acids and 1% penicillin-streptomycin. Adjustments of the pH to 7.4 with NaOH were also performed.

Cells were kept in storage buffer during experiments. When performing online long-term-imaging fluorescence experiments storage buffer containing 10% FCS was applied to the cells.

Depolarization buffer, which was used to depolarize mitochondria during the long-term-imaging fluorescence experiments contained 5 µM Antimycin-A1 and 10 µM Oligomycin-A diluted in storage buffer with 10% FCS.

For depolarization of mitochondria and measurement of the mistargeting of the FP-based probes as an endpoint readout treatment was done in the incubator. Cells were incubated in cell culture medium containing: DMEM (see description below; in the chapter cell culture and transfection), 10% FCS, 100 U mL^{-1} penicillin, 100 µg mL^{-1} streptomycin and 2.5 µg mL^{-1} fungizone (Thermo Fisher Scientific). Afterwards 5 µM Antimycin-A1 and 10 µM Oligomycin-Awere were diluted in the described cell culture medium.

The buffer, which was used to trigger the protein biosynthesis during the long-term-imaging fluorescence experiments contained 5 µM suberanilohydroxamic acid (SAHA) diluted in storage buffer with 10% FCS.

3.2. Generation of the FP-based constructs

One part of the constructs were purchased from the synthesis company Gene Universal Inc. (Newark, USA). The other part was cloned.

Cloning of the FP-based probes:

Standard cloning protocols, which are provided by the manufacturer were applied to perform the cloning. All cloned constructs, after having the final plasmid were verified by sequencing (Microsynth, Vienna, Austria). The Primers used for cloning were obtained from ThermoFisher Scientific (Vienna, Austria). Herculase II fusion DNA polymerase (Agilent, Santa Clara, CA, USA) was used to perform the PCR reactions. For the generation of 2mt-sfGFP an established mitochondrial targeting sequence (MTS) of the COXVIII subunit was applied (136). The MTS was utilized as a tandem dimeric repeat and fused N-terminally to the super-folder green fluorescent protein (sfGFP). SfGFP-N1 was obtained from Addgene (plasmid number 54737) and was used for the isolation and PCR-amplification of sfGFP. The MTS was N-terminally fused to the sfGFP as an insert between the restriction sites NheI and EcoRI in an mammalian expression vector pdDNA3.1(-) (Invitrogen, Austria) to obtain the mitochondrially targeted sfGFP, namely the 2mt-sfGFP.

For the generation of mtDsRed, following cloning procedure was performed: Firstly DsRed was ordered from Addgene (plasmid number 11151). Afterwards isolation of the DsRed was performed via PCR-amplification. To get mtDsRed, the tandem dimeric repeat of the MTS of the COXVIII subunits (136) was N-terminally fused to the DsRed.

Transformation of the ligated constructs was done by using Top 10 chemically competent *E. coli* cells and heat shot at 42°C for 60 seconds. The cells were plated on LB-Agar plates, which where supplemented with ampicillin and individual selection of clones were done for the inoculation of 5 ml of ampicillin containing LB liquid medium. The mixture of cells and LB medium was incubated over night at 37 °C in a shaker. To isolate the plasmid DNA, on the next day STET mini preparation was performed and the verification of the insert according to their size was confirmed by PCR with the following sequencing primers: pcDNA3.1 (-) for 5'-CACTGCTTACTGGCTTATCG-3' and pcDNA3.1 (-) rev 5'-CAACAGATGGCTGGCAACTA-3'. The positively verified clones were exploited for the inoculation of 200 ml LB-liquid medium, which was supplemented with ampicillin and the mixture was incubated for around 16 hours at

37 °C in a shaker under permanent conditions of 200 rpm. PureVield™ Plasmid Maxiprep System (Promega, Germany) with nuclease-free water was used to purify the plasmids.

FP-based probes purchased from the company:

The designed constructs (inserts) were inserted in the mammalian expression vector pcDNA3.1 (-). Following constructs were purchased from Gene Universal Inc.:

Table 1: Plasmids purchased from Gene Universal Inc.

Construct Name	**Description**
seCFP-omp25	seCFP-omp25
Sirt4-sfGFP	Sirt4-sfGFP
Sirtuin4-sfCherry2_{11}	Sirtuin4-sfCherry2_{11}
MTS-sfCherry$_{1\text{-}10}$	MTS-sfCherry$_{1\text{-}10}$
Sirt4-sfCherry$_{11}$	Sirt4-sfCherry$_{11}$
mito-STAR	MTS-sfCherry$2_{1–10}$-SC-Sirt4-sfCherry2_{11}-SC-sfCherry$2_{1–10}$-NLS
PRIMA 1.0	2MT-B1-NLS-SC-GA-NLS
n4mt-sfGFP	$MTS_{COXVIII}$-MTS_{GDH}-MTS_{PDH}-MTS_{OTC}-sfGFP

MTS refers to mitochondrial targeting sequence, utilizing N-terminally a tandem repeat of - of the COXVIII (136) ; SC indicates a self-cleavage peptide, namely the 2A self-cleaving peptide (137) with following sequence: MGSGATNFSLLKQAGDVEENPGP; NLS refers to the nuclear localizing sequence as a repetition of three times (138) as depicted here: DPKKKRKVDPKKKRKVDPKKKRKV.

For the n4mt-sfGFP we chose four mitochondrial proteins, of which we picked the N-terminal targeting sequences respectively and fused these domains next to each other followed by sfGFP: mitochondrial COXVIII subunit (136), mitochondrial glutamate dehydrogenase (GDH) (158) , mitochondrial pyruvate dehydrogenase (PDH) (159) and ornithine transcarbamylase (160).

FP-based probes purchased from addgene:

Table 2: *E. coli* glycerol stocks purchased from addgene

Construct Name	Description
GA-NLS	MonomerA of ddFP fused to NLS (Plasmid-code of addgene: #50852)
B-NLS	MonomerB of ddFP fused to NLS (Plasmid-code of addgene: #50836)

3.3. Cell culture and cells

Following cell lines were used in this work: HeLa S3, mouse embryonic fibroblasts (MEFs) and H9C2 and INS-1 832/13 (INS-1). HeLa S3 cells were obtained from ATCC; MEFs were a gift from Thomas Simmen, Department of Cell Biology, University of Alberta, Canada. H9C2 were a gift from Heiko Bugger, Devision of Cardiology, Medical University of Graz. Supply of INS1-cells was done by C.B. Newgard, Department of Pharmacology and Cancer Biology, Duke University School of Medicine, USA.

Hela, MEFs and H9C2 were grown in Dulbecco´s modified eagle´s medium (DMEM) containing 10% FCS, 100 U/ml penicillin, 100 µg/ml streptomycin, 2.5 µg/ml amphotericin B and 2 mM glutamine, further on termed as full DMEM.

INS-1 were cultivated in GIBCO RPMI Medium 1640, which was ordered at Thermo Fisher Scientific and was additionally supplemented with 10% FCS, 10 mM HEPES, 1 mM sodium pyruvate, 0.05 mM 2- mercaptoethanl, 100 U mL−1 penicillin, 100 µg mL−1 streptomycin and 2.5 µg mL−1 fungizone (Thermo Fisher Scientific).

The material needed for the cell culture was obtained from Life Technologies (Vienna, Austria) and Carl Roth (Karlsruhe, Germany). All cells were maintained in a humidified incubator and cultivated and grown at 37°C with 5% CO_2 and 95% air conditions in the incubator.

3.4. Transfection

Cells were seeded in 30 mm glass imaging dishes in 6-well plates, IBIDI glass bottom dishes, 35mm (Ibidi, Munich, Germany) or in 4-chamber glass bottom dishes (Greiner Bio One International GmbH, Austria, Kremsmünster).

Transfection was done at a confluency of 60% using transfection reagent PolyJet (SigmaGen Laboratories, Rockville, MD, USA) and 1µg DNA, unless otherwise specified. DMEM, free of antibiotic and serum was used to transfect the cells with the respective plasmids.

Cells were transfected, when performed as an endpoint measurement 24 hours prior to measurement, meaning that the cells were incubated with Polyjet for 8 hours and after removal they were maintained in full DMEM. For online long-term imaging cells were transfected with PolyJet and 1µg DNA (unless otherwise specified). After 8 hours of incubation with PolyJet, the cells were maintained on storage buffer containing 10% FCS and the respective treatment.

3.5. Mitochondrial Staining

To perform colocalization analysis, firstly the cells were washed with storage-buffer containing, in mM, 2 $CaCl_2$, 135 NaCl, 5 KCl, 1 $MgCl_2$, 1 HEPES, 2.6 $NaHCO_3$, 0.44 KH_2PO_4, 0.34 Na_2HPO_4, 10 d-glucose (Roth), 0.1% vitamins, 0.2% essential amino acids, and 1% penicillin/streptomycin (Gibco). The pH of the storage buffer was adjusted at 7.4. Afterwards the cells were incubated in a solution of loading buffer, which was prepared containing either 0.2 µM MitoTracker™ Green FM or 0.2 µM MitoTracker™ Red FM for 20 min.

Cells were then washed three times with loading buffer and imaged in the same. Excitation of the MitoTracker™ Red FM was done at 561 nm, the emission was captures at 644 nm. Applying a wavelength of 488 nm excited the MitoTracker™ Green FM and the emission was captures at 516 nm.

Loading of the Tetramethylrhodamine methyl ester (TMRM; catalog number T668, Invitrogen) was done likewise for 40 minutes with a concentration of the TMRM of 50 nM. Excitation of the TMRM was done at 550 nm and emission was caught at 600 nm. During the measurements the TMRM remained on the cells.

3.6. Submitochondrial Localization of Sirt4-sfGFP and 2mt-sfGFP

To determine the submitochondrial localization of Sirt4-sfGFP and 2mt-sfGFP following constructs as plasmids were used to transfect HeLa cells: Sirt4-sfGFP, 2mt-sfGFP, seCFP-OMP25, MTS-sfCherry2_{1-10}, Sirt4-sfCherry2_{11}, mito-STAR, or mCherry-TOM22. Additionally the cells were stained with MitoTracker™ Green FM or MitoTracker™ Red FM, respectively. Fluorescence imaging experiments were performed on a super structural illumination microscopy (SIM) or array confocal laser scanning microscope (ACLSM). ImageJ plugin 'coloc2' was applied for the co-localization studies and analysis to measure the Pearson correlation coefficient.

3.7. Structural design and construction of the FP-based probes

For the construction of the mitochondrial protein import sensors various FP-technologies were applied, such as the self-complementation split FP-technology (139), single-FP technology (140) and the dimerization dependent FP-technology (141).

For modelling of the probes the online tool Phyre2 (Protein Homolgy/analygy Recognition Engine V2.0) was used. The modelling consists of 3D structure prediction of the respective constructs. The structure predictions are performed by using profile-profile alignment algorithm of the desired protein by entering the sequence of the protein of interest into the online tool. Markov models via HHsearch were utilized to perform the alignment, which improves the accuracy of the alignment and of the detection rate.

DeepView/Swiss Pdb viewer V4.1.0 (Swiss Institute for Bioinformatics – SIB, Lausanne, Switzerland), obtained from Expasy was applied for the the calculcation, modification and analysis of the 3D-models of the predicted proteins and probes. By using evolutionarily related structures sensitive sequences of a library of experimentally determined protein structures can be found. This is how the software identifies proteins, meaning that proteins, which are related to the target protein are generated in a 3D-structure manner of the protein of interest (142).

3.8. Fluorescence Imaging

3.8.1. Confocal Imaging

The cells were imaged with an array confocal laser scanning microscope (ACLSM), which is . The microscope is based on a Zeiss Observer Z.1 inverted microscope, which is equipped with a Yokogawa CSU-X1 Nipkow spinning disk system, a piezoelectric z-axis motorized stage (CRWG3-200; Nippon Thompson Co., Ltd., Tokyo, Japan), and a CoolSNAP HQ2 CCD Camera (Photometrics Tucson, Arizona, USA). The setup is equipped with oil-immersion objectives (Zeiss). An objective of 100x or 40x was used to image the cells.

Table 2: Excitation and emission parameter of the various FP-based sensors

Construct	**Excitation [nm]**	**Emission [nm]**
2mt-sfGFP	488	516
seCFP-omp25	445	477
mtDsRed	561	644
mCherry-TOM22	561	644
Sirt4-sfGFP	488	516
Sirtuin4-sfCherry2$_{11}$	561	644
MTS-sfCherry$_{1-10}$	561	644
Sirt4-sfCherry$_{11}$	561	644
mito-STAR	561	644
PRIMA 1.0	488	516
PRIMA 2.0	488	516
PRIMA-RFP	488/561	516/644
MiNts	488	516
mito-TIMER	488/561	516/644

The software which was used for data acquisition and control is VisiView Premier Acquisition software (2.0.8, Visitron Systems, Puchheim, Germany).

3.8.2. Structural illumination microscopy (SIM)

The excitation laser of the SIM set up consists of following wavelengths: 405-, 488-, 515-, 532- and a 561-nm. A CFI SR Apochromat TIRF × 100-oil (NA 1.49) objective was arranged on a Nikon Structured Illumination Microscopy (N-SIM) System in combination a with standard filter sets of wide-field microscopy and SIM. In addition to that, two Andor iXon3 EMCCD cameras, which were placed to a two-camera imaging adapter (Nikon Austria, Vienna, Cells 2019, 8, 1583 5 of 19 Austria), where part of the Apochromat. This was done in order to achieve super-resolution.

Both, ImageJ (National Institutes of Health (NIH), Bethesda, MA, USA) and Metamorph (Molecular Devices) were applied for the calibration and reconstruction of the SIM images. Prior to each measurement, the laser beam was projected through the objective at the top cover of the bright field arm of the microscope, to ensure laser adjustment. For this process NIS-Elements Advanced Research (AR) (4.51, Nikon Corporation, Tokio, Japan) was installed and ran automatically.

3.9. Mitochondrial morphology assessment

Following parameters were assessed and evaluated to determine the mitochondrial morphology: mitochondrial area (a), perimeter (p), minor (x), and major (y) axes of the mitochondria. ImageJ particle analyzer was applied to obtain the results.

The calculation of the aspect ratio was done as depicted here: $= \frac{\mathrm{x}}{\mathrm{y}}$.

To evaluate the form factor (FF), following formula was applied: $= \frac{p^2}{4\pi \mathrm{a}}$.

The freeware program ImageJ was used to perform the image analysis.

3.10. Data analysis and statistical analysis

Following programs were applied to analyze the obtained data: GraphPad Prism 5 Software (GraphPad Software, Inc., La Jolla, CA, USA) and Excel (2013, 15.0, Microsoft). To perform the image analysis MetaMorph (Molecular Devices) and the freeware program ImageJ (NIH, MA, USA) were used.

To calculate the ratio values of the nuclear fluorescence to the cytosolic fluorescence or the mitochondrial fluorescence, respectively, first, the ACLSM images were background subtracted on MetaMorph using a background region of interest (ROI).

Each further steps, which was required for the analysis of the images were done with MetaMorph. Region measurement by drawing region randomly in the cytosol or by bordering the complete nucleus enabled the determination of the cytosolic and the nuclear fluorescence. In the case that bordering of the complete nucleus was not possible, for instance, because of mitochondrial structures, a region measurement was done by randomly picking a position in the nucleus. An auto threshold for light objects in MetaMorph was used to set a mask and by doing so the mitochondrial fluorescence could be determined. The threshold was set manually to encompass mitochondrial structures. Afterwards, the average mitochondrial fluorescence within the mask was evaluated.

To do the statistical analysis and evaluation GraphPad Prism 5 was applied, by using statistical tests such as unpaired double-sided Student's t-test or a one-way ANOVA with a Bonferroni post-hoc test. The number of independent experiments is indicated in the figure legends. The total number of measured cells is also indicated in the figure legends. Data are either shown ±SEM or ±SD as indicated in the figure legends.

4. Results

Some sections of the results described in this work are part of my first-author publication and are hence discussed in a similar manner as in (1).

4.1. 2mt-sfGFP, a fast maturing GFP-variant fused to a mitochondrial targeting sequence locates to the mitochondrial matrix

Amongst a palette of various fluorescent proteins (FPs), we decided to fuse the super-folder GPF (sfGFP) to the mitochondrial targeting sequence (MTS) of interest in order to detect the localisation of the probe, hence determine the efficiency of the mitochondrial targeting efficiency **(Figure 1A)**. The sfGFP has a maturation time of a few minutes (143) (144), meaning that upon biosynthesis it becomes fluorescent within minutes. This feature of the sfGFP represents the ideal candidate, since imaging cells, which synthesize the respective constructs makes an acute visualization of the probe under various conditions possible.

Regarding the MTS we decided to pick the established MTS of the COXVIII subunit (136) for the probe and generated thereby 2mt-sfGFP **(Figure 1A)**. This specific MTS is known to target FPs efficiently into the respective organelle (136).

Sometimes more than one repeat of the signal sequence is required for an efficient targeting to mitochondria, depending on the rest of the length of the translated protein or probe (136) (145). As indicated, 2mt-sfGFP harbors a 71 amino acid (aa) dimeric tandem repeat of the MTS of COXVIII **(Figure 1A)**.

Before we determined the efficiency of the mitochondrial targeting in HeLa cells under physiological conditions, we wanted to check with super-resolution microscopy whether the MTS of the COXVIII targets the sfGFP to the mitochondrial matrix, as it is supposed to do. Therefore we applied structural illumination microscopy (SIM) and co-expressed 2mt-sfGFP with mCherry-TOM22, a marker for the outer mitochondrial membrane and mtDSred, respectively. No co-localization was detectable by co-expression 2mt-sfGFP with mCherry-TOM22 **(Figure 1B and D)** (1). In contrast to that we could confirm the matrix localization of 2mt-sfGFP by a high co-localization with mtDsRed **(Figure 1C and D)** (1).

Figure 1

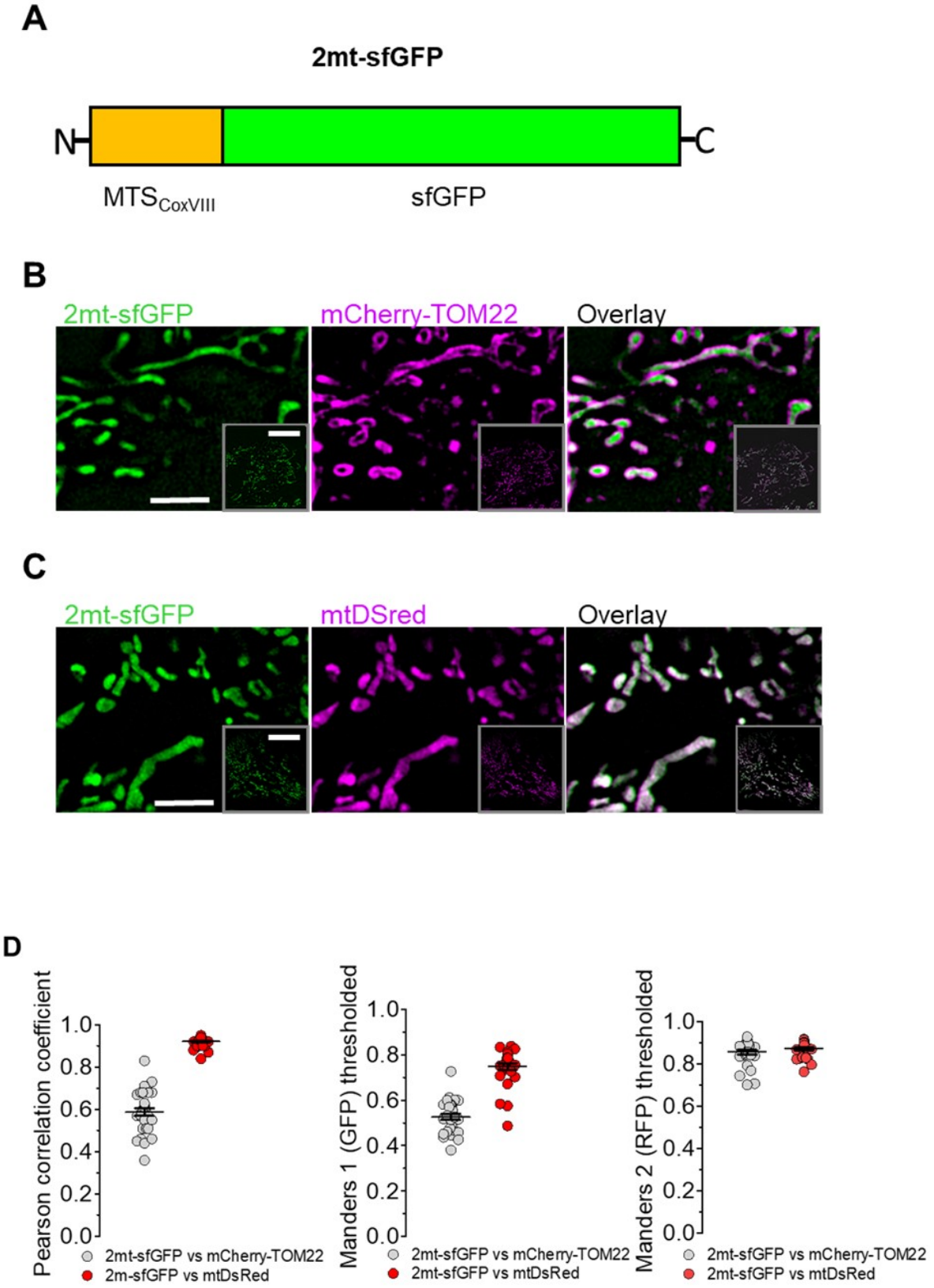
A
2mt-sfGFP
N
C
MTS$_{CoxVIII}$
sfGFP
B
2mt-sfGFP
mCherry-TOM22
Overlay
C
2mt-sfGFP
mtDSred
Overlay
D
Pearson correlation coefficient
1.0
0.8
0.6
0.4
0.2
0.0
2mt-sfGFP vs mCherry-TOM22
2m-sfGFP vs mtDsRed
Manders 1 (GFP) thresholded
1.0
0.8
0.6
0.4
0.2
0.0
2mt-sfGFP vs mCherry-TOM22
2mt-sfGFP vs mtDsRed
Manders 2 (RFP) thresholded
1.0
0.8
0.6
0.4
0.2
0.0
2mt-sfGFP vs mCherry-TOM22
2mt-sfGFP vs mtDsRed

Figure 1. **Co-localization analysis of 2mt-sfGFP. (A)** Dimeric tandem repeat of the mitochondrial targeting sequence of the CoxVIII subunit, referred to as $MTS_{CoxVIII}$ (orange) fused on N-terminus of the sfGFP (green). **(B)** Representative SIM-images of HeLa cells co-expressing 2mt-sfGFP (green) and mCherry-TOM22 (magenta). Merged channels are shown in the third illustration. Scale bar, 2.5 µm. Squares in the lower right show the whole cell. Scale bar represents 10 µm. **(C)** SIM-images shown as representative images of HeLa cells co-expressing 2mts-sfGFP (green) and mtDsRed (magenta). Illustration of merged channels. Scale bar, 2.5 µm. Squares in the lower right show the whole cell. Scale bar represents 10 µm. Shown experiments in **(B)** and **(C)** are representative of 3 independent experiments, including 30 different cells **(D)** Statistical analysis of the co-localization of 2mt-sfGFP and mCherry-TOM22 and mtDsRed, respectively. Evaluation of the *Pearson* correlation coefficient, comparing 2mt-sfGFP with mCherry-TOM22 and mtDsRed, respectively (left panel). Evaluation of the thresholded *Manders 1* coefficient (GFP), comparing 2mt-sfGFP with mCherry-TOM22 and mtDsRed, respectively (middle panel). Evaluation of the thresholded *Manders 2* coefficient (RFP), comparing 2mt-sfGFP with mCherry-TOM22 and mtDsRed, respectively (middle panel).). [Figure panels reproduced from Ramadani-Muja et al., Cells 2019.]

4.2. 2mt-sfGFP is suitable for the qualitative and quantitative determination of mitochondrial targeting efficiency

To demonstrate the suitability of the 2mt-sfGFP for the assessment of mitochondrial targeting efficiencies we manipulated the mitochondrial protein import machinery by provoking mitochondrial protein import disturbances. Expression of 2mt-sfGFP in untreated HeLa cells showed a nice mitochondrial staining, indicating the efficient import of 2mt-sfGFP into the mitochondrial matrix **(Figure 2A)**.

Treatment of HeLa cells expressing 2mt-sfGFP with oligomycin-A and and antimycin-A1, a combination of well-known mitochondrial toxins, which completely depolarize the mitochondrial membrane potential (146) and hence should impair the import of 2mt-sfGFP into the matrix, depicted a brighter fluorescence arising from mitochondria **(Figure 2B)**. In addition to that we detect a fluorescence signal coming from the cytosol **(Figure 2B)**. These observations indicate that the probe was firstly imported into mitochondria and after import inhibition the probe could not be imported anymore and hence it accumulated in the cytosol.

Incubation of HeLa cells with oligomycin-A and antimycin-A1 and the simultaneous transfection with 2mt-sfGFP led us to the observation of typical dark mitochondrial tubular structures

surrounded by green fluorescence, which is here shown as a monochromatic illustration **(Figure 2C)**. This result showed that the probe directly accumulates in the cytosol and was never imported into mitochondria **(Figure 2C)**, indicating the mitochondrial protein import inhibition before the probe was synthesized and could be transported to mitochondria.

These observations show, that 2mt-sfGFP is suitable for the qualitative assessment of mitochondrial targeting efficiencies by capturing not only the fluorescence signal coming from mitochondria, but also by taking the mistargeting also into consideration.

However, rarely someone has exploited the mistargeting of mitochondrially targeted proteins to assess mitochondrial targeting efficiencies in a quantitative, statistical and systematic manner. This was the motivation for us to overcome these restrictions and come up with a quantification approach of mitochondrially targeted proteins.

Firstly we decided to blot the fluorescence intensity values of 2mt-sfGFP from the cytosol on the x-axis of a diagram against the fluorescence intensity values coming from mitochondria on the y-axis **(Figure 2D)**. By doing so we can analyze the distribution of the fluorescence of the 2mt-sfGFP signal of each individual cell. Additionally we calculated the fluorescence intensity ratio of the cytosol and mitochondria and plotted the values ranking from 0 to 1 against the fluorescence intensity values of mitochondria **(Figure 2E)**. This enabled us to provide a quantitative description of the targeting efficiencies of 2mt-sfGFP.

We also generated a category or grading system ranking from targeting to weak and moderate mistargeting, over strong mistargeting to even total mistargeting **(Figure 2E)**. Cells falling in the ratio 0.0 – 0.2 belong to the category targeting **(Figure 2E)**. Weak Mistargeting covers the cells from 0.2 – 0.4 **(Figure 2E)**. Cells, which are located between 0.4 – 0.6 are part of the category moderate mistargeting **(Figure 2E)**. If strong mistargeting is the case the cells fall in the ratio 0.6 – 0.8 **(Figure 2E)**. Cells with ratio values between 0.8 – 1.0 belong to the category total mistargeting **(Figure 2E)**. In addition to that we depicted a representative image of each of each of the dots on the ratio-diagram **(Figure 2F)**.

Figure 2

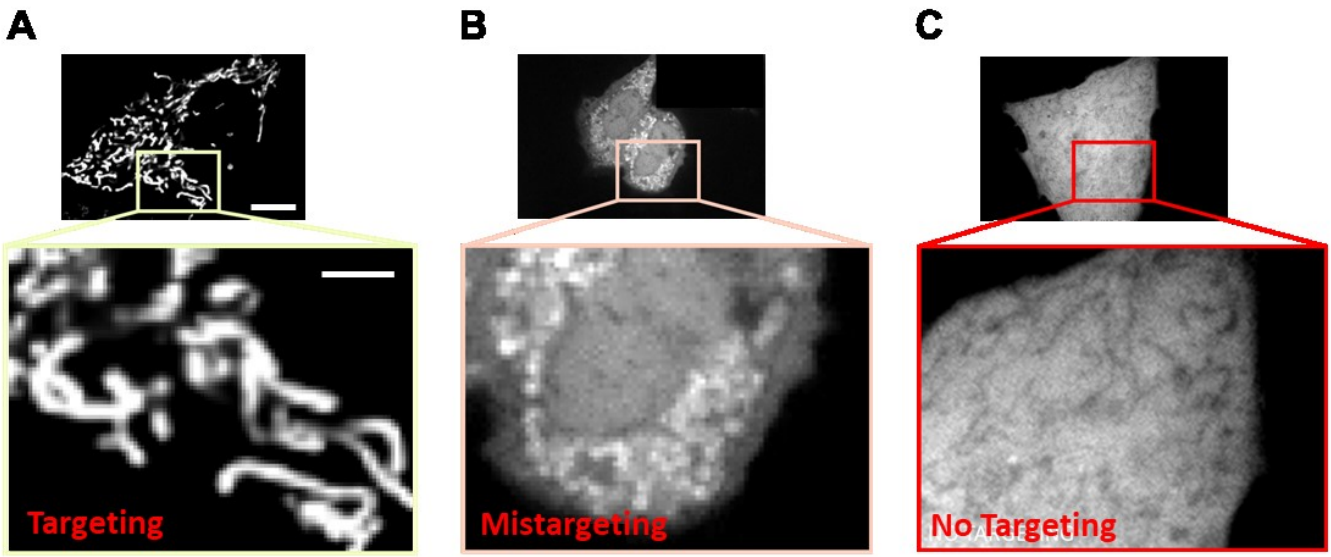
A
B
C
Targeting
Mistargeting
No Targeting

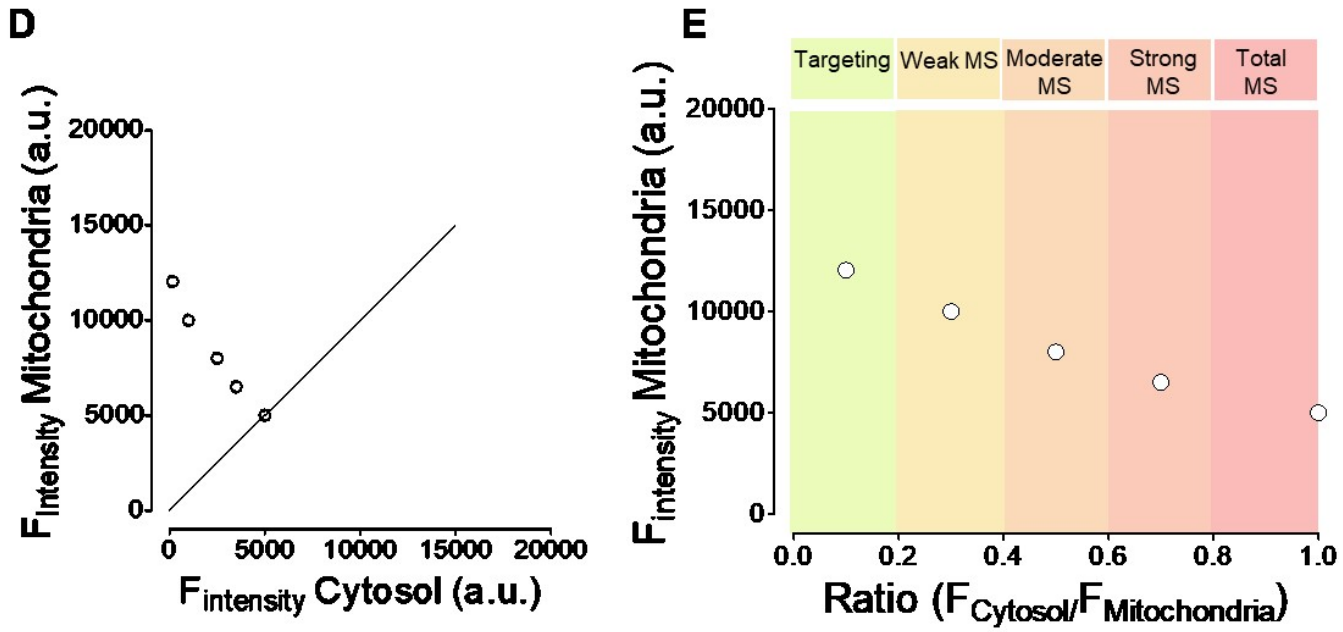
D
F intensity Mitochondria (a.u.)
20000
15000
10000
5000
0
0
5000
10000
15000
20000
F intensity Cytosol (a.u.)
E
Targeting
Weak MS
Moderate MS
Strong MS
Total MS
F intensity Mitochondria (a.u.)
20000
15000
10000
5000
0
0.0
0.2
0.4
0.6
0.8
1.0
Ratio (F Cytosol/F Mitochondria)

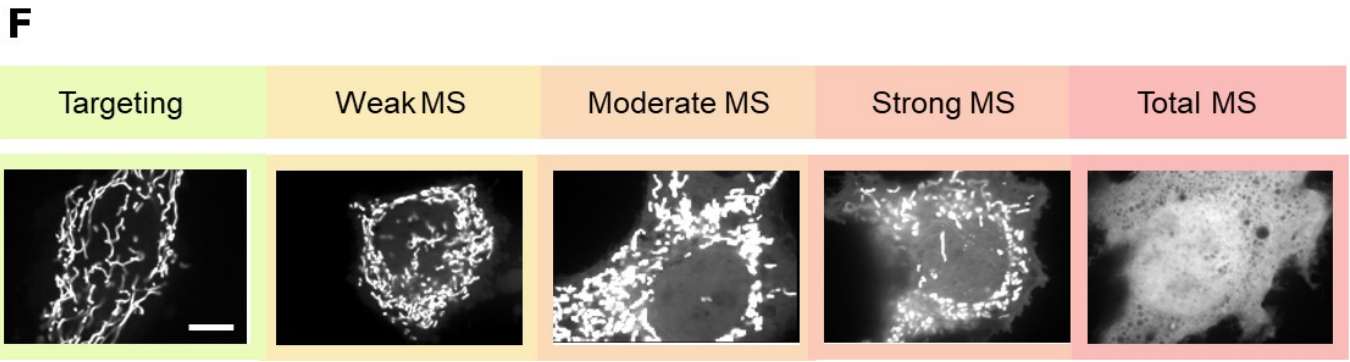
F
Targeting
Weak MS
Moderate MS
Strong MS
Total MS

Figure 2. **Establishment of an approach to quantify the targeting efficiency to mitochondria using 2mt-sfGFP. (A)** Representative confocal image of HeLa cells expressing 2mt-sfGFP (in monochromatic). Illustration of tubular mitochondrial structures. Scale bar indicates 10 µm. Magnification of a representative cut-out showing individual mitochondria harboring 2mt-sfGFP (in monochromatic). Scale bar corresponds to 3µm. **(B)** Representative confocal image of HeLa cells expressing 2mt-sfGFP, showing mistargeting of the respective probe (in monochromatic). Scale bar indicates 10 µm. Magnification of a representative cut-out showing individual mitochondria and the cytosol carrying 2mt-sfGFP (in monochromatic). Scale bar indicates 3µm. **(C)** Representative confocal image of HeLa cells expressing 2mt-sfGFP (in monochromatic). Illustration of negatively stained mitochondria, surrounded by a fluorescence signal (in monochromatic). Magnification of a representative cut-out showing dark tubular mitochondrial structures, surrounded by a fluorescence signal (in monochromatic). Scale bar corresponds to 3µm. **(D)** HeLa cells expressing 2mt-sfGFP, illustrated as fluorescence intensity values, and plotted as cytosolic fluorescence intensities against the mitochondrial fluorescence intensities. **(E)** Diagram of HeLa cells expressing 2mt-sfGFP, illustrated as ratio of cytosolic fluorescence to mitochondrial fluorescence and plotted against the mitochondrial fluorescence intensity in a cell. MS indicates Mistargeting and will be further on denoted in Figures as MS **(F)** Image series of representative images of each of the dots shown in **(D)** and **(E)**. Scale bar indicates 10 µm.

4.3. Cancer cells import high amounts of 2mt-sfGFP into mitochondria very efficiently

Next, we wanted to address following question: What is the capacity of cancer cell mitochondria to import mitochondrially targeted proteins? To answer that question we applied the approach of determining the targeting efficiency of mitochondria by using 2mt-sfGFP as described above **(Figure 2)**.

First, we established a protocol **(Figure 3A)**, in which we used HeLa cells to visualize and determine the mitochondrial protein import capacity as an endpoint readout. The procedure starts with transfection of the cells with the 2mt-sfGFP, meaning that most likely two to three hours after transfection the probe is imported into mitochondria **(Figure 3A)**. The cells are imaged on a confocal microscope 24 hours after transfection **(Figure 3A)**, thereby capturing the mitochondrial targeting efficiency of HeLa cells on the single cell level.

All HeLa cells expressing 2mt-sfGFP showed a nice fluorescence signal coming from mitochondria under control conditions **(Figure 3B)**. Cytosolic fluorescence signal was not detectable in any of the HeLa cells. The expression level of the mitochondrial fluorescence signal was spread over a wide range **(Figure 3B)**. Quantification of the fluorescence signal of HeLa cells expressing 2mt-sfGFP unveiled that no cell showed a fluorescence signal arising from the cytosol, even when very high fluorescence signals i.e. high expression levels of the construct were obtained **(Figure 3C, D)**. In contrast to that, plotting the fluorescence intensity values of mitochondria and the cytosol and evaluating the cytosolic to mitochondria ratio of the fluorescence values revealed that all cells fell under the category targeting **(Figure 3C and D)**. In line with the images, quantification of 2mt-sfGFP showed that the expression level of the probe ranges from very low culminating in even saturation of the confocal set-up.

Taken these observations together, we concluded that HeLa cells constantly and very efficiently import very high amounts of 2mt-sfGFP into mitochondria, indicating a very high capacity of the mitochondrial protein import machinery in this cell type under these conditions.

Figure 3

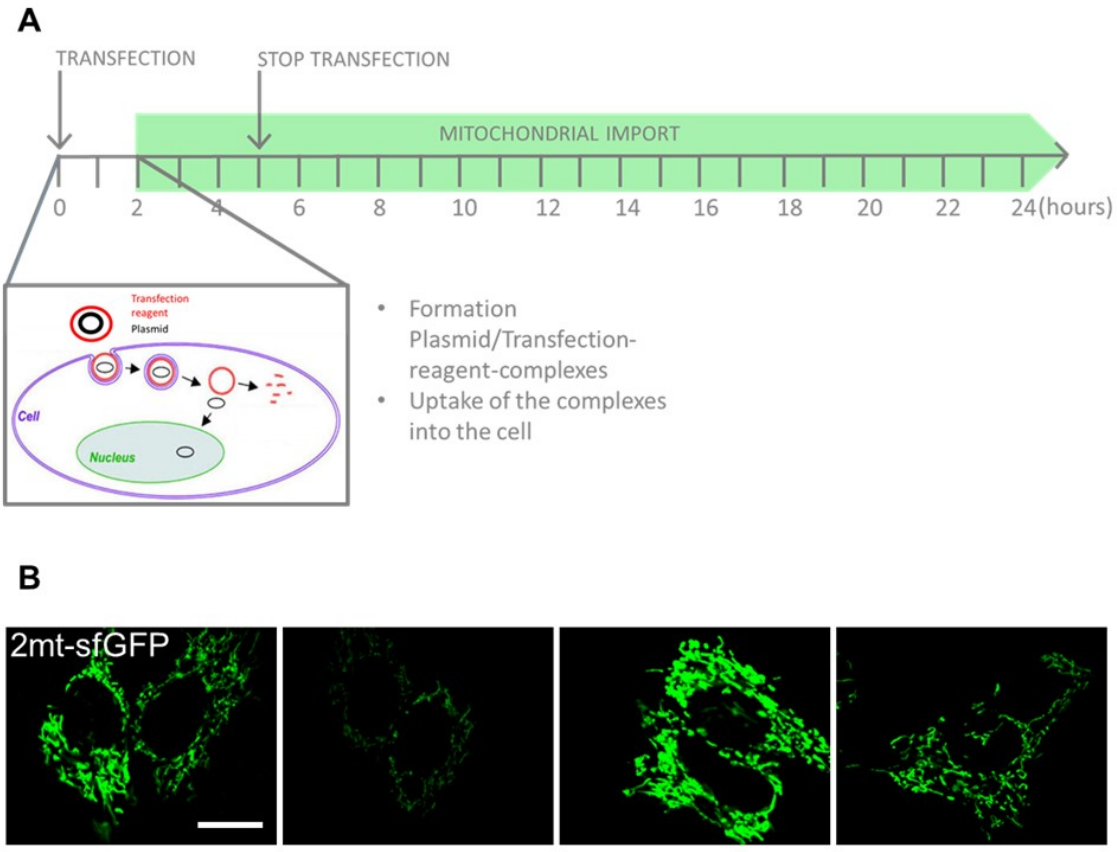

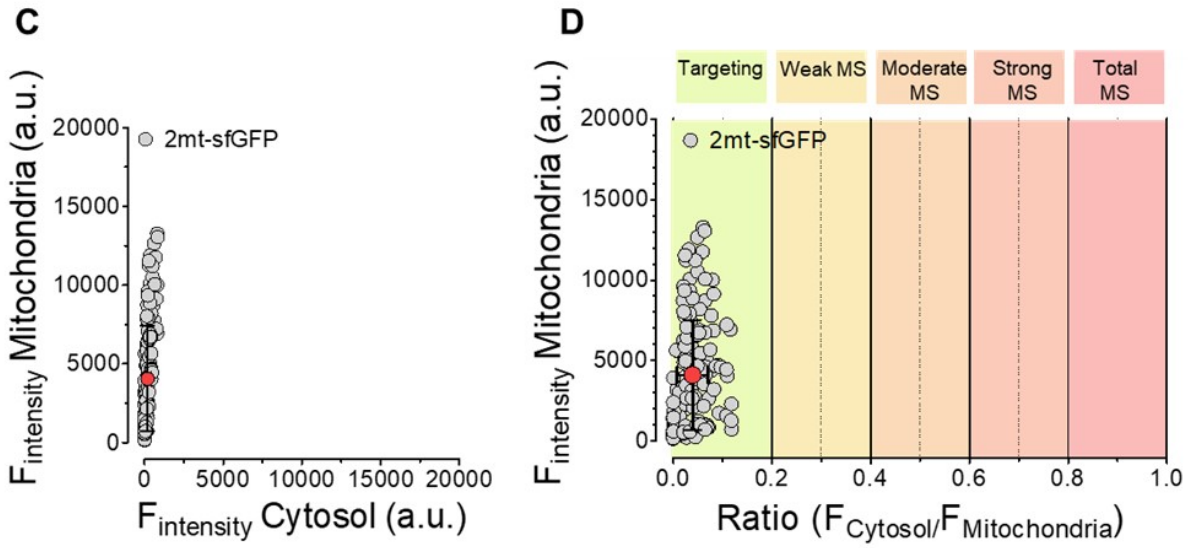

Figure 3. **Evaluation of the mitochondrial protein import capacity of HeLa cells under control conditions using 2mt-sfGFP. (A)** Procedure of the experimental set-up illustrated as a timeline **(B)** Representative confocal images of HeLa cells expressing 2mt-sfGFP (green). All images are shown with the same contrast settings. Scale bar indicates 10 µm. **(C)** Illustration of HeLa cells expressing 2mt-sfGFP under control conditions. Fluorescence intensity values of the cytosol are plotted on the x-axis against the fluorescence intensity values of mitochondria on the y-axis. Six independent experiments were performed for the control condition. Dots are depicted as ratio values ± SD; n = 146 cells. **(D)** HeLa cells expressing 2mt-sfGFP shown as the calculated ratio between the cytosolic fluorescence intensity values and the mitochondrial fluorescence intensity values, which are plotted against the mitochondrial fluorescence intensity values. Six independent experiments were performed for the control condition. Data are depicted as raw intensity values with the mean n ± SD; n = 146 cells. MS indicates Mistargeting.

4.4. Only a strong overload of the mitochondrial protein import machinery triggers an accumulation of 2mt-sfGFP in the cytosol

In the previous result section we demonstrated the high capacity of cancer cell mitochondria to import mitochondrially targeted proteins, when cells were transfected using a standard transfection procedure **(**see methods and **Figure 3)**. Next, we wanted to check whether it is possible to overload the mitochondrial protein import machinery by further overexpressing 2mt-sfGFP.

We decided to increase the DNA-concentration of the plasmid coding for 2mt-sfGFP in order to probably boost the amount of mitochondria targeted fluorescent proteins, which then have to be imported by the mitochondrial protein import machinery into the lumen of mitochondria. Indeed, those cells expressing 0.5 µg DNA and 1.0 µg DNA, of the 2mt-sfGFP respectively showed a nice mitochondrial fluorescence signal, indicating again the efficient targeting of the probe into mitochondria **(Figure 4A, B, E, F, I and J)**. We were not able to detect cells with any fluorescence signal arising from the cytosol under these conditions **(Figure 4A, B, E, F, I and J)**.

Yet, increasing the DNA concentration to 1.5 µg DNA, clearly showed that still around **85%** of the HeLa cells expressing 2mt-sfGFP have an exclusive mitochondrial fluorescence signal, indicating again the efficient import of the protein into mitochondria **(Figure 4C,G, I and J)**. However, the remaining **15%** of the HeLa cells expressing 2mt-sfGFP now showed a clear fluorescence signal, coming from the cytosol, in addition to that one coming from mitochondria when transfecting cells with higher amounts of DNA **(Figure 4C,G, I and J)**. In line with the observation, that mitochondria of HeLa cell have a high capacity to import mitochondrially targeted proteins, we observed a positive correlation between the expression level and mistargeting **(Figure 4G and I)**. This means, that those cells that displayed a clear mistargeting showed very high expression level of mitochondria targeted sfGFP **(Figure 4G and I)**.

We obtained similar results by incubating HeLa cells, expressing 2mt-sfGFP with up to 2.0 µg DNA. Increasing the DNA-concentration to 2.0 µg led to a population of cells, making up around **28/%**, which clearly showed a fluorescence signal arising from the cytosol, additionally to that one coming from mitochondria **(Figure 4D, H, I and J)**. The remaining **72%** of the cells, expressing 2mt-sfGFP with a DNA concentration of 2.0 µg depicted exclusive mitochondrial fluorescence **(Figure 4D, H, I and J).**

The observations of this result section again emphasize the high capacity of mitochondria in HeLa cells to import the mitochondrially targeted sfGFP. Additionally these results indicate, that increasing the amount of proteins, which have to be imported into mitochondria can overload the import machinery, hence triggering an accumulation of the 2mt-sfGFP in the cytosol **(Figure 4C, D, G, H, I and J)**.

Figure 4

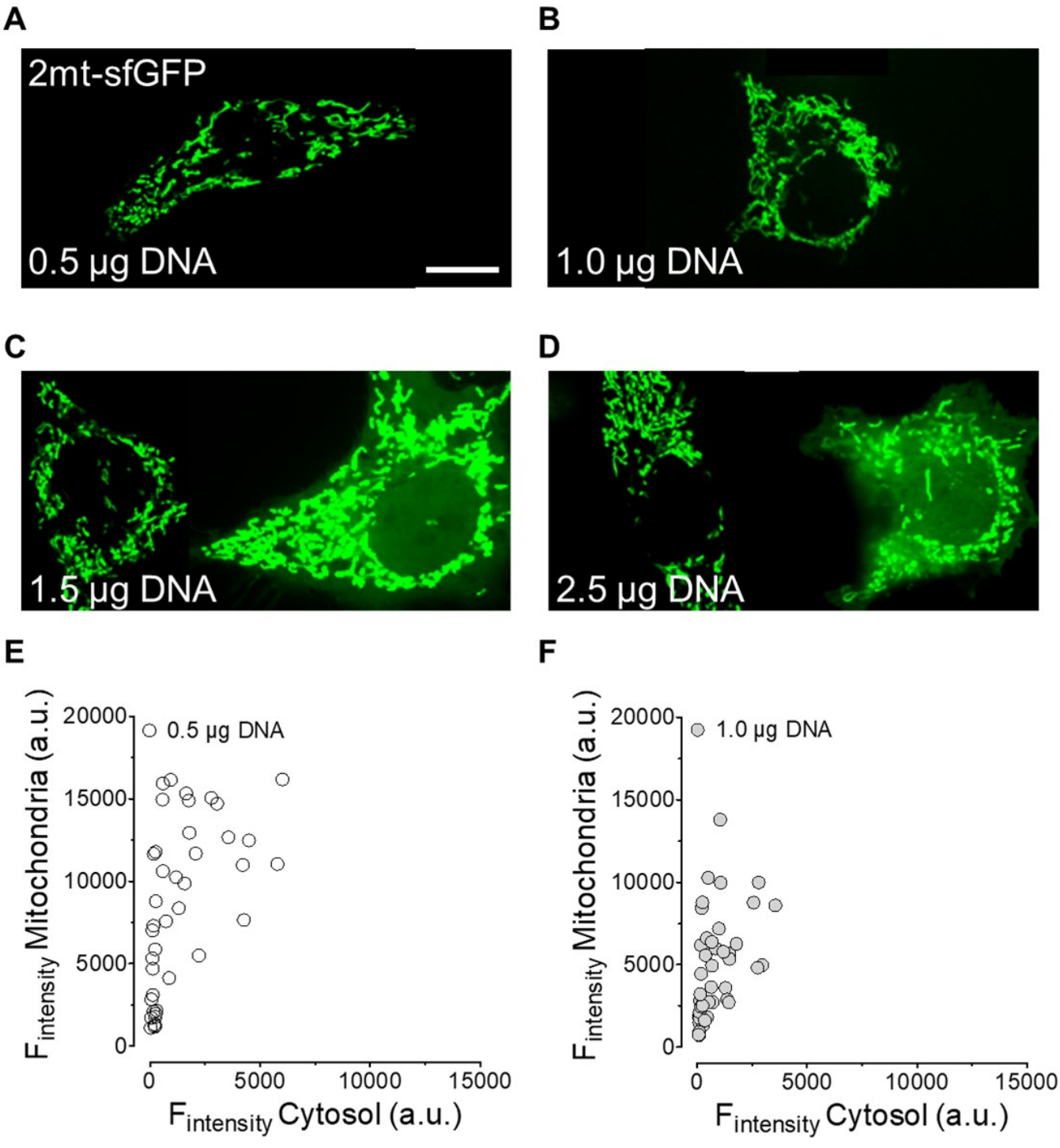
A
2mt-sfGFP
0.5 µg DNA
B
1.0 µg DNA
C
1.5 µg DNA
D
2.5 µg DNA
E
0.5 µg DNA
F
1.0 µg DNA
F intensity Mitochondria (a.u.)
F intensity Cytosol (a.u.)
0
5000
10000
15000
20000

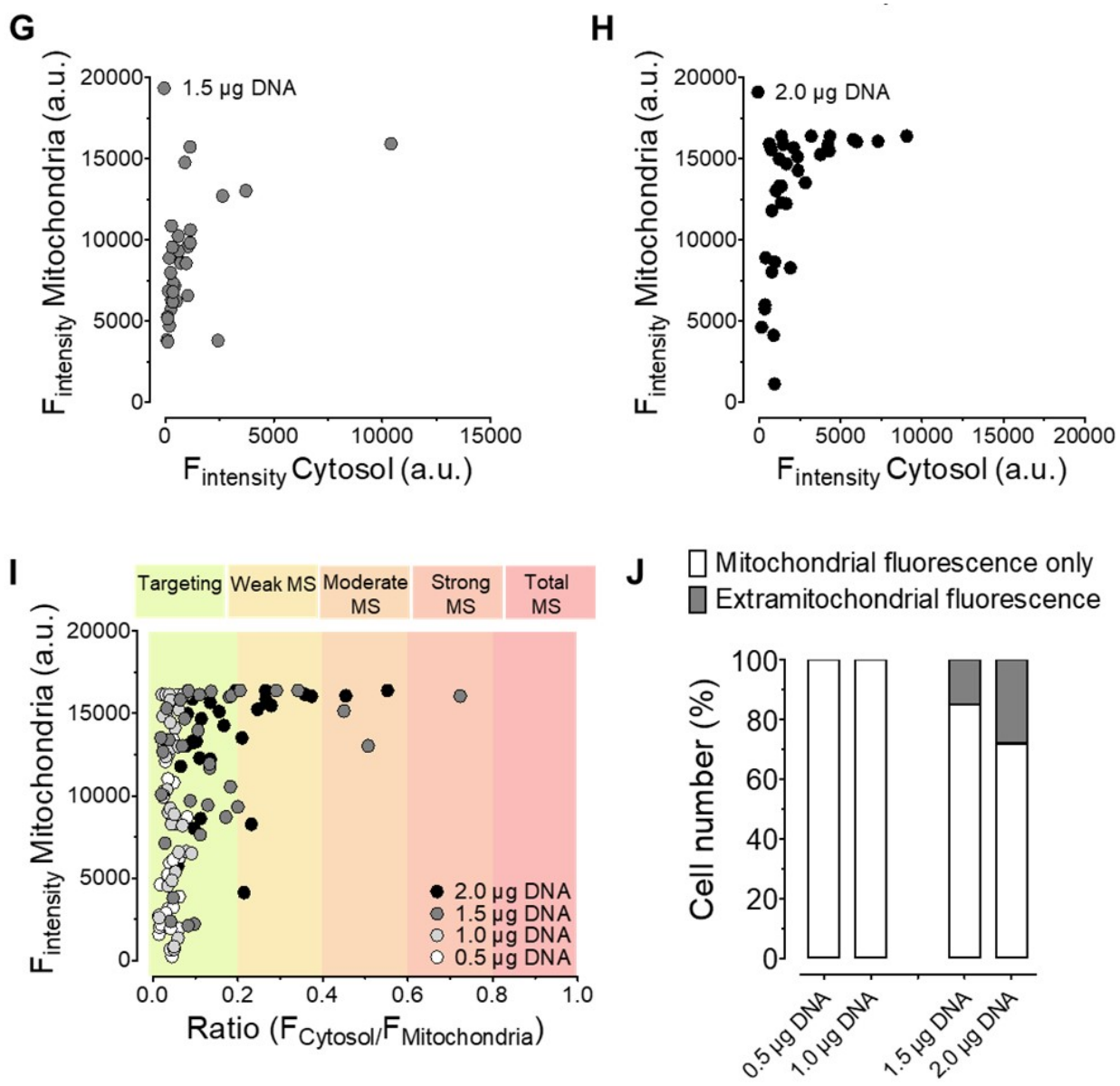

Figure 4. Visualization of the accumulation of 2mt-sfGFP in the cytosol, triggered by an overload of the mitochondrial protein import. (A) Representative confocal image of 2mt-sfGFP (green), expressed in HeLa cells in the amount of 0.5 µg DNA. Scale bar indicates 10 µm in the whole image section of Figure **(B)** Representative confocal recording of HeLa cells expressing 2mt-sfGFP (shown in green; 1.0 µg DNA) **(C)** Representative confocal images of HeLa cells, which expressed 2mt-sfGFP, being incubated with 1.5 µg DNA (illustrated in green, left image and right image). Left image shows typical mitochondrial structures. Right image shown mitochondrial structures and additionally a fluorescence signal coming from the cytosol. **(D)** HeLa cells expressing 2mt-sfGFP (2.0 µg DNA) shown in representative confocal images (depicted in green, left image and right image). Right image is a representative image of a cell with a fluorescence signal coming from mitochondria. Left image represents cells with a fluorescence signal arising from the cytosol.

(E) HeLa cells, expressing 2mt-sfGFP under conditions of 0.5 µg DNA shown as fluorescence intensity values of the cytosol, which are plotted on the x-axis against the fluorescence intensity values of mitochondria on the y-axis. Three independent experiments were performed. n = 41 cells. **(F)** Identical experiment as this in **(E)**, but the amount of DNA is 1.0 µg. Three independent experiments were done. n = 47 cells **(G)** Identical experiment as this in **(E)**, however HeLa cells are incubated with 1.5 µg DNA. Three independent experiments were performed. n = 31 cells (**H)** Identical experiment as this in **(E)**, but incubation of HeLa cells was done with 2.0 µg DNA. Three independent experiments were performed. n = 36 cells.

4.5. Depolarization of mitochondria leads to severe mistargeting, independently of the expression of 2mt-sfGFP

Many studies suppose, that the mitochondrial membrane potential is essential in the presequence import pathway of mitochondrially targeted protein into the inner membrane and the lumen of mitochondria (100) (147) (148). However, in many cases those statements are mostly assumptions and theoretical models and concepts.

We established again a protocol **(Figure 5A)**, where we decided to treat HeLa cells with a combination of well-known mitochondrial toxins, which completely depolarize the mitochondrial membrane potential, namely oligomycin-A and antimycin-A1 (146).

As expected, treatment of HeLa cells with oligomycin-A and antimycin-A1 expressing 2mt-sfGFP led to a severe mistargeting of the matrix targeted probe in the cytosol, compared to HeLa cells expressing 2mt-sfGFP under physiological conditions, which represents the control group **(Figure 5B, C, D and E)**. The grade of mistargeting occurred independently of the expression level, pointing to an impairment in the mitochondrial protein import machinery **(Figure 5D)** by the depolarization of the IMM. Cells in the control condition showed exclusive mitochondrial fluorescence, indicating the efficient import of the 2mt-sfGFP into mitochondria **(Figure 5B, D and E)**. In contrast, cells treated with oligomycin-A and antimycin-A1 displayed a strong fluorescence signal arising from the cytosol, in addition to the mitochondrial fluorescence signal **(Figure 5C, D and E)**. This indicates the mistargeting of the 2mt-sfGFP, which accumulates in the cytosol upon resynthesis, since the 2mt-sfGFP cannot be transported into mitochondria anymore due to complete depolarization of mitochondria upon cell treatment with oligo/antimycin.

Applying the category system emphasized and confirmed the observation that treatment of HeLa cells expressing 2mt-sfGFP leads to severe mistargeting of the probe, since all cells in

the control group fell under the category targeting and all cell treated with oligomycin-A and antimycin-A1 displayed a mistargeting ranking from weak up to total mistargeting **(Figure 5D)**. This indicates that every cell, which was treated with the mixture of the mitochondrial toxins was not able to import the 2mt-sfGFP into mitochondria anymore.

Figure 5

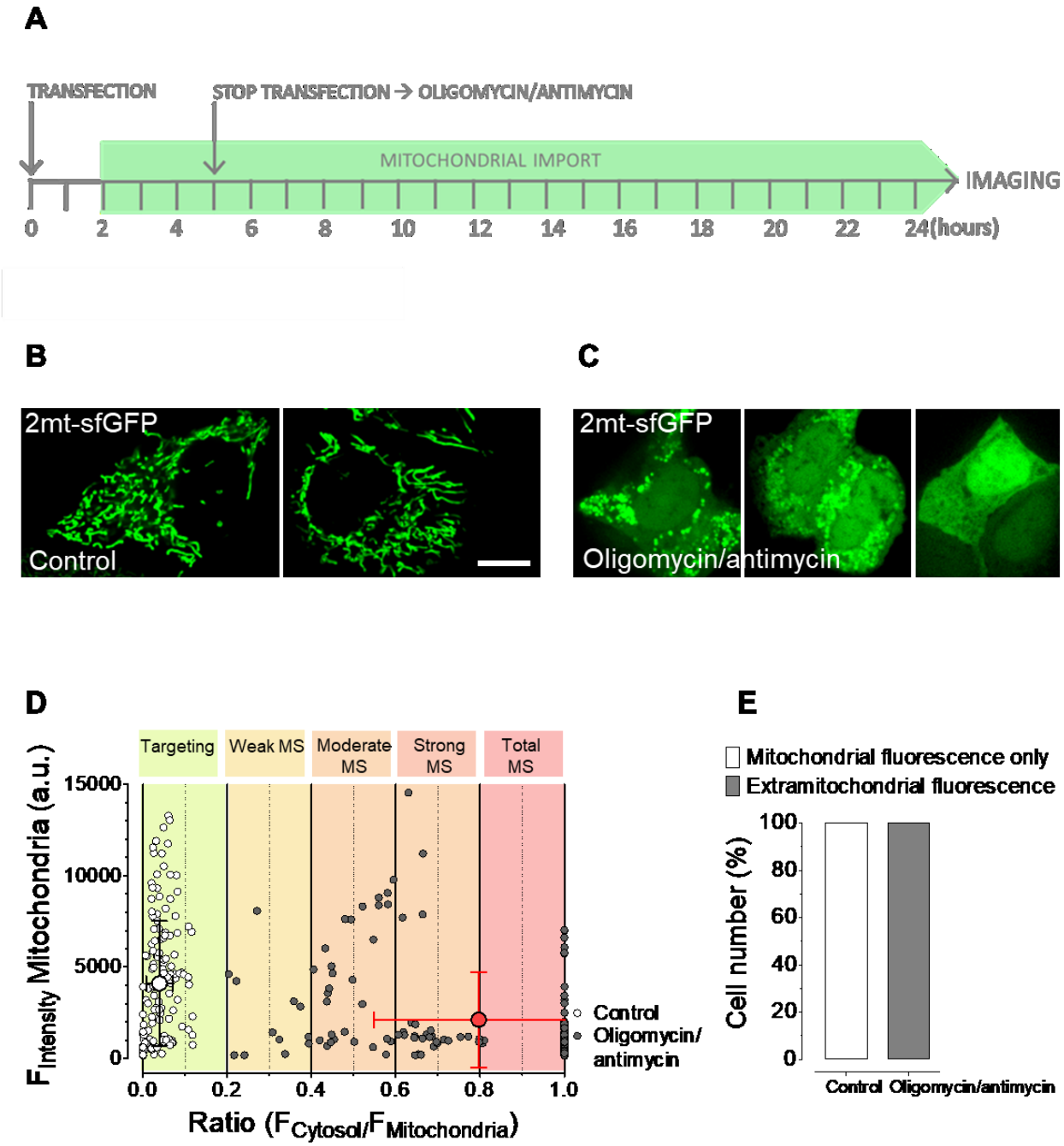

Figure 5. Visualization of the mistargeting of 2mt-sfGFP in the cytosol as an endpoint read-out, triggered by impairments in the mitochondrial protein uptake machinery upon

depolarization of the mitochondrial membrane potential. (A) Illustration of the protocol procedure for the endpoint determination of the mitochondrial protein import deficiency upon oligomycin-A and antimycin-A1. **(B)** Representative confocal images (left and right image, in green) of 2mt-sfGFP expressed in HeLa cells under control conditions. Scale bar indicates 10 µm. **(C)** Confocal images which represent different stages of mistargeting of HeLa cells expressing 2mt-sfGFP, treated with oligomycin-A and antimycin-A1. **(D)** HeLa cells expressing 2mt-sfGFP plotted as ratio of the cytosolic fluorescence and mitochondrial fluorescence intensity values against the mitochondrial fluorescence intensities. Control group and cells treated with oligomycin-A and antimycin-A1 are illustrated on the diagram. Four independent experiments were performed. Dots are shown as calculated ratio values ± SD; n (control group) = 144 cells, n (oligomycin-A and antimycin-A1) = 159 cells. **(E)** Percentage of HeLa cells expressing 2mt-sfGFP under control conditions and treated with oligomycin-A and antimycin-A1, respectively, showing the fluorescence signal coming from mitochondria only or additionally outside of mitochondria, n = 144 cells (control group), n = 159 cells (condition treated with oligomycin-A and antimycin-A1).

4.6. Depolarization of the mitochondrial membrane potential instantly affects the targeting of 2mt-sfGFP into mitochondria

Previously described data in this result section clearly showed that depolarization of the mitochondrial membrane potential inhibits the import of 2mt-sfGFP **(Figure 5B, C, D and E)**. Next we wanted to address the question, when the inhibition of the mitochondrial protein import machinery occurs, by depolarizing the mitochondrial membrane potential. This issue requires a more challenging experimental procedure, meaning that for this concern for the first time we tested whether the 2mt-sfGFP is suitable for long-term online-measurements. In order to tackle our question, we established a measurement protocol **(Figure 6A)**, which enables the dynamic visualization of de novo protein synthesis of the 2mt-sfGFP in living cells under various conditions.

Treatment of HeLa cells expressing 2mt-sfGFP with oligomycin-A and antimycin-A1 led to an accumulation of the probe in the cytosol around 20 minutes after adding the compounds, pointing to a fast and total inhibition of the mitochondrial protein import of 2mt-sfGFP under these conditions **(Figure 6B)**.

This means that depolarization of the mitochondrial membrane potential instantly affects the targeting of 2mt-sfGFP into mitochondria, namely a complete inhibition of the transport of 2mt-sfGFP into the organelle.

In contrast to that long-term online-imaging of HeLa cells expressing 2mt-sfGFP under control conditions showed an exclusive mitochondrial fluorescence during the complete measurement **(Figure 6B)**, indicating the efficient import of 2mt-sfGFP into mitochondria, which is constantly maintained.

Additionally, cells expressing 2mt-sfGFP and treated with oligomycin-A and antimycin-A1 showed a continuous increase in the fluorescence signal coming from the cytosol **(Figure 6B)**, indicating a constant de novo synthesis of 2mt-sfGFP. Mitochondria of HeLa cells of the control group expressing 2mt-sfGFP showed no appreciable morphological changes, indicating high and constant import of the fluorescent construct did not affect the shape of mitochondria **(Figure 6C)**. In contrast to that HeLa cells expressing 2mt-sfGFP, which were treated with oligomycin-A and antimycin-A1 exhibited evident morphological alterations **(Figure 6B)**, which in addition to the mistargeting indicates the effect of the mitochondrial toxins.

Our data so far prove the suitability of 2mt-sfGFP for the long-term online imaging of mitochondrial import deficiencies in living cells. In addition to that, those results demonstrate, that the established approach with the 2mt-sfGFP can be also exploited as a reporter system or technique for the protein biosynthesis rate.

Figure 6

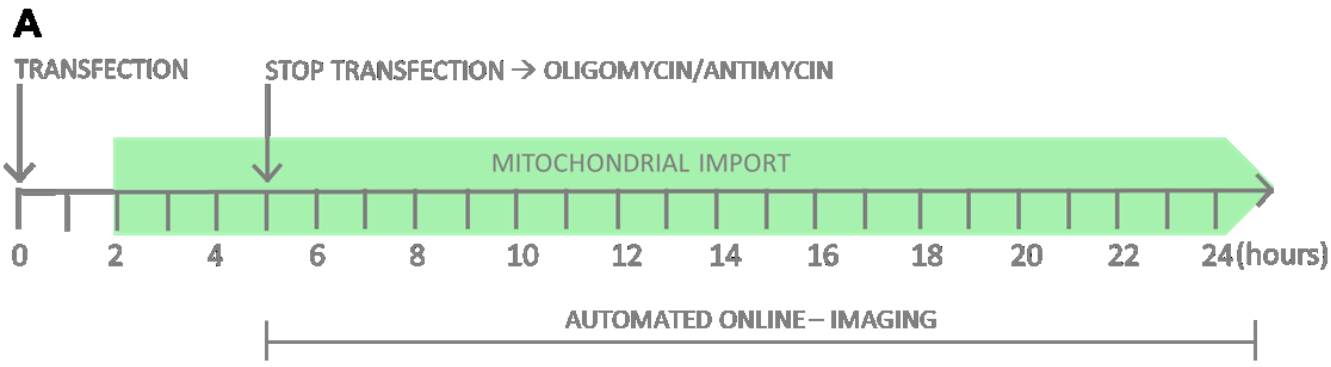

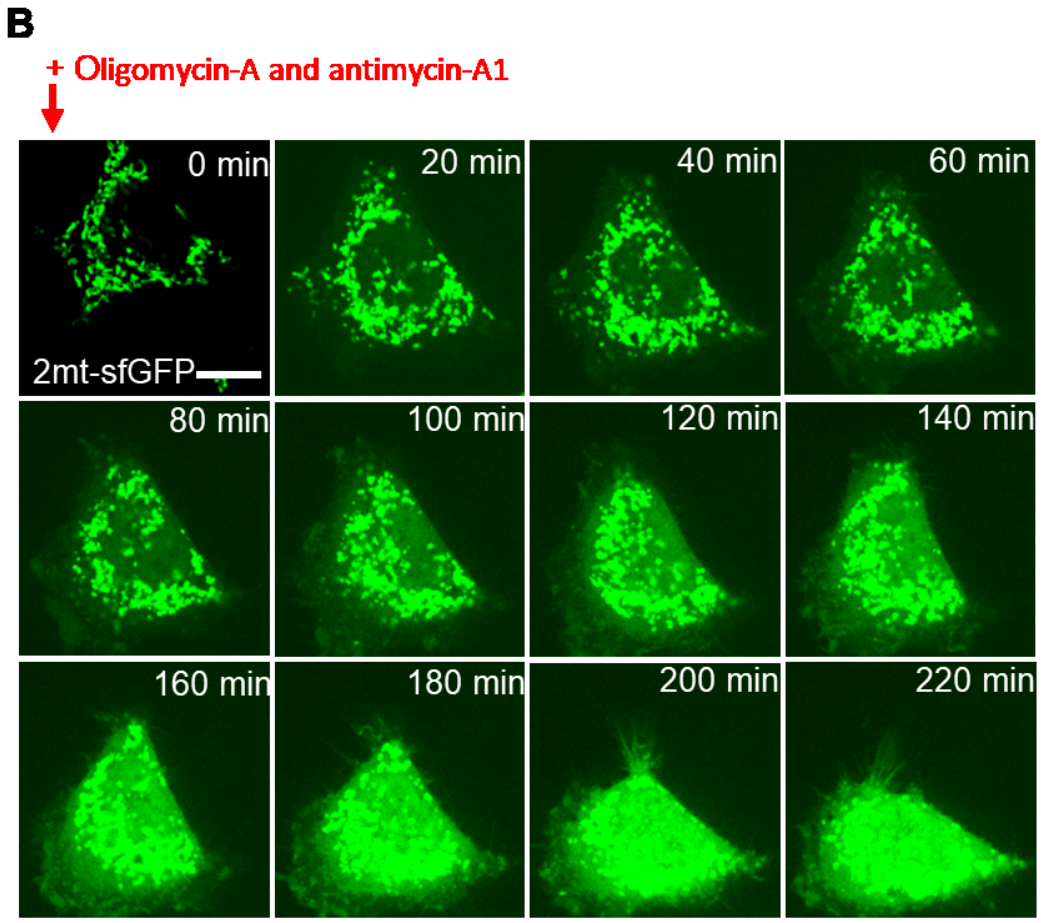
B
+ Oligomycin-A and antimycin-A1
0 min
20 min
40 min
60 min
2mt-sfGFP
80 min
100 min
120 min
140 min
160 min
180 min
200 min
220 min

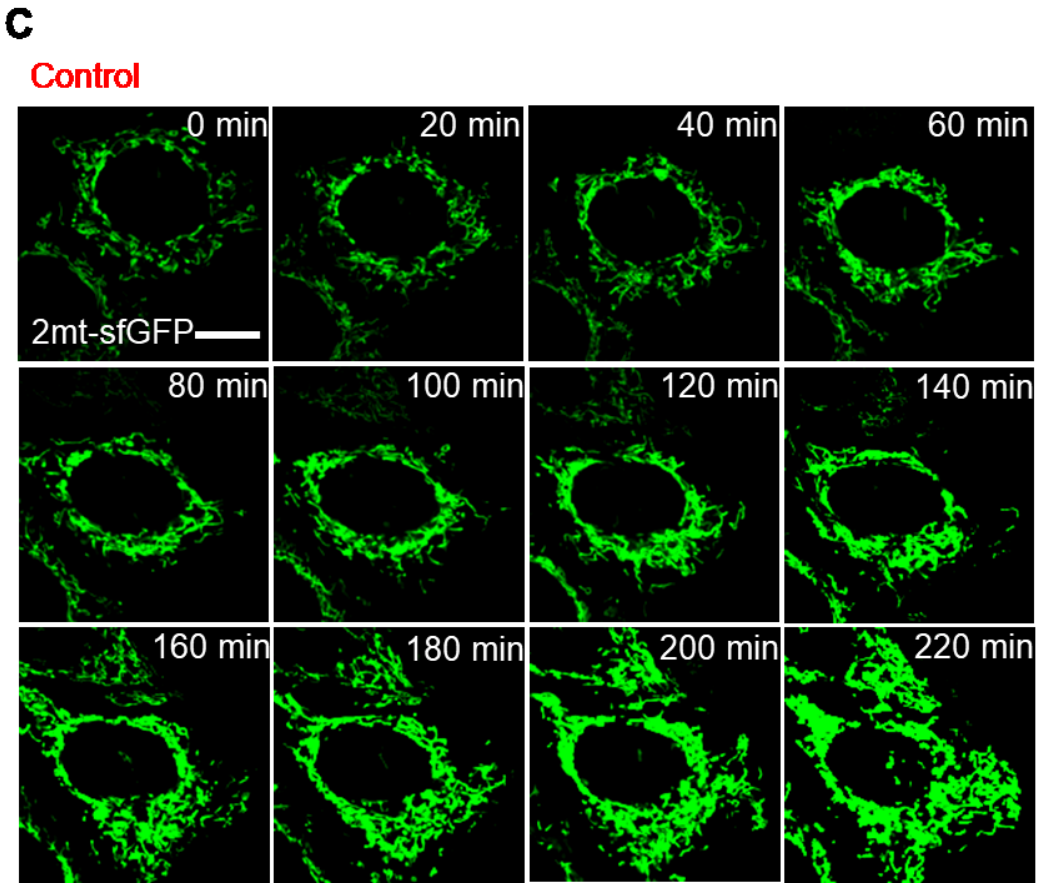
C
Control
0 min
20 min
40 min
60 min
2mt-sfGFP
80 min
100 min
120 min
140 min
160 min
180 min
200 min
220 min

Figure 6. Online long-term imaging of mitochondrial protein import deficiencies using the targeting-analysis approach with 2mt-sfGFP. (A) Overview of the protocol procedure for the long-term online measurement for the determination of the mitochondrial protein import deficiency upon treatment with oligomycin-A and antimycin-A1. **(B)** Image series of HeLa cells expressing 2mt-sfGFP imaged on a confocal microscope, treated with oligomycin-A and antimycin-A1. Scale bar corresponds to 10 µm. **(C)** Confocal time-lapse recordings of HeLa cells expressing 2mt-sfGFP under control conditions. Scale bar corresponds to 10 µm.

4.7. seCFP-OMP25, a cyan FP-variant targeted to the outer mitochondrial membrane shows no mistargeting upon depolarization of mitochondria

Since, depolarization of the mitochondrial membrane potential led to an instant accumulation of 2mt-sfGFP in the cytosol (Figure 5G), indicating an immediate inhibition of the import of 2mt-sfGFP into mitochondria, we were wondering, whether proteins, which are destined for the outer mitochondrial membrane also depend upon an intact mitochondrial membrane potential.

To check that, we exploited the seCFP-OMP25, a super-enhanced variant of the cyan FP (seCFP), targeted to the outer mitochondrial membrane, using an established targeting peptide (149).

Expression of seCFP-OMP25 in HeLa cells under control condition showed in 100 % of all positively transfected cells an exclusive mitochondrial fluorescence signal, indicating the efficient import and insertion of the protein into the outer mitochondrial membrane, as expected **(Figure 7A, C and D)**. Interestingly, treatment of HeLa cells with oligomycin-A and antimycin-A1 triggered no accumulation of seCFP-OMP25 in the cytosol, meaning that we could only detect a fluorescence signal coming from mitochondria **(Figure 7B, C and D)**. This indicates that depolarization of the mitochondrial membrane potential does not affect the insertion of a protein which harbors a targeting peptide for the outer membrane of mitochondria.

Next, we compared the subcellular distribution of seCFP-OMP25 with that one of 2mt-sfGFP after treatment with oligomycin-A and antimycin-A1. 100% of HeLa cells expressing seCFP-OMP25 exhibited a prominent mitochondrial fluorescence **(Figure 7B, C, D, E and F)**. However, all HeLa cells expressing 2mt-sfGFP showed a clear fluorescence signal arising from the cytosol, in addition to the fluorescence signal detected in mitochondria **(Figure 7E and F)**.

This comparison leads to the assumption that proteins harboring a classic N-terminal mitochondrial targeting sequence, which are imported through the presequence pathway into the lumen of mitochondria (42) depend upon the mitochondrial membrane potential. This is not the case for proteins, which carry a targeting peptide for the outer mitochondrial membrane, since disrupting the mitochondrial membrane potential showed no mistargeting of the seCFP-OMP25, representing a protein of the outer mitochondrial membrane.

Figure 7

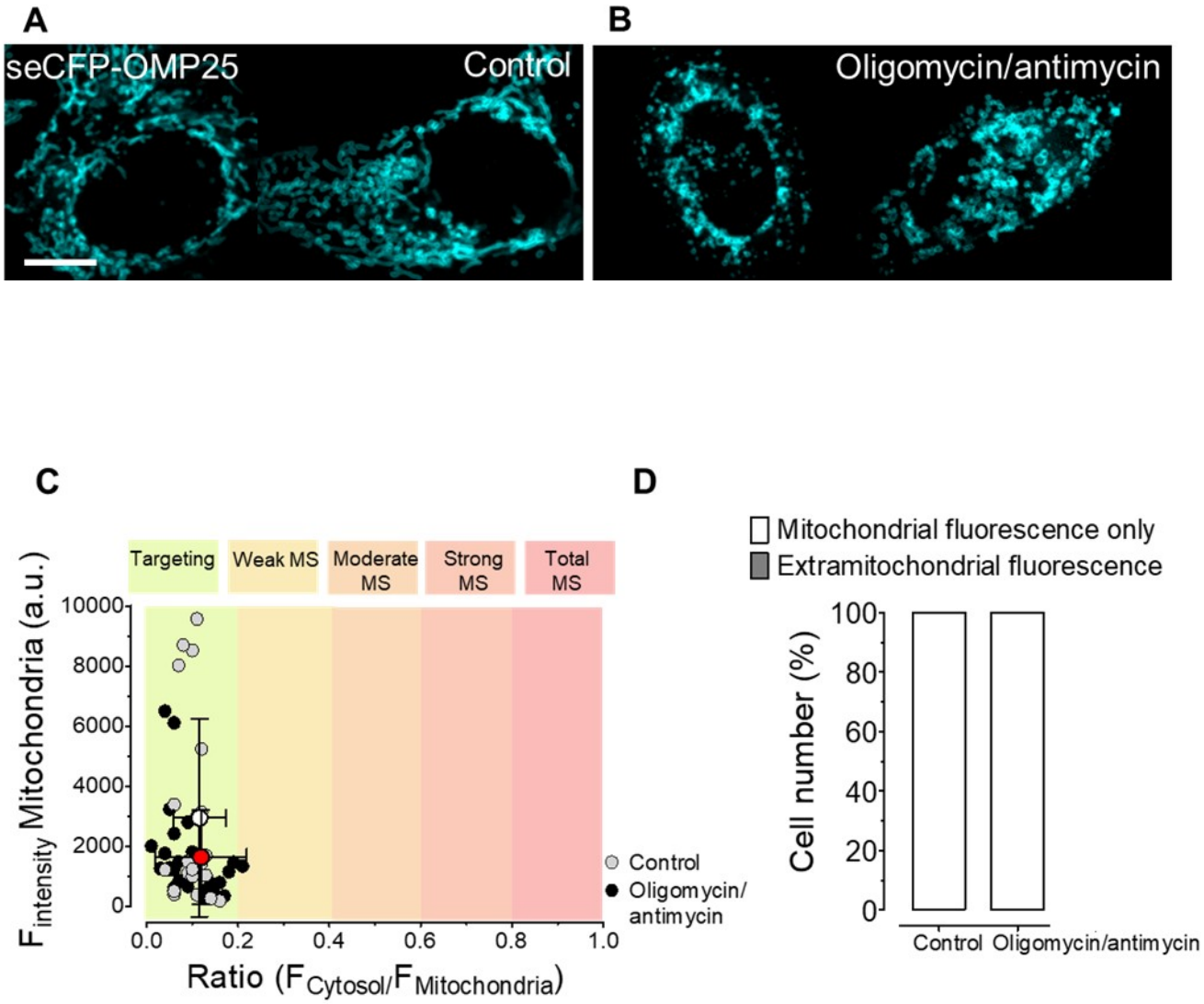

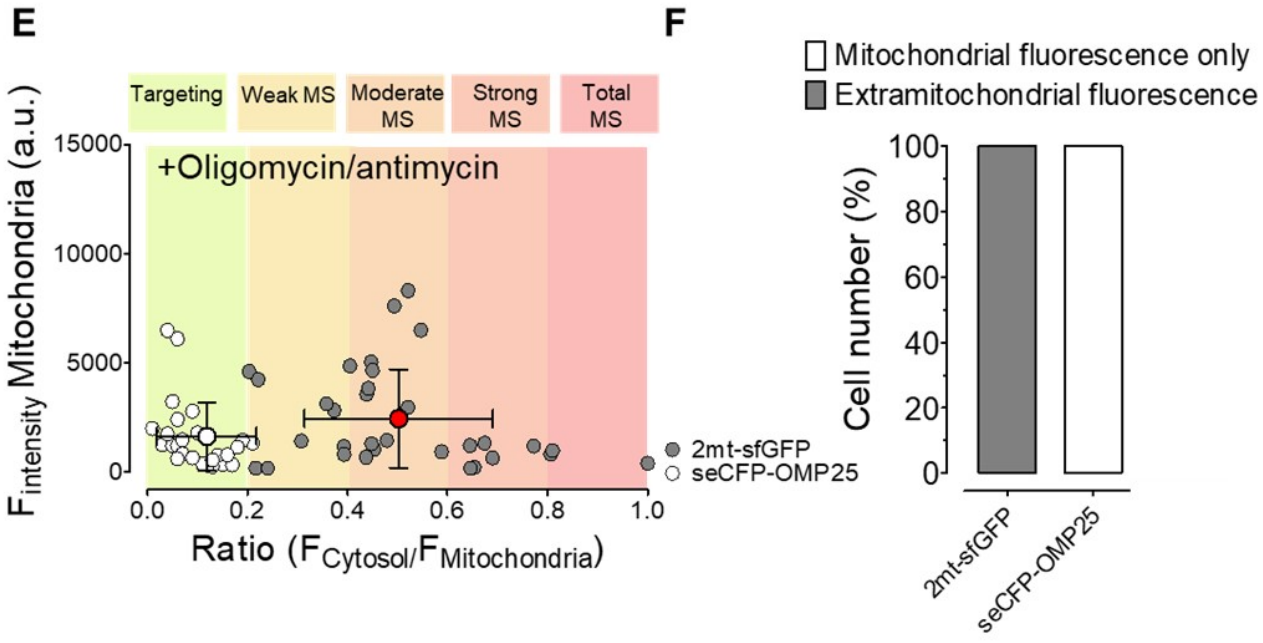

Figure 7. Visualization of mitochondrial protein insertion of seCFP-OMP25 upon depolarization of the mitochondrial membrane potential. (A) Representative confocal images of HeLa cells expressing seCFP-OMP25 under control conditions. Scale bar represents 10 µm. **B)** HeLa cells expressing seCFP-OMP25 shown as representative confocal images upon treatment with oligomycin-A and antimycin-A1. **(C)** HeLa cells expressing seCFP-OMP25 plotted as ratio values of the cytosolic fluorescence and mitochondrial fluorescence intensities against the mitochondrial fluorescence intensities. Cells are shown in 2 different condition, namely control group compared to cells treated with oligomycin-A and antimycin-A1. Three experiments were performed. Dots are shown as calculated ratio values ± SD; n (control group) = 23 cells, n (oligomycin-A and antimycin-A1) = 27 cells. **(D)** HeLa cells expressing seCFP-OMP25 as a control group compared to cells treated with oligomycin-A and antimycin-A1, illustrated in percentage. The bars are showing the fluorescence signal coming from mitochondria only or additionally outside of mitochondria, n = 23 cells (control group), n = 27 cells (condition treated with oligomycin-A and antimycin-A1). **(E)** Illustration of HeLa cells expressing either seCFP-OMP25 or 2mt-sfGFP, calculated as ratio of the cytosolic fluorescence and mitochondrial fluorescence intensity values against the mitochondrial fluorescence intensities. Cells transfected with seCFP-OMP25 and 2mt-sfGFP are treated with oligomycin-A and antimycin-A1, respectively. Three experiments were performed. Dots are represented as calculated ratio values ± SD; n (seCFP-OMP25) = 27 cells, n (2mt-sfGFP) = 32 cells. **(F)** HeLa cells treated with oligomycin-A and antimycin-A1 expressing seCFP-OMP25 and 2mt-sfGFP, respectively portrayed in percentage. The bars are showing the fluorescence signal coming from mitochondria only or additionally outside of mitochondria, n (seCFP-OMP25) = 27 cells, n (2mt-sfGFP) = 32 cells.

4.8. Application of the mitochondrial protein import analysis approach to Sirtuin4, a mitochondrial sirtuin isoform

Our results so far demonstrate and prove the suitability of 2mt-sfGFP being exploited as a proper tool to study mitochondrial protein import activities, efficiencies and impairments in living cells under various conditions.

Additionally we expanded the approach by implementing another FP-based probe, which makes it possible to study not only the presequence pathway of mitochondrial proteins harboring a classic N-terminal MTS, but also to visualize the import and insertion of mitochondrial proteins into the outer membrane of the organelle.

We generated data, which emphasize the power of fusing targeting peptides to fluorescent proteins in order to make various mitochondrial protein import pathways visible in living cells. These obtained data pushed us to test whether this technique is applicable to other mitochondrial proteins of interest.

Given the importance of mitochondrial sirtuins in the regulation of various essential cellular processes related to metabolism and stress (18) (17), we decided to take a closer look into Sirtuin4 (Sirt4), since its subcellular distribution is still debatable (150) (151) (152).

Screening the literature we found out that Sirt4 harbors a classic N-terminal MTS, making up 28 amino acids of the complete protein (153). Using computational 3D-prediction tools pointed the insertion of a flexible linker between Sirt4 and sfGFP out, because of the bulky structures of the two proteins. Given the importance of the classical N-terminal MTS of mitochondrial matrix proteins it is essential to fuse the sfGFP C-terminally to the protein (154). Otherwise the MTS is not efficient in its targeting properties. Considering the computational predictions and the aspects of the N-terminal MTS we fused the sfGFP C-terminally to the protein and inserted a flexible GS-Linker between the two proteins, generating the construct Sirt4-sfGFP **(Figure 8A)**.

Figure 8

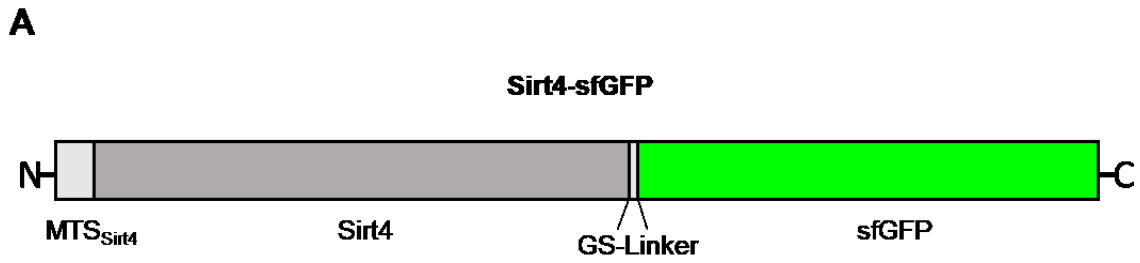

Figure 8. Design and schematic overview of the Sirt4-sfGFP. (A) In light grey the mitochondrial targeting sequence is illustrated, indicated as MTS_{Sirt4}, followed by the rest of Sirt4, which is shown in dark grey. Sirt4 is fused to the C-terminus of the sfGFP, shown in bright green.

4.9. Sirt4-sfGFP is less efficiently targeted and imported into mitochondria of HeLa cells compared to 2mt-sfGFP

In order to determine the efficiency of the mitochondrial targeting of Sirt4-sfGFP, we first investigated the subcellular localization of the FP-based pro in HeLa cells. Sirt4 acting by regulating important cellular processes acts as a tumor suppressor in cancer, therefore we decided to perform the first experiments in our cancer cell model, name in HeLa cells (155) For the analysis of the subcellular localization we applied array confocal laser scanning microscopy.

Applying the established 2mt-sfGFP enabled the comparison of the subcellular distribution of Sirt4-sfGFP with the matrix-targeted sfGFP. In 60% of all HeLa cells expressing Sirt4-sfGFP harboring a 28 amino acid long MTS **(Figure 7A)** we detected an exclusive mitochondrial fluorescence signal **(Figure 9A, C and D)** (1) . Yet, 40% of HeLa cells expressing Sirt4-sfGFP displayed a dominant fluorescence signal, coming from the cytosol and the nucleus **(Figure 9A, C and D)** (1). In the cells were we could detect a fluorescence signal coming from the cytosol and the nucleus, also a mitochondrial fluorescence signal was captured **(Figure 9A, C and D)** (1).

Even when HeLa cells expressed rather low levels of Sirt4-sfGFP we found a population of cells with a prominent extra-mitochondrial fluorescence signal, although we calculated a significant positive correlation between the expression levels and mitochondrial targeting efficiency **(Figure 9C)** (1). A threshold of ratio $F_{Nucleus}/F_{Mitochondria} \geq 0.33$ was set and denoted by gray areas, which were defined as areas of significant extra-mitochondrial localization **(Figure 9C)** (1).

Comparing Sirt4-sfGFP with 2mt-sfGFP unveiled that all HeLa cells expressing 2mt-sfGFP displayed an exclusive mitochondrial fluorescence signal independent of the expression level of the mitochondria targeted FP variant **(Figure 9B, C and D)** (1).

These observations led us to the conclusion that the mitochondrial targeting efficiency of Sirt4-sfGFP in HeLa cells is rather weak, compared to the targeting efficiency of 2mt-sfGFP to mitochondria.

Figure 9

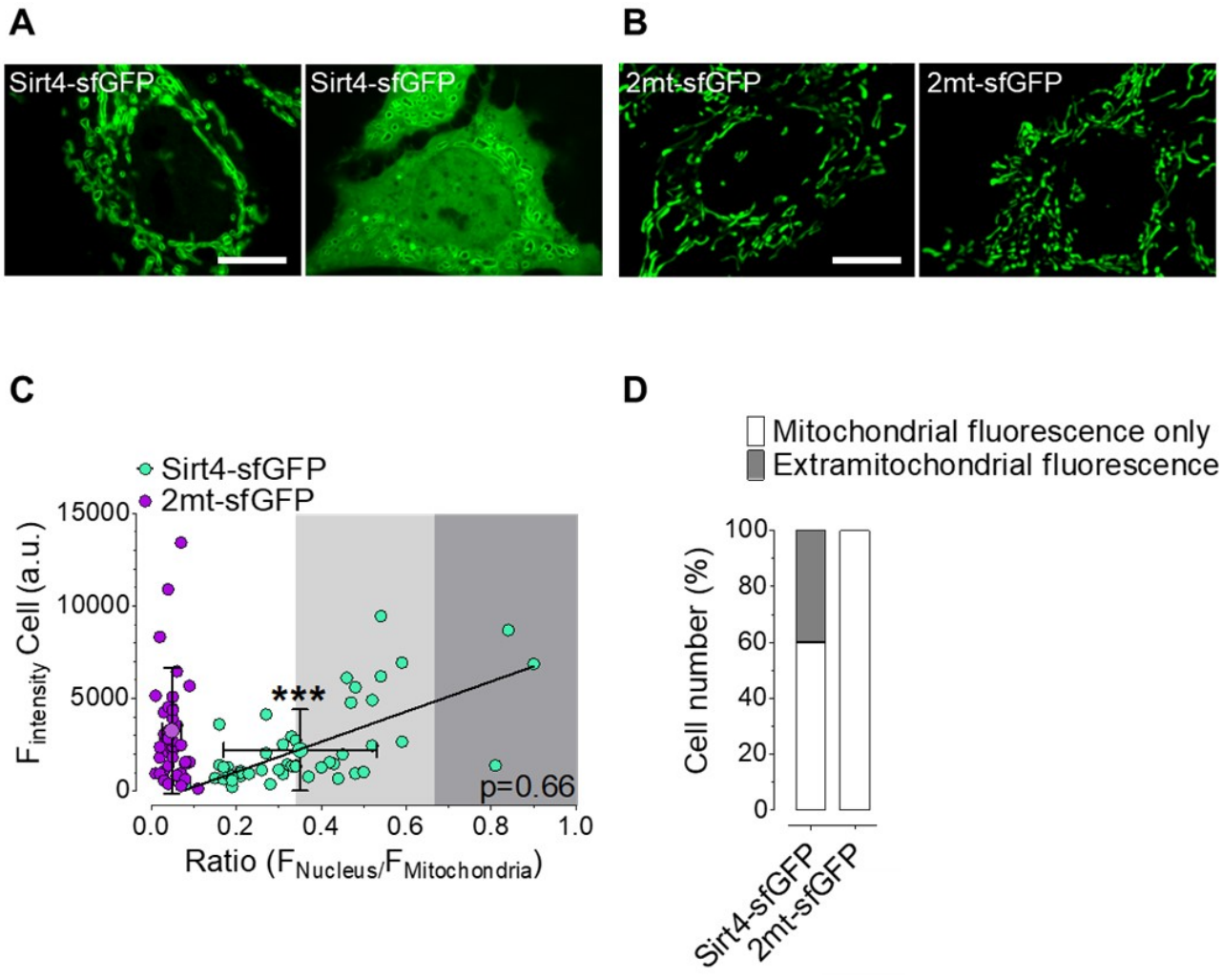

Figure 9. Visualization of the subcellular distribution of Sirt4-sfGFP in living HeLa cells. **(A**) HeLa cells expressing Sirt4-sfGFP shown as representative images of a confocal imaging system. On the left image, Sirt4-sfGFP is illustrated being located to mitochondria. Right image displays Sirt4-sfGFP located in addition to mitochondria also extra mitochondrially. Scale bar corresponds to 10 µm. **(B**) Representative images of HeLa cells expressing 2mt-sfGFP recorded on a confocal imaging system. Left and right image show the exclusive localization of 2mt-sfGFP to mitochondria. Scale bar indicates 10 µm. **(C**) Calculation of the ratio of nuclear fluorescence to mitochondrial fluorescence and plotted against whole cell fluorescence intensity, generated by recordings of HeLa cells expressing either 2mt-sfGFP or Sirt4-sfGFP. A mathematical function was applied to describe the correlation of Sirt4-sfGFP between $F_{Nucleus}$ and $F_{Mitochondria}$ with the Pearson coefficient shown in the lower right corner, indicated with "p". Three independent experiments were performed for each condition. Data are shown as ratios with the mean ± SD; n = 97 cells. (*** $p < 0.0001$, unpaired double-sided t-test). [Figure panels reproduced from Ramadani-Muja et al., Cells 2019.]

4.10. INS-1 cells also target and import Sirt4-sfGFP with a lower efficiency to mitochondria, compared to 2mt-sfGFP

We thought that it would make sense to check the subcellular distribution of Sirt4-sfGFP in the pancreatic beta cell line, the INS-1 cells, given the role of Sirt4 in insulin secretion through the leucine metabolism (152).

Expression of Sirt4-sfGFP in INS-1 cells also showed two different populations: We could detect in almost 80% of INS-1 cells expressing Sirt4-sfGFP a dominant fluorescence signal, coming from outside of mitochondria, in addition to that fluorescence signal arising from mitochondria **(Figure 10A, C and D)** (1). The remaining 20% of all INS-1 cells expressing Sirt4-sfGFP displayed a dominant fluorescence signal, which was exclusively located to mitochondria **(Figure 10A, C and D)** (1). Similarly like in HeLa cells, also in INS-1 cells we found some cells with a clear extra-mitochondrial fluorescence signal, despite the rather low expression levels of Sirt4-sfGFP and a significant positively calculated correlation between the expression level and mistargeting of Sirt4-sfGFP **(Figure 10C)** (1). Again, a threshold of ratio $F_{Nucleus}/F_{Mitochondria} \geq 0.33$ was set and denoted by gray areas, which were defined as areas of significant extra-mitochondrial localization.

In analogy to the results we obtained in HeLa cells, also INS-1 cells positive for 2mt-sfGFP showed a prominent fluorescence signal arising exclusively from mitochondria **(Figure 10B, C and D)** (1), indicating the efficient mitochondrial targeting of the respective probe in this cell model as well. In contrast to the subcellular localization of the Sirt4-sfGFP, which was distributed between mitochondria, the cytosol and nucleus, we concluded that also in INS-1 cells the targeting efficiency to mitochondria of Sirt4-sfGFP is weak, compared to the uptake efficiency of 2mt-sfGFP into mitochondria.

Figure 10

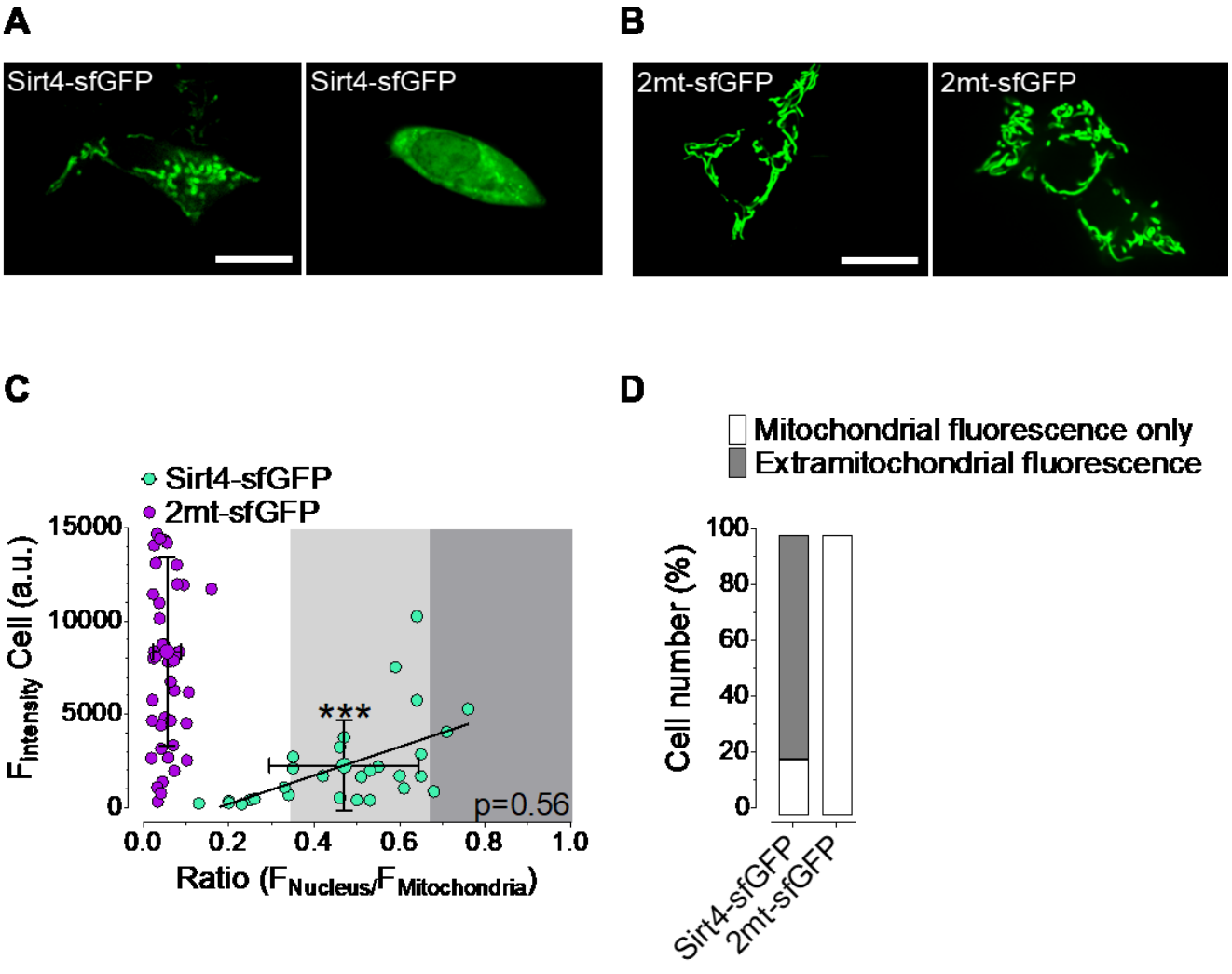

Figure 10. Confocal imaging of the subcellular distribution of Sirt4-sfGFP in living INS-1 cells. (A) INS-1 cells expressing Sirt4-sfGFP shown as representative images of a confocal imaging system. On the left image, Sirt4-sfGFP is illustrated being located to mitochondria. Right image displays Sirt4-sfGFP located in addition to mitochondria also extra

mitochondrially. Scale bar corresponds to 10 µm. **(B**) Representative images of INS-1 cells expressing 2mt-sfGFP recorded on a confocal imaging system.

Left and right image show the exclusive localization of 2mt-sfGFP to mitochondria. Scale bar indicates 10 µm. **(C**) Calculation of the ratio of nuclear fluorescence to mitochondrial fluorescence and plotted against whole cell fluorescence intensity, generated by recordings of HeLa cells expressing either 2mt-sfGFP or Sirt4-sfGFP. A mathematical function was applied to describe the correlation of Sirt4-sfGFP between $F_{Nucleus}$ and $F_{Mitochondria}$ with the Pearson coefficient shown in the lower right corner, indicated with "p". Three independent experiments were performed for each condition. Data are shown as ratios with the mean ± SD; n = 73 cells. (*** $p < 0.0001$, unpaired double-sided t-test). [Figure panels reproduced from Ramadani-Muja et al., Cells 2019.]

4.11. Sirt4-sfGFP is equally distributed between the nucleus and the cytosol in HeLa and INS-1 cells

Zeng et al. described in their work, that Sirt4, as a regulator of metabolic activities in mitochondria, might also regulate processes within the nucleus (156). Therefore we thought about the possibility of Sirt4-sfGFP to accumulate in the nucleus as well, once it is not efficiently imported into mitochondria. To address this issue we analyzed the images we generated on the confocal microscope for a putative accumulation of Sirt4-sfGFP within the nucleus of individual cells.

Interestingly, we found out by calculating the ratio of the fluorescence signal coming from the cytosol and the nucleus, respectively that Sirt4-sfGFP is equally distributed amongst these compartments in HeLa cells **(Figure 11A and B)** (1). Based on that observation we draw the conclusion that Sirt4-sfGFP does not accumulate in the nucleus upon mistargeting outside of mitochondria, but enters this organelle due to its small size allowing the passage of nuclear pores (157) .

We made the same observation when we performed the experiment in INS-1 cells. The abundance of Sirt4-sfGFP, expressed by INS-cells in the nucleus and the cytosol was equally strong, **(Figure 11C and D)** (1). This indicates that Sirt4-sfGFP has no preference for the nucleus, upon mistargeting outside of mitochondria also in INS-1 cells.

Figure 11

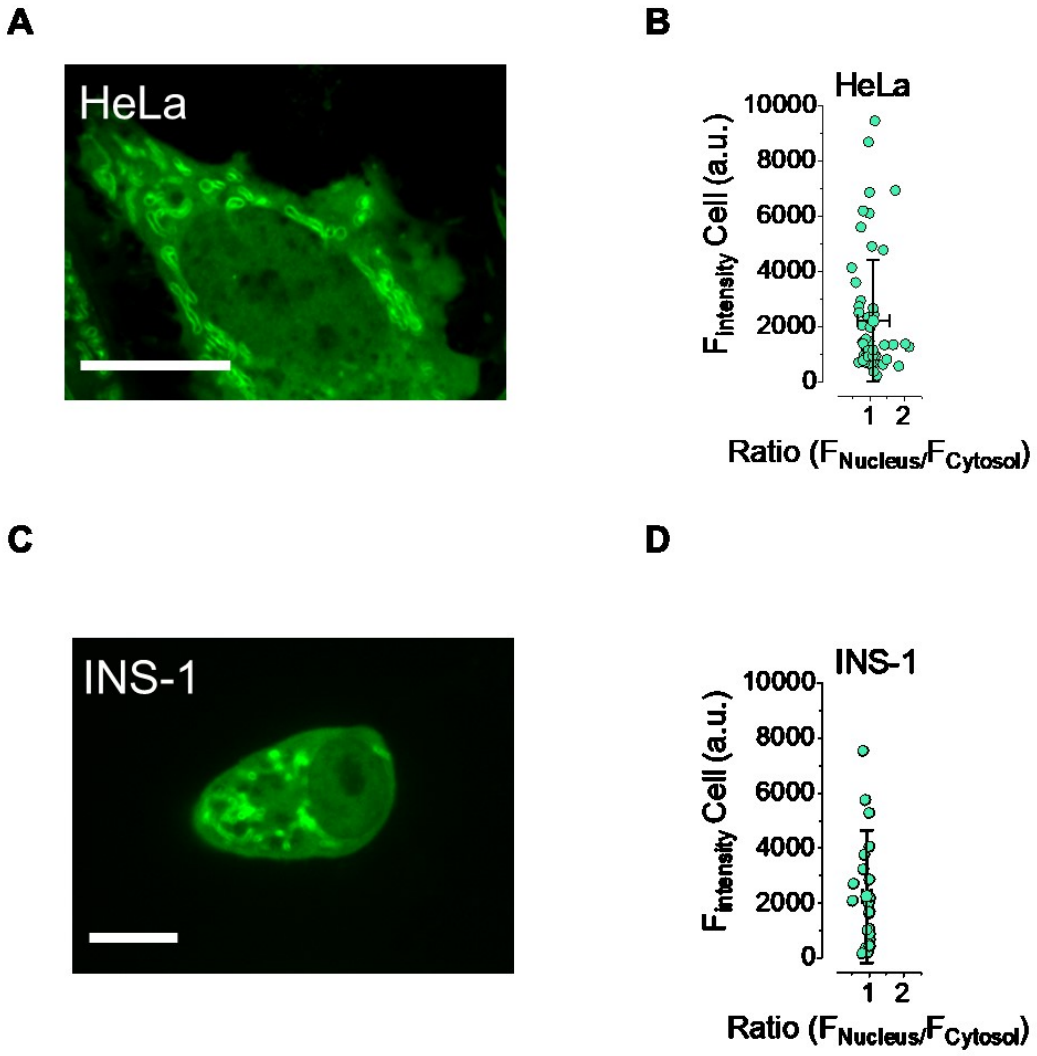

Figure 11. Visualization of the distribution of Sirt4-sfGFP between the nucleus and cytosol in HeLa cells and INS-1 cells. (A) Representative image of a HeLa cell expressing Sirt4-sfGFP recorded with a confocal microscope, showing a fluorescence signal coming from mitochondria and from the nucleus and cytosol, respectively. Scale bar indicates 10 µm. **(B**) Illustration of HeLa cells expressing Sirt4-sfGFP, shown as ratio values of the nucleus fluorescence and the cytosolic fluorescence, which were plotted against the whole cell fluorescence intensity. Dots are shown as ratios with mean ± SD; n = 52 cells. Three independent experiments were done. **(C**) INS-1 cell expressing Sirt4-sfGFP, represented as a confocal imaging, showing a fluorescence signal coming from mitochondria and from the nucleus and cytosol, respectively. Scale bar indicates 10 µm. **(D**) Calculation of the ratio of nuclear fluorescence to cytosolic fluorescence of Sirt4-sfGFP in INS-1 cells plotted against the whole cell fluorescence intensity. Data are shown as ratios with the mean ± SD; n = 29 cells. Three independent experiments were done. [Figure panels reproduced from Ramadani-Muja et al., Cells 2019.]

4.12. Fusion of four different mitochondrial targeting sequences to sfGFP lead to accumulation of the probe in the nucleus upon mitochondrial mistargeting

Next, we decided to create and design a novel mitochondrial targeting sequence (nMTS) by fusing different N-terminal mitochondrial targeting sequences of various mitochondrial proteins to super-folder GFP **(Figure 12A)**. The idea behind this purpose was to establish a so far not existing artificial MTS, which upon mistargeting would not distribute within the complete cell, instead harboring a dual targeting information, such as one for the nucleus. This would result in a nice separation of the fluorescence signal upon mistargeting, therefore facilitating image analysis. By screening the literature, we came up with following four mitochondrial proteins, of which we picked the N-terminal targeting sequences respectively and fused these domains next to each other followed by sfGFP: mitochondrial COXVIII subunit (136), mitochondrial glutamate dehydrogenase (GDH) (158) , mitochondrial pyruvate dehydrogenase (PDH) (159) and ornithine transcarbamylase (160) **(Figure 12A)**. As a result we generated a construct, which we named n4mt-sfGFP (new 4 repeat MTS fused to sfGFP) **(Figure 12A)**.

Indeed, expression of n4mt-sfGFP in HeLa cells showed a dominant mitochondrial fluorescence in 22% of all positively transfected cells **(Figure 12B, E and F)**, indicating the import of the probe into mitochondria. However, HeLa cells expressing n4mt-sfGFP exhibited a population of cells, namely 34%, where the probe clearly displayed extramitochondrial fluorescence, in addition to the fluorescence signal coming from mitochondria **(Figure 12C, E and F)**. This indicates that in some cells the mitochondrial targeting efficiency of n4mt-sfGFP was not as strong as we found it for 2mt-sfGFP. Additionally we found that in 44%- of HeLa cells the fluorescence signal was extremely dominant in the nucleus, meaning that under certain condition the probe severely accumulates in the nucleus upon mistargeting **(Figure 12D, E and F)**. Next, we wanted to test the suitability of n4mt-sfGFP for the visualization of mitochondrial stress induced by treatment of the cells with oligomycin-A and antimycin-A1. All HeLa cells, expressing n4mt-sfGFP treated with the combination of the two mitochondrial toxins exhibited no mitochondrial fluorescence at all, but only a dominant fluorescence signal coming from the nucleus **(Figure 12G and H)**. Taken these results together we concluded that due to the fact that we found also cells with a fluorescence signal outside of mitochondria, it seems that we generated a fluorescent construct, which seems quite sensitive to report already slight defects in mitochondrial protein import. The probe is also highly suitable for the

visualization of severe mitochondrial stress induced by mitochondrial toxins, which depolarize the mitochondrial membrane potential.

Figure 12

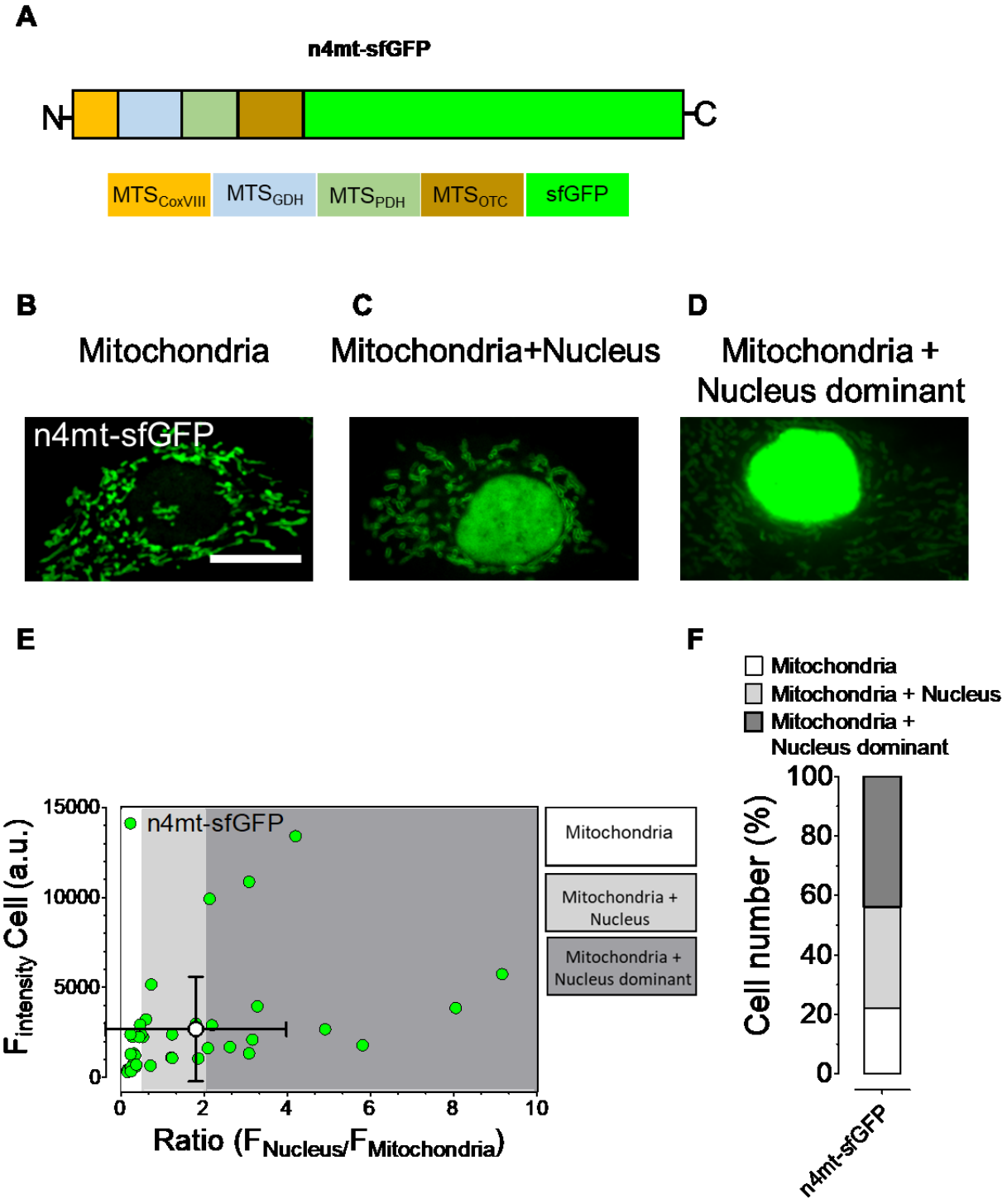

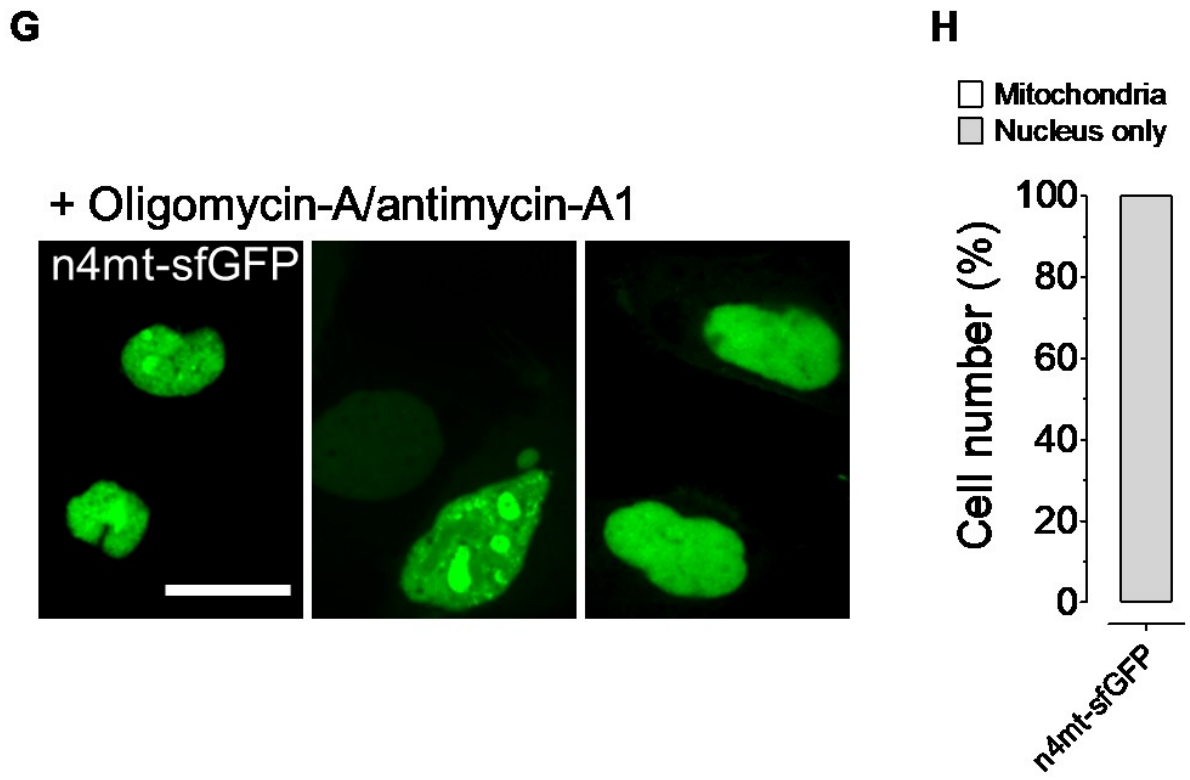

Figure 12. Generation of n4mt-sfGFP, an artificial four times repeat of different MTSs fused to sfGFP, to visualize mitochondrial mistargeting as an accumulation of the respective probe in the nucleus. (A) Scematic overview of the construction of n4mt-sfGFP. Four different mitochondrial targeting sequences of distinct mitochondrial proteins are fused one after the other, shown in yellow ($MTS_{CoxVIII}$), light blue (MTS_{GDH}), light green (MTS_{PDH}) and brown (MTS_{OTC}), followed by sfGFP (bright green). **(B)** Representative confocal image of HeLa cell expressing n4mt-sfGFP, showing mitochondrial fluorescence signal. Scale bar indicates 10µm. **(C)** HeLa cell expressing n4mt-sfGFP, depicted as a confocal recording, showing a fluorescence signal coming from mitochondria and the nucleus, respectively. **(C)** Representative confocal image of HeLa cell expressing n4mt-sfGFP illustrating weak fluorescence signal arising from mitochondria and a very strong signal coming from the nucleus. **(E)** Diagram, showing HeLa cells expressing n4mt-sfGFP, where the dots are depicted as ratio values of the nucleus fluorescence and the mitochondrial fluorescence and plotted against the whole cell intensity. Definition of a new categorization for the mitochondrial mistargeting, defined with a threshold of ratio $F_{Nucleus}/F_{Mitochondria} \leq 0.30$ as a white area of mitochondrial signal, 0.30 – 1.0 as an light grey area of mitochondria and the nucleus respectively and ≥ 1.0 as an dark grey area of mitochondrial signal and a strong and dominant nuclear fluorescence signal. Two independent experiments were done. Dots are shown as ratios with the mean ± SD; n = 38 cells.

(F) Percentage of HeLa cells expressing n4mt-sfGFP showing the fluorescence signal coming from mitochondria, mitochondria and nucleus respectively or from mitochondria and mainly the nucleus only. Two independent experiments were done. n = 38 cells. **(G)** Representative images recorded on a confocal microscope, showing HeLa cells, which express n4mt-sfGFP under treatment of oligomycin-A and antimycin-A1. Scale bar corresponds to 10 µm. **(H)** Percentage of HeLa cells expressing n4mt-sfGFP showing the fluorescence signal coming from the nucleus only. Two independent experiments were performed. n = 31 cells.

4.13. The n4mt-sfGFP as well as Sirt4-sfGFP locates to the outer mitochondrial membrane

Surprisingly, when we took a closer look at the high-resolution images, which we recorded by the array confocal laser scanning microscope (ACLSM), we observed mitochondrial structures enclosing darker mitochondrial matrices in HeLa cells expressing n4mt-sfGFP **(Figure 13A)**. This finding might indicate the localisation of n4mt-sfGFP to the outer mitochondrial membrane.

Since we noticed a localisation to the outer mitochondrial membrane of sfGFP fused to a classic N-terminal MTSs, we were curios whether this is also the case for Sirt4-sfGFP. Due to the fact that Sirt4 also harbors a classic N-terminal mitochondrial targeting sequence (153), we expected Sirt4-sfGFP to be located to the lumen of mitochondria. Interestingly enough, we made a similar observation, when we applied high-resolution microscopy to HeLa cells, which were transfected with Sirt4-sfGFP and detected a nice mitochondrial structure, however inside omitted **(Figure 13B)** (1).

We exploited therefore seCFP-OMP25, as a marker for the outer mitochondrial membrane and observed a similar pattern with seCFP based probe **(Figure 13C)** (1). Performing co-localization experiments in HeLa cells expressing Sirt4-sfGFP and stained with MitoTracker™ Red FM, a marker for the inner mitochondrial membrane (28) resulted in a red fluorescence signal surrounded by a green fluorescence, indicating the low co-localization between the two channels respectively **(Figure 13D)**.

Figure 13

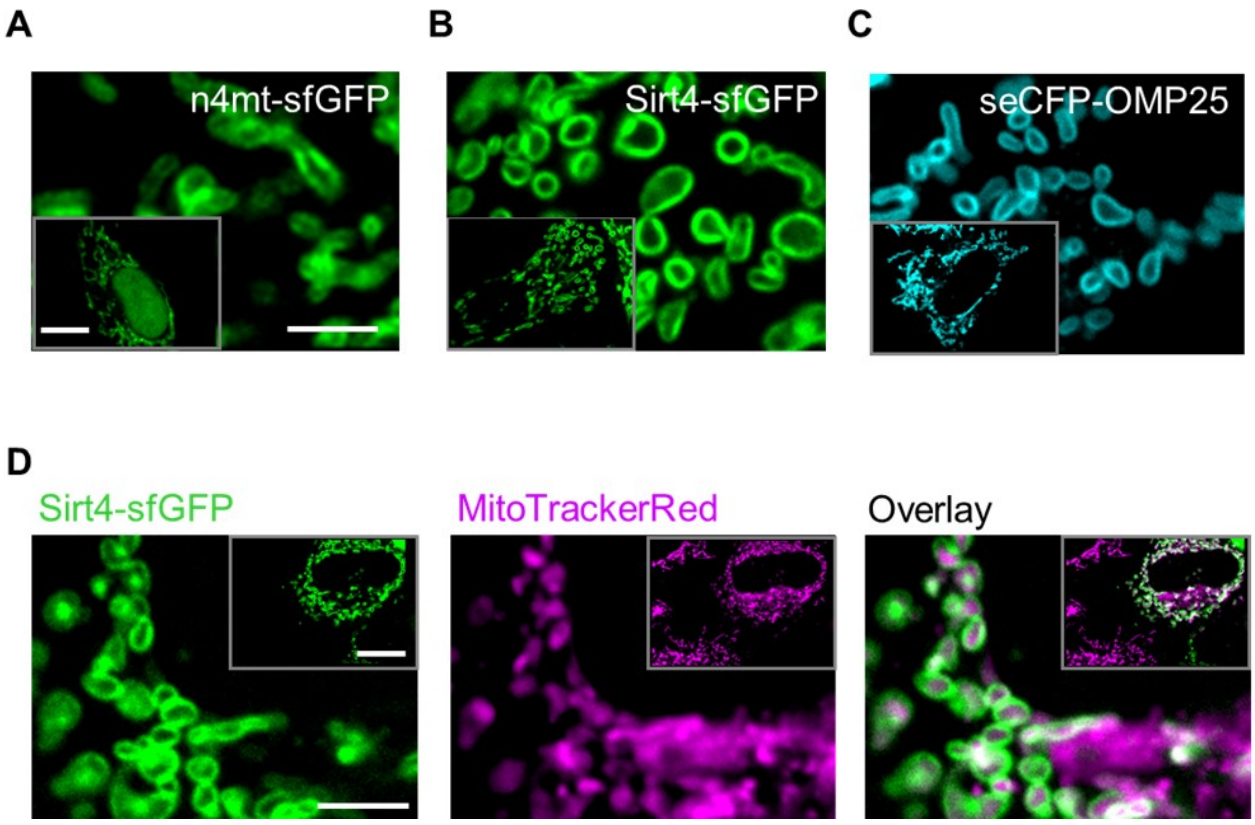

Figure 13. Imaging of the localization of Sirt4-sfGFP to the outer mitochondrial membrane using high-resolution microscopy. (A) Representative confocal image of HeLa cells expressing n4mt-sfGFP. Scale bar corresponds to 2.5 µm in the zoomed image. In the lower left square the whole cell is shown respectively with a scale bar corresponding to 10 µm. **(B)** Identical experiment as this in **(A)**, but using HeLa cells expressing Sirt4-sfGFP. **(C)** Same experimental approach as in **(A)** and **(B)** exploiting HeLa cells transfected with seCFP-OMP25. **(D)** Confocal recordings representing HeLa cells expressing Sirt4-sfGFP (green) and stained with MitoTracker™ Red FM (magenta). On the right panel the merged image is illustrated. Scare bar indicating 2.5 µm. Scare in the upper right displaying the whole cell respectively. Scale bar corresponds to 10 µm. [Figure panels reproduced from Ramadani-Muja et al., Cells 2019.]

4.14. Applying super-resolution microscopy confirmed the localization of Sirt4-sfGFP to the outer mitochondrial membrane

To verify the previously described observations of the localization of Sirt4-sfGFP to the outer mitochondrial membrane we applied super-resolution microscopy, exploiting a structural illumination microscope (SIM). Using the SIM we planned to determine the sub-mitochondrial localization of Sirt4-sfGFP being expressed by HeLa cells. Having a look at the cells recorded by the SIM revealed strong co-localizations between Sirt4-sfGFP and Tetramethylrhodamine methyl ester (TMRM) **(Figure 14A)** (1).The analysis of the generated images in the form of line scans confirmed the co-localization of Sirt4-sfGFP with TMRM **(Figure 14B)** (1), pointing to the localization of Sirt4-sfGFP to the outer mitochondrial membrane.

By analyzing the images and performing respective line scans we obtained similar results of HeLa cells expressing Sirt4-sfGFP, which were stained with the matrix targeted DsRed (mtDsRed), namely the observation of a low co-localization of the green and red fluorescence respectively **(Figure 14C and D)** (1). This finding also indicates the presence of Sirt4-sfGFP to the outer membrane of mitochondria.

Moreover, by generating a series of imaging data recorded with the SIM in intact HeLa cells expressing Sirt4-sfGFP we emphasize the localization of Sirt4-sfGFP to the outer mitochondrial membrane, since we demonstrated a strong co-localization between the respective probe and mCherry-TOM22 **(Figure 14E)** (1). When we performed line scan analysis we could verify the high co-localization between Sirt4-sfGFP and mCherry-TOM22, respectively **(Figure 14F)** (1). We also did cross-section intensity profiles of Sirt4-sfGFP and mCherry-TOM22 with subpixel accuracy exploiting the mathematical analysis of a double Gauss fit and found out that the respective constructs overlap with a uncertainty of 12 nm (SD, n = 30/59 cells/mitochondria), being a strong indicator for the existence of Sirt4-sfGFP to the outer membrane of the organelle.

Taken these results together we concluded that Sirt4-sfGFP locates exclusively at the outer mitochondrial membrane.

Figure 14

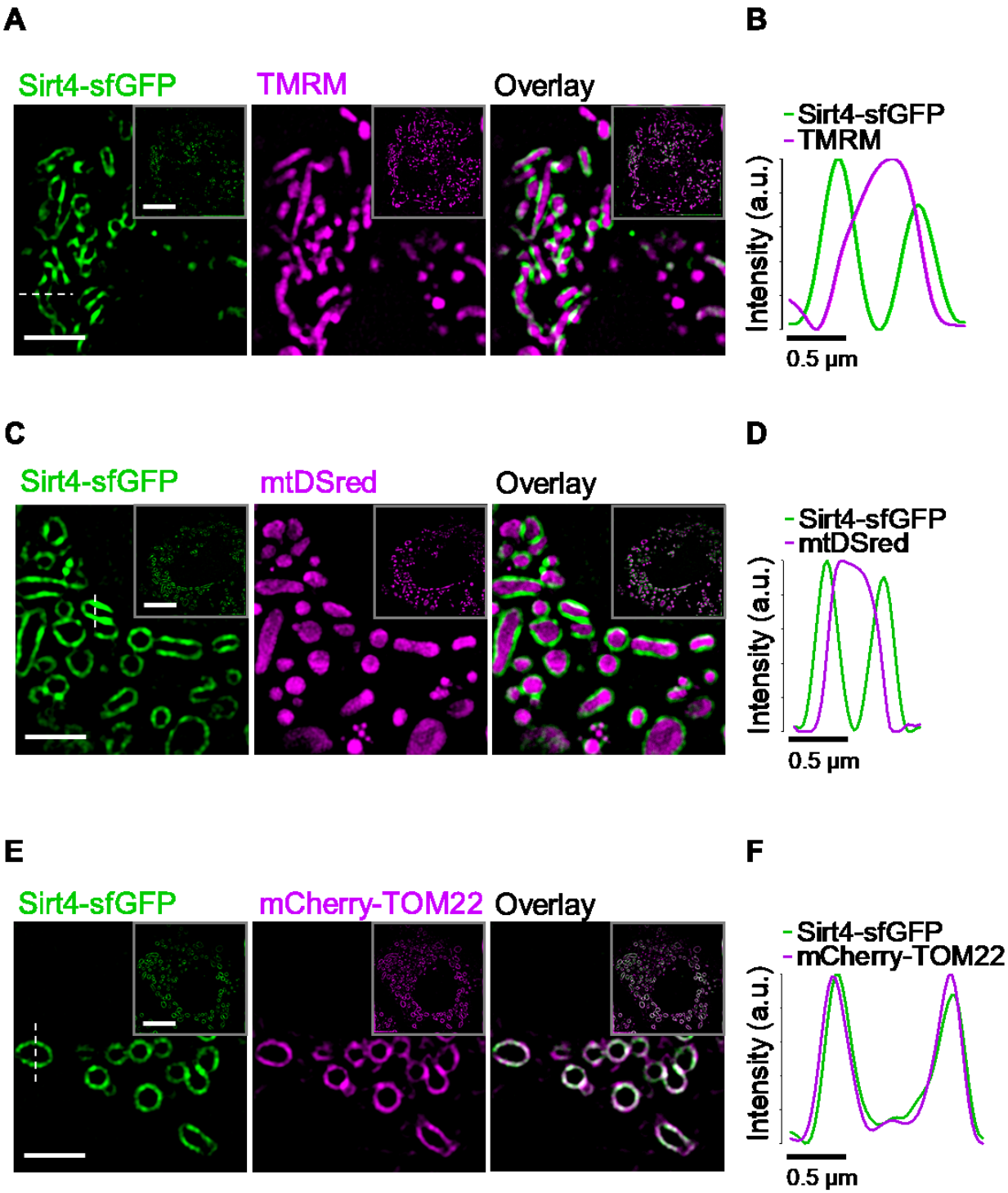

Figure 14. Visualization of the localization of Sirt4-sfGFP using super resolution microscopy. (A) Representative SIM images of HeLa cells expressing Sirt4-sfGFP (left image in green), TMRM (middle image in magenta) and illustrated as an overlay of Sirt4-sfGFP and TMRM. Scale bar represents 2.5 µm in the zoomed image. In the lower left square the whole cell is displayed with a scale bar corresponding to 10 µm.

Pearson correlation coefficient: 0.34 (mean) with a standard deviation of 0.14, n = 3. **(B)** Line scan as a representative of an individual mitochondrion like in the illustration shown in **(A)** (left panel, white dashed line). **(C)** Identical experiment as this in **(A)**, but using mtDsRed to stain the cells. **(D)** Same performance of a line scan as this in **(B)**, but by staining cells with mtDsRed. Pearson correlation coefficient: 0.33 (mean) with a standard deviation of 0.07, n = 3. **(E)** Identical image series as this in **(A),** but transfecting cells with mCherry-TOM22. **(F)** Line scan analysis as this in **(B)**, but with the expression of mCherry-TOM22 in HeLa cells. Pearson correlation coefficient: 0.74 (mean) with a standard deviation of 0.10, n = 3. [Figure panels reproduced from Ramadani-Muja et al., Cells 2019.]

4.15. Expression of Sirt4-sfGFP induced mitochondrial swelling

Having a closer look at the images recorded by the confocal microscope we observed peculiar mitochondrial structures in HeLa cells expressing Sirt4-sfGFP compared to 2mt-sfGFP, namely blown up mitochondria **(Figure 15A and B)** (1)**.** Therefore we applied the SIM by using 2mt-sfGFP and mCherry-TOM22 as markers to find out, whether Sirt4-sfGPF expressed in HeLa cells might induce mitochondrial swelling. We calculated the aspect ratio, as the ratio between the major (height) and minor (width) axes of the ellipse equivalent to the mitochondrion and we determined the mitochondrial area. Both, the minor of mitochondria and the mitochondrial area in HeLa cells expressing Sirt4-sfGFP were significantly higher compared to cells expressing 2mt-sfGFP **(Figure 15C and D)** (1)**.** These calculations indicate that expression of Sirt4-sfGFP is responsible for the swelling of mitochondria.

The major axis and the form factor between HeLa cells expressing 2mt-sfGFP or Sirt4-sfGFP did not show any significant differences, indicating that the overall morphology of swelled mitochondria was not affected by Sirt4-sfGFP **(Figure 15C and E)** (1)**.**

Figure 15

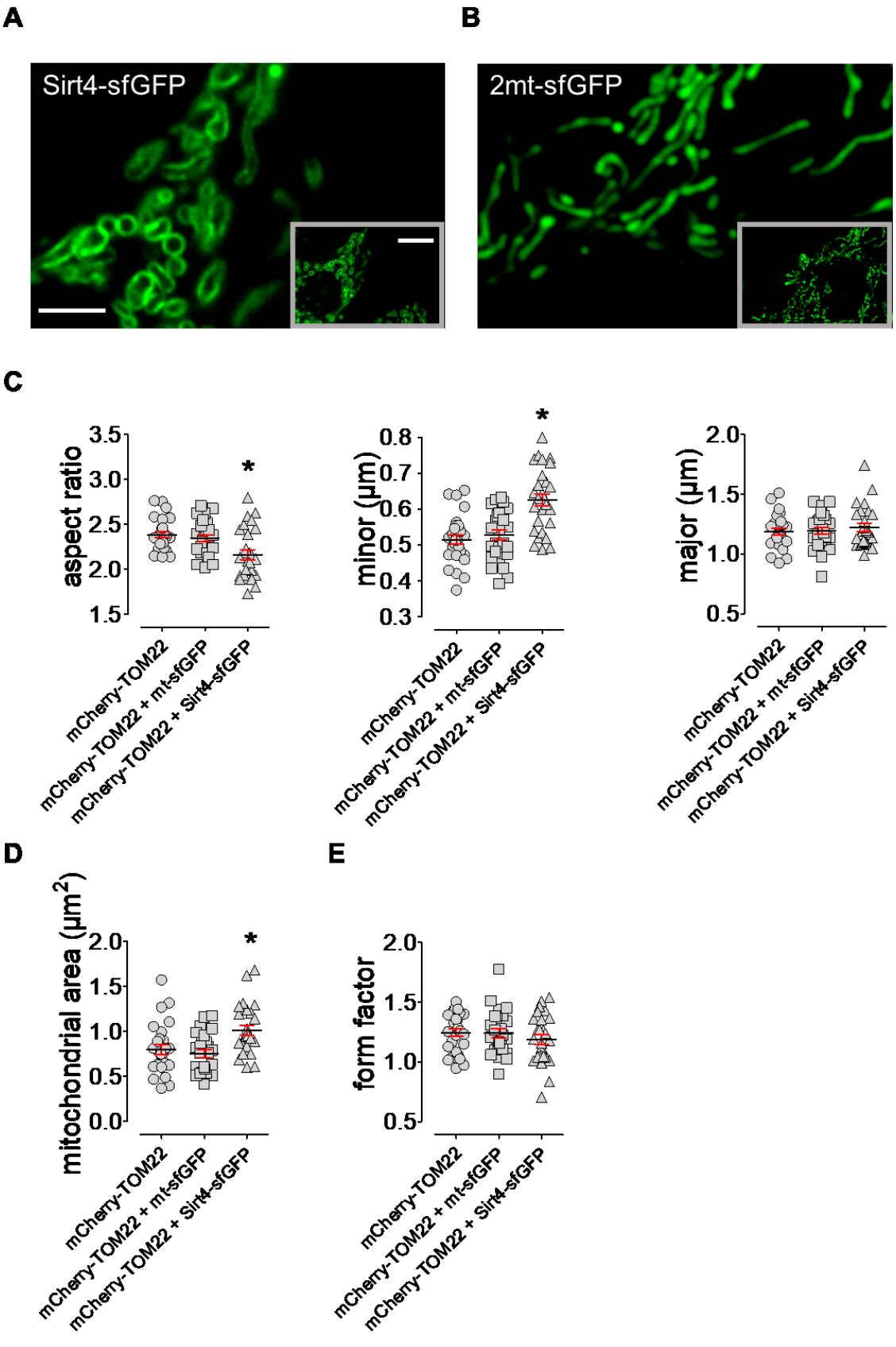
A
B
Sirt4-sfGFP
2mt-sfGFP
C
aspect ratio
minor (µm)
major (µm)
D
mitochondrial area (µm²)
E
form factor
mCherry-TOM22
mCherry-TOM22 + mt-sfGFP
mCherry-TOM22 + Sirt4-sfGFP
*

Figure 15. Determining mitochondrial morphology by the calculation of various established parameters. (A) Representative confocal image of HeLa cell expressing Sirt4-sfGFP. Scale bar indicating 2.5 µm in the zoomed image. In the right left square the whole cell is shown with a scale bar representing 10 µm. **(B)** Identical experiment as this in **(A)**, but using HeLa cells expressing 2mt-sfGFP. **(C)** Diagram on the left side showing values of the aspect ratio. Middle and right diagram display the minor and major values, respectively. **(D)** Diagram showing the values of the mitochondrial area. **(E)** Diagram, which illustrates the form factor. For all conditions, cells are represented in grey shapes, respectively. Data are shown as the mean ± SEM; n= 30 cells. For testing significance ANOVA with Bonferroni post-hoc test was used. (*P< 0.05) [Figure panels reproduced from Ramadani-Muja et al., Cells 2019.]

4.16. Fusion of slower maturing FPs to Sirt4 improve the targeting efficiency to mitochondria

Due to the fact, that Sirt4 harbors a classic N-terminal mitochondrial targeting sequence (153), it should be imported into the lumen of mitochondria. Our results so far however clearly demonstrate the localization of Sirt4-sfGFP exclusively to the outer membrane of mitochondria. That is the reason, why we were thinking whether the fast maturation kinetic of sfGFP prevents the complete import of Sirt4 into the mitochondrial matrix, because folding of sfGFP precedes the transport of Sirt4-sfGFP into the organelle and as a result the probe is trapped to the outer mitochondrial membrane.

Accordingly we decided to fuse Sirt4 to FPs with slower maturation kinetics and find out, whether the targeting efficiency is improved, compared to that one of Sirt4-sfGFP.

Thus, we fused Sirt4 to a FP with a slightly slower maturation time than sfGFP, namely to enhanced GFP (eGFP) (144) and generated thereby Sirt4-eGFP **(Figure 16A)**. The second construct we designed was Sirt4-mCherry, where we fused Sirt4 to an even slower maturing FP than eGFP, such as the mCherry **(Figure 16B)** (144).

We expressed Sirt4-sfGFP, Sirt4-eGFP and Sirt4-mCherry in intact living HeLa cells respectively.

Fusion of eGFP to Sirt4 showed a slight improvement in the targeting efficiency into mitochondria up to 65%, compared to that one of Sirt4-sfGFP where in 60% of all cells the respective probe was located to mitochondria only **(Figure 16C)**.

As expected HeLa cells expressing Sirt4-mCherry displayed a significant improvement in the mitochondrial targeting efficiency of up to 90% compared to that one of Sirt4-sfGFP (60%) and Sirt4-eGFP (65%), respectively **(Figure 16C)**.

Our results so far might indicate, that fusion of Sirt4 to slower folding FPs lead to a better targeting efficiency to mitochondria compared to fusion constructs with faster folding FP, such as sfGFP or eGFP. We also think that these data emphasize our hypothesis of a rather weak mitochondrial targeting efficiency of Sirt4, particularly if it is fused to fast maturating FPs.

Figure 16

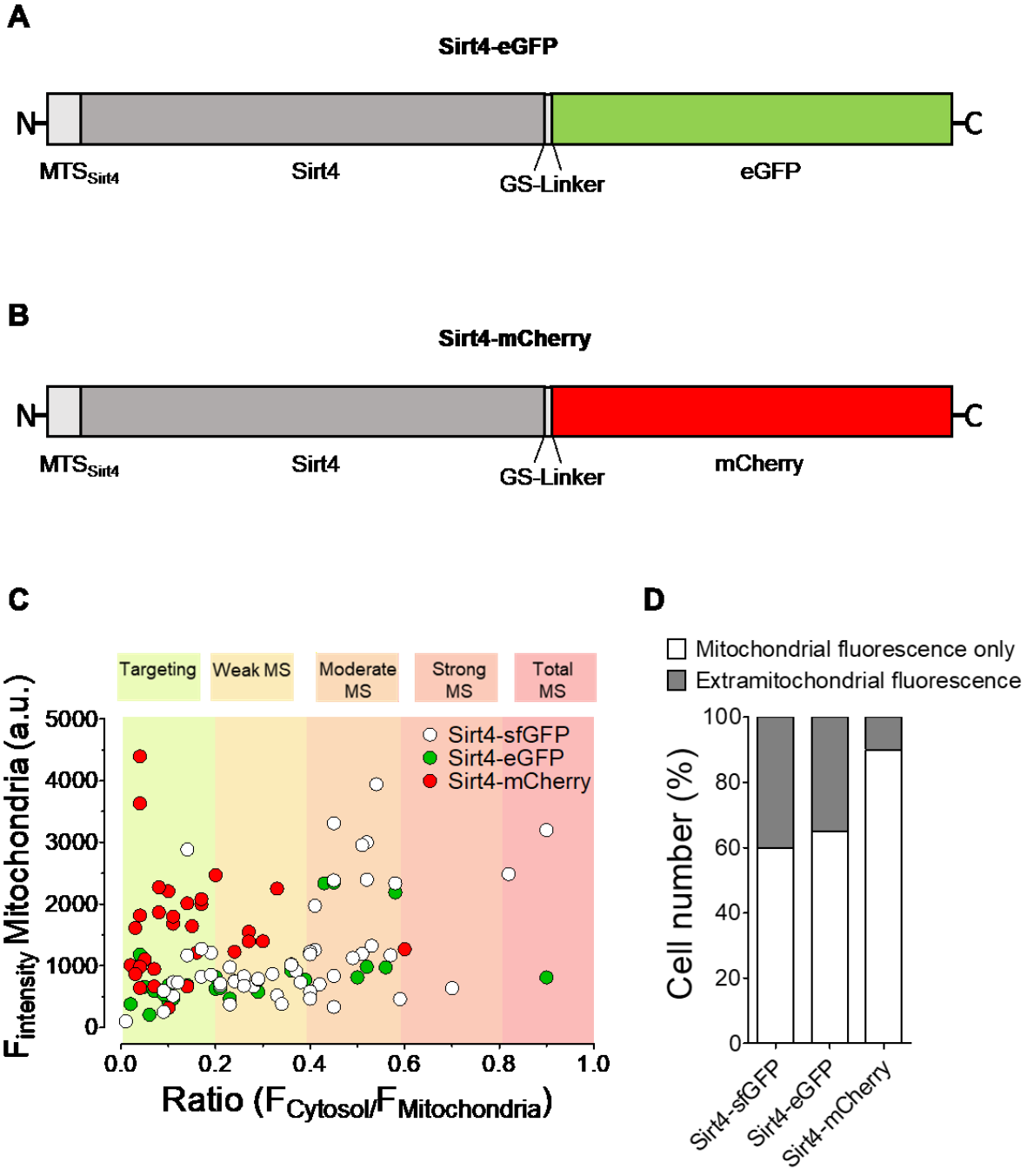

Figure 16. Visualization of the mitochondrial targeting efficiency of Sirt4-eGFP and Sirt4-mCherry respectively, compared to Sirt4-sfGFP. (A) Scematic overview of Sirt4-eGFP. Illustration of the mitochondrial targeting sequence of Sirt4 (MTS_{Sirt4}) shown in light grey, followed by the rest of Sirt4, which is depicted in dark grey (Sirt4). Sirt4 is fused to the C-terminus of the eGFP, shown in green (eGFP). **(A)** Scematic illustration of Sirt4-mCherry, identical construct as in **(A)** but Sirt4 is fused to mCherry, shown in red (mCherry). **(C)** Diagram, displaying HeLa cells expressing Sirt4-sfGFP, Sirt4-eGFP and Sirt4-mCherry, respectively where the dots are depicted as ratio values of the cytosolic fluorescence and the mitochondrial fluorescence and plotted against the mitochondrial fluorescence intensity values. Two independent experiments were done. n = 30 cells (Sirt4-mCherry), n = 25 cells (Sirt4-eGFP), n = 52 cells (Sirt4-sfGFP).

4.17. Import of Sirt4 into the mitochondrial matrix visualized by the self-complementing split-FP variant of sfCherry2

We could show so far, that fusion of full FPs varying in their maturation kinetics can drastically influence the mitochondrial targeting efficiency, such as it is the case with Sirt4 fused to sfGFP, eGFP and mCherry, respectively **(Figure 16)**. Fusion of Sirt4 to sfGFP also led to trapping of the probe to the outer mitochondrial membrane and induced mitochondrial swelling **(Figure 13, 14 and 15)**.

To avoid these kind of unintentional effects, we end up with fusion of a small tag to Sirt4. This tag represents a 17 amino acids short β-barrel strand of sfCherry2, which we linked on the C-terminus of Sirt4, generating thereby Sirt4-sfCherry2_{11} **(Figure 17A)** (1) (161). On the other hand we targeted the complementary part of the sfCherry2, namely the sfCherry2_{1-10} (161) to the mitochondrial matrix, using the established mitochondrial targeting sequence of the COXVIII in the dimeric tandem repeat (136) and got by that MTS-sfCherry2_{1-10} **(Figure 17B)** (1)**.** Red fluorescence would be detectable due to the self-complementation of Sirt4-sfCherry2_{11} with MTS-sfCherry2_{1-10} if Sirt4-sfCherry2_{11} is completely imported into the lumen of mitochondria **(Figure 17C)** (1).

We were able to confirm the import of Sirt4-sfCherry2_{11} to the mitochondrial matrix by exploiting this established approach (162). Co-expression of Sirt4-sfCherry2_{11} and MTS-sfCherry2_{1-10} in HeLa cells resulted in a dominant red fluorescence signal, arising from mitochondria **(Figure 17D)** (1), indicating the entire import of Sirt4-sfCherry2_{11} into the mitochondrial matrix.

Additionally, performing a series of co-localization experiments on the confocal microscope proved the import of Sirt4-sfCherry2$_{11}$ into the lumen of mitochondria. Staining HeLa cells with MitoTracker^{TM} Green FM, which co-expressed Sirt4-sfCherry2$_{11}$ and MTS-sfCherry2$_{1-10}$ showed a high co-localization when we overlaid the images **(Figure 17E)** (1). Furthermore, analyzing the images of HeLa cells co-expressing Sirt4-sfCherry2$_{11}$ and MTS-sfCherry2$_{1-10}$ with both 2mt-sfGFP **(Figure 17F)** (1) and seCFP-OMP25 **(Figure 17G)** (1), respectively verified the localization of Sirt4-sfCherry2$_{11}$ complemented with MTS-sfCherry2$_{1-10}$ exclusively to the mitochondrial matrix.

Figure 17

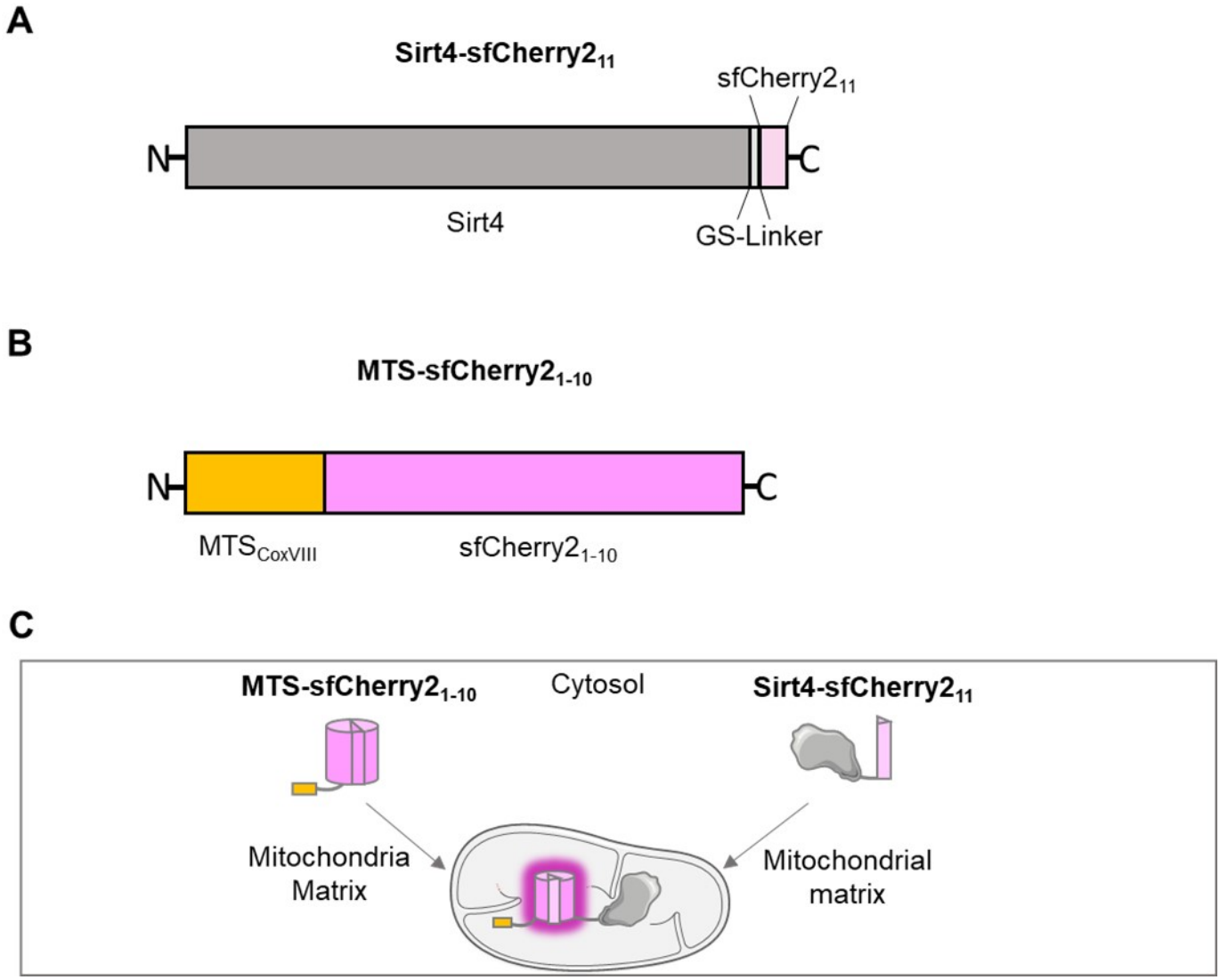

D

MTS-sfCherry2$_{1-10}$ + Sirt4-sfCherry2$_{11}$

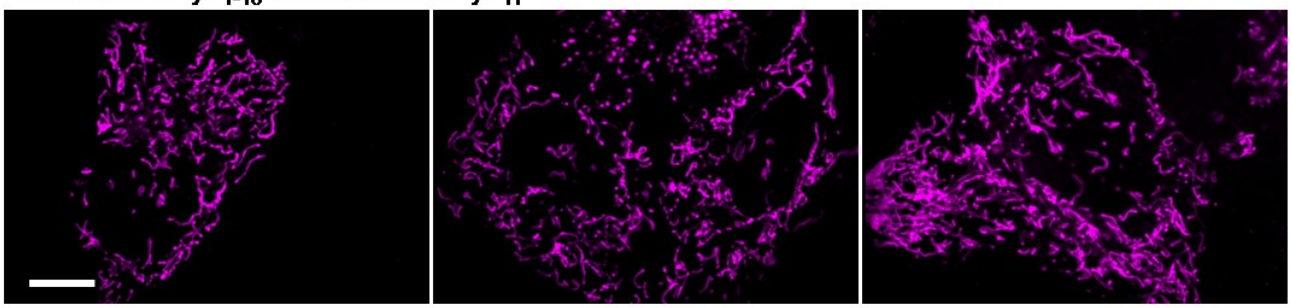

E

MTS-sfCherry2$_{1-10}$ + Sirt4-sfCherry2$_{11}$ | mitoTrackerGreen | Overlay

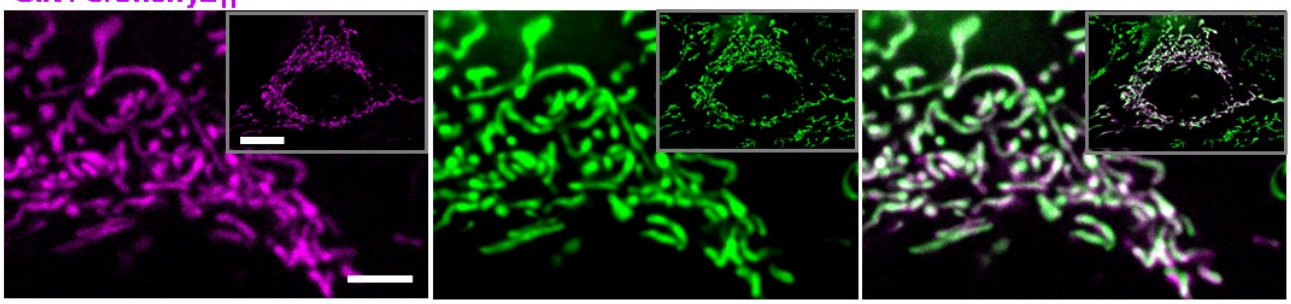

F

MTS-sfCherry2$_{1-10}$ + Sirt4-sfCherry2$_{11}$ | 2mt-sfGFP | Overlay

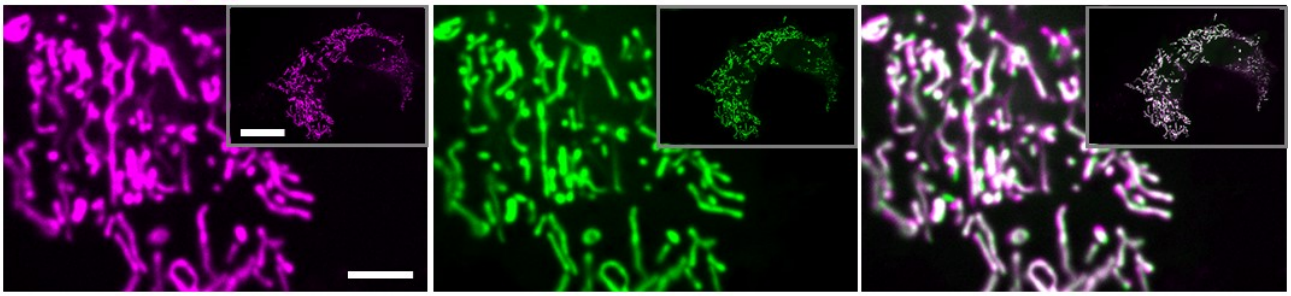

G

MTS-sfCherry2$_{1-10}$ + Sirt4-sfCherry2$_{11}$ | seCFP-OMP25 | Overlay

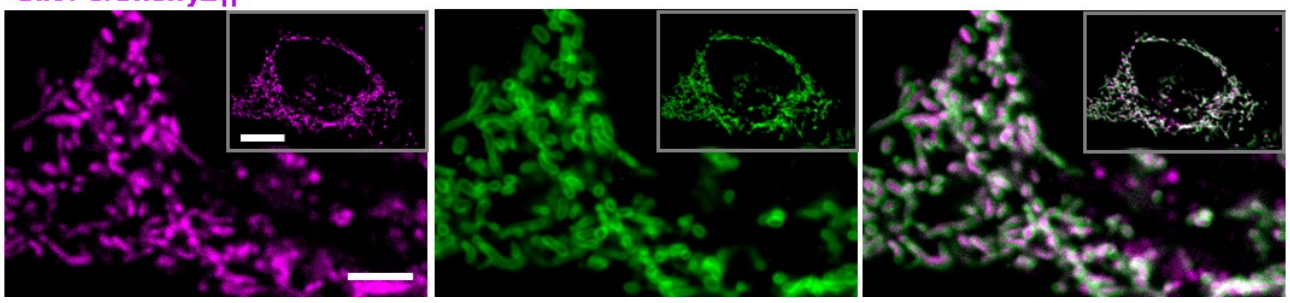

Figure 17. Application of the established split-sfCherry2 approach enables the visualization of the import of Sirt4-sfCherry2$_{11}$ into the lumen of mitochondria. (A) Scematic image of the Sirt4, shown in dark grey, followed by a GS-linker (in light grey) and sfCherry2$_{11}$ (light pink). **(B)** Scematic overview of the MTS-sfCherry2$_{1-10}$, starting with the mitochondrial targeting sequence (MTS$_{CoxVIII}$) shown in orange and fused C-terminally to the sfCherry2$_{1-10}$, here depicted in dark pink. **(C)** Scematic illustration of the self-complementation split-FP approach, containing sfCherry2$_{1-10}$ fused N-terminally to the mitochondrial targeting sequence of the COXVIII (MTS-sfCherry2$_{1-10}$) and the Sirt4 fused to the complementary sfCherry2$_{11}$ (Sirt4-sfCherry2$_{11}$). Red luminal mitochondrial fluorescence is detectable upon self-complementation of sfCherry2 in the mitochondrial matrix. **(D)** Three confocal images representing HeLa cells co-expressing both MTS-sfCherry2$_{1-10}$ and Sirt4-sfCherry2$_{11}$ shown as fluorescence signals in magenta. Scale bar corresponds to 10 µm. **(E)** Representative confocal recordings of HeLa cells expressing MTS-sfCherry2$_{1-10}$ and Sirt4-sfCherry2$_{11}$ (magenta) and stained with MitoTracker^{TM} Green FM (green). The third illustration shows the merged channels. Scale bar indicates 2.5 µm. In the upper right corner of each individual image of the series a square is shown respectively representing the whole cell. Scale bar 10 µm. Pearson correlation coefficient: 0.73 (mean) with a standard deviation of 0.07. **(F)** Same experiments as those in **(E)**, but expressing 2mt-sfGFP (green). Pearson correlation coefficient: 0.78 (mean) with a standard deviation of 0.12. **(G)** Identical experiments as in **(E)**, but using seCFP-OMP25 (green). Pearson correlation coefficient: 0.64 (mean) with a standard deviation of 0.09. Three independent experiments were done, encompassing 30 different cells. [Figure panels reproduced from Ramadani-Muja et al., Cells 2019.]

4.18. mito-STAR, a tripartite self-complementing FP-based probe enables the visualization of the distribution of Sirt4 between mitochondria and the nucleus in living cells

By applying the self-complementation split-FP approach we could show that Sirt4 is entirely imported into the lumen of mitochondria **(Figure 17)**. However, Zeng et al. demonstrate the possibility of Sirt4 being also abundant in the nucleus (156).

Therefore we aimed to expand the bimolecular approach based on self-complementation split-FP in order to visualize the possible distribution of Sirt4 between mitochondria and the nucleus. For this purpose we added a nuclear-located non-fluorescent sfCherry2$_{1-10}$ (sfCherry2$_{1-10}$-NLS) by exploiting an established nuclear localizing sequence (NLS) (138), which is repeated three times **(Figure 18A)** (1).

For the design of the tripartite self-complementation split-FP probe we also incorporated the P2A peptide, which has a strong self-cleavage activity to achieve equal amounts of all three part, namely of MTS-sfCherry2_{1-10}, Sirt4-sfCherry211 and sfCherry2_{1-10}-NLS respectively and to avoid low efficient expression levels upon co-transfection **(Figure 18A)** (1). The novel design probe bears the name mito-STAR, meaning **mito**chondrial **S**irt4 **T**ripartite **A**bundance **R**eporter (1).

A red fluorescence signal would be detectable by the self-complementation of the two non-fluorescent sfCherry2_{1-10}, which are located in the mitochondria and the nucleus respectively, with Sirt4-sfCherry2_{11} **(Figure 18B)** (1). The fluorescence signal represents a direct measure of the subcellular distribution of Sirt4 in a particular cell.

When we expressed mito-STAR in HeLa cells we found out that in 80% of the transfected cells the two split-FPs self-complemented to sfCherry2 exclusively within the mitochondrial matrix **(Figure 18C, E and F)** (1), indicating the occurrence of Sirt4-sfCherry2_{11} in the lumen of mitochondria only.

However, we found a population of cells, namely 20% of all HeLa cells expressing mito-STAR, where a red fluorescence signal was detectable within the nucleus, indicating the self-complementation of sfCherry2 hence the abundance of Sirt4-sfCherry2_{11} in the nucleus additionally to mitochondria **(Figure 18C, E and F)** (1).

We demonstrated that in HeLa cells expressing mito-STAR the expression level of the particular probe, represented as the overall fluorescence intensity did not positively correlate with the nuclear fluorescence under control conditions (generated pearson coefficient of 0.11) (1).

Next we applied mito-STAR to study the subcellular distribution of Sirt4-sfCherry2_{11} in INS-1 cells. 70% of all INS-1 cells expressing mito-STAR showed a red fluorescence signal coming from mitochondria only, indicating the self-complementation of sfCherry2 in the matrix of mitochondria **(Figure 18C, E and F)** (1). This means that in these cells Sirt4-sfCherry2_{11} occurs in mitochondria only. Yet, in 30% of all positively transfected INS-1 cells, which expressed mito-STAR we detected a red fluorescence signal arising from the nucleus, indicating the presence of Sirt4-sfCherry2_{11} in the nucleus **(Figure 18C, E and F)** (1).

Figure 18

A

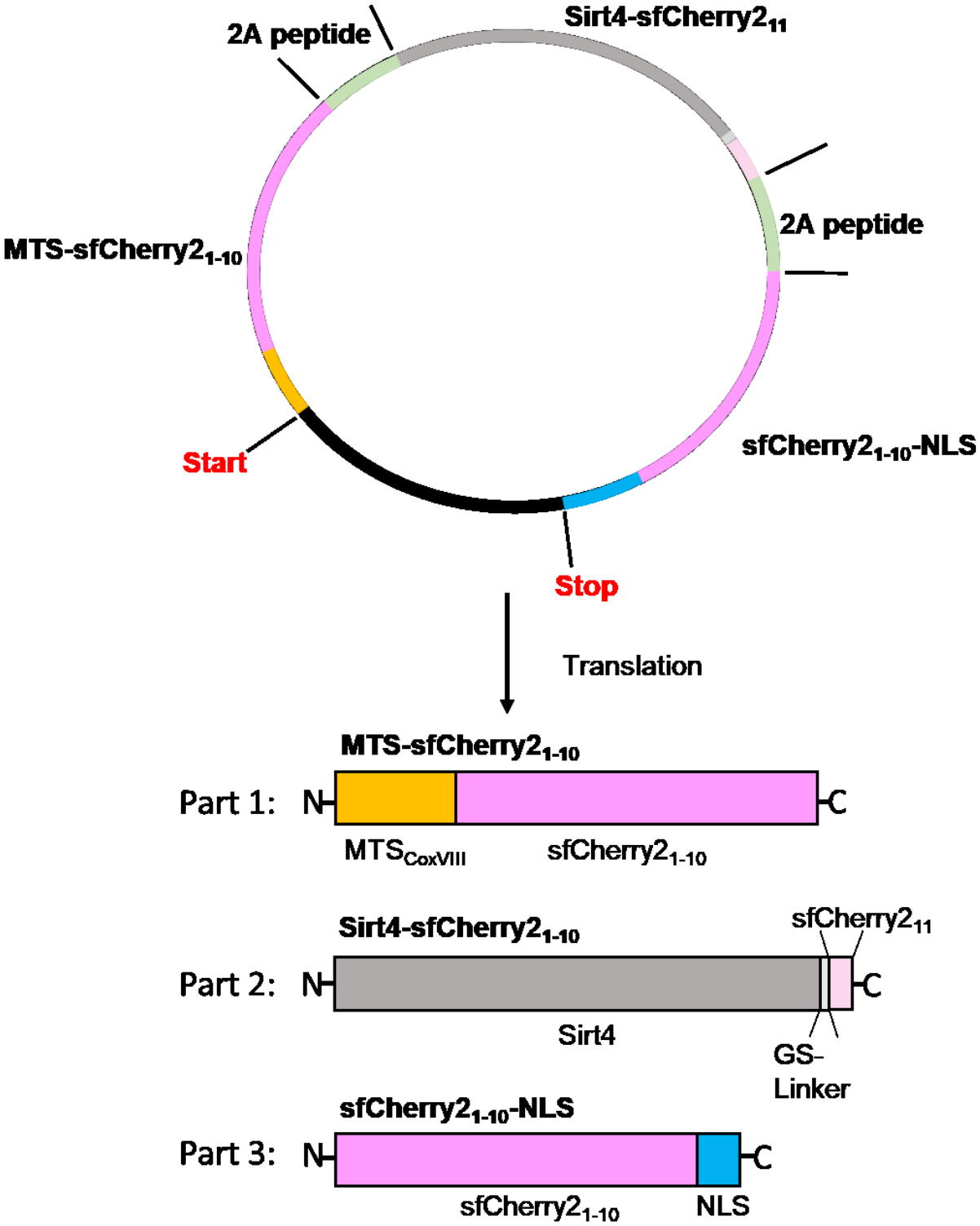
2A peptide
Sirt4-sfCherry2$_{11}$
MTS-sfCherry2$_{1-10}$
2A peptide
Start
sfCherry2$_{1-10}$-NLS
Stop
Translation
MTS-sfCherry2$_{1-10}$
Part 1: N C
MTS$_{CoxVIII}$
sfCherry2$_{1-10}$
Sirt4-sfCherry2$_{1-10}$
sfCherry2$_{11}$
Part 2: N C
Sirt4
GS-
Linker
sfCherry2$_{1-10}$-NLS
Part 3: N C
sfCherry2$_{1-10}$
NLS

B

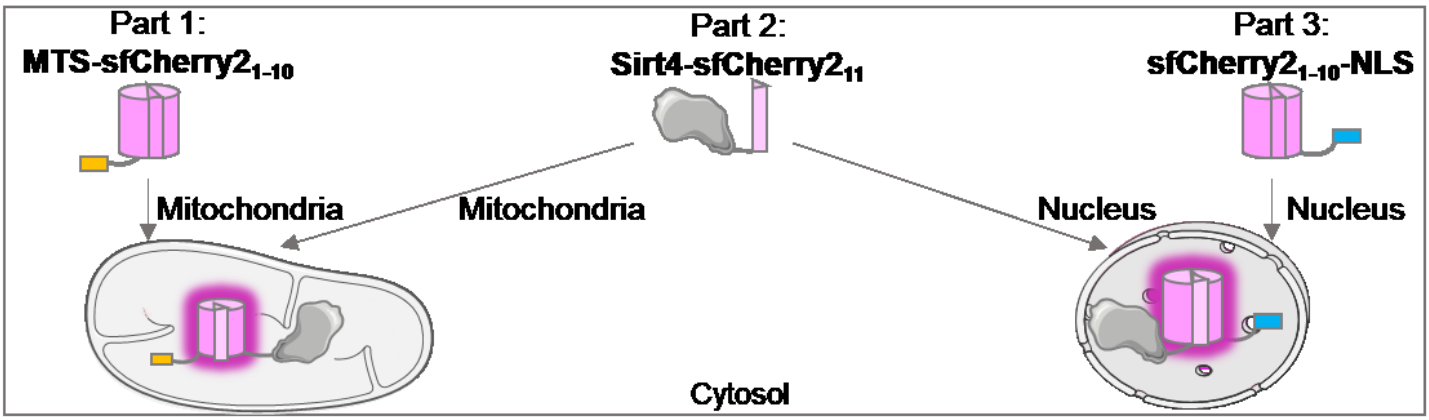
Part 1:
MTS-sfCherry2$_{1-10}$
Part 2:
Sirt4-sfCherry2$_{11}$
Part 3:
sfCherry2$_{1-10}$-NLS
Mitochondria
Mitochondria
Nucleus
Nucleus
Cytosol

C

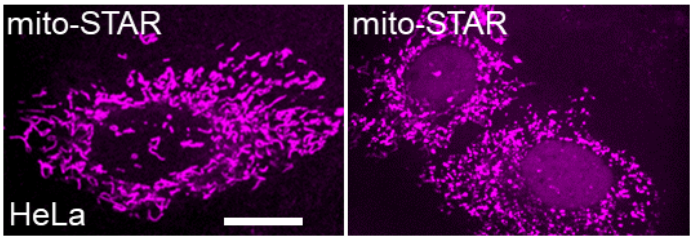
mito-STAR
mito-STAR
HeLa

D

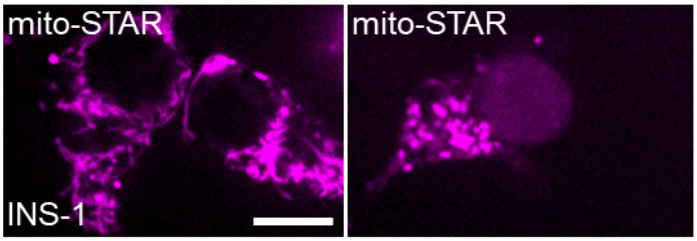
mito-STAR
mito-STAR
INS-1

E

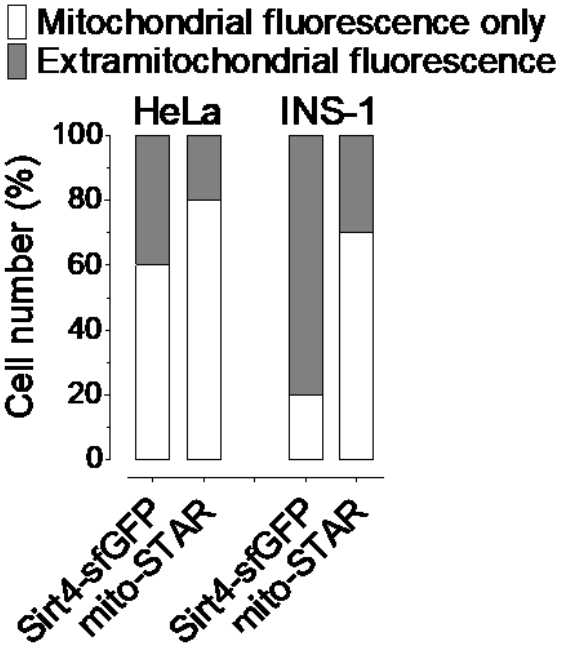
Mitochondrial fluorescence only
Extramitochondrial fluorescence
HeLa
INS-1
Cell number (%)
100
80
60
40
20
0
Sirt4-sfGFP
mito-STAR
Sirt4-sfGFP
mito-STAR

F

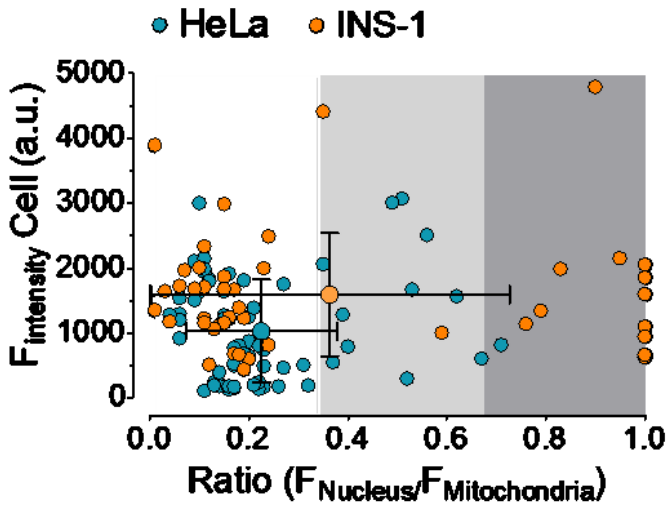
HeLa
INS-1
$F_{intensity}$ Cell (a.u.)
5000
4000
3000
2000
1000
0
0.0
0.2
0.4
0.6
0.8
1.0
Ratio ($F_{Nucleus}/F_{Mitochondria}$)

Figure 18. Application of the established split-sfCherry2 approach enables the visualization of the import of Sirt4-sfCherry2$_{11}$ into the lumen of mitochondria. (A) Overview of the sensor design of mito-STAR. Scematic depiction of the plasmid coding for mito-STAR, harboring three parts (MTS-sfCherry2$_{1-10}$, Sirt4-sfCherry2$_{11}$ and sfCherry21$_{1-10}$-NLS). Between each part a 2A peptide with self-cleavage activity is inserted (green). The probe results in three differentially targeted individual parts upon translation. Part 1 illustrating MTS-sfCherry2$_{1-10}$. Part 2 shows Sirt4-sfCherry2$_{1-10}$. Part 3 displays sfCherry2$_{11}$-NLS. **(B)** Scematic summary of the principle of mito-STAR in the cell. Sirt4-sfCherry2$_{11}$ upon import into mitochondria or the nucleus is shown as a red fluorescence signal (displayed in magenta) in mitochondria and/or the nucleus, respectively. **(C)** Confocal images, representing HeLa cells expressing mito-STAR with Sirt4-sfCherry2$_{11}$ being located in mitochondria only (left image) and Sirt4-sfCherry2$_{11}$ being distributed in addition to mitochondria also extra mitochondrially (right image). Scale bar corresponds to 10 µm. **(D)** Identical experiments as in **(C)**, but representing INS-1 cells. Scale bar indicates 10 µm. **(E)** Illustration of the percentage of Hela cells and INS-1 cells. Expressing either Sirt4-sfGFP or mito-STAR, which is representing mitochondrial fluorescence only or extra mitochondrial fluorescence. N = 120 cells (HeLa); n = 74 cells (INS-1). **(F)** Diagram of dots, which are calculated as nuclear fluorescence to cytosolic fluorescence of HeLa cells and INS-1 cells expressing mito-STAR. Calculated values are plotted against the whole cell fluorescence intensity. Data are shown as ration with the mean ± SD; n = 67 cells (HeLa); n = 45 cells (INS-1); three independent experiments were performed, respectively. [Figure panels reproduced from Ramadani-Muja et al., Cells 2019.]

4.19. mito-STAR does not induce mitochondrial swelling in HeLa cells

Performing a series of imaging experiments we observed that Sirt4-sfCherry2$_{11}$ displayed a high co-localization with 2mt-sfGFP in the lumen of mitochondria **(Figure 19A)** (1) . We also verified the trapping of Sirt4-sfGFP to the outer mitochondrial membrane **(Figure 19B)** (1). Additionally we demonstrated that expression of mito-STAR in HeLa cells did not in induce mitochondrial swelling, as it was the case with Sirt4-sfGFP **(Figure 19C)** (1).

Figure 19

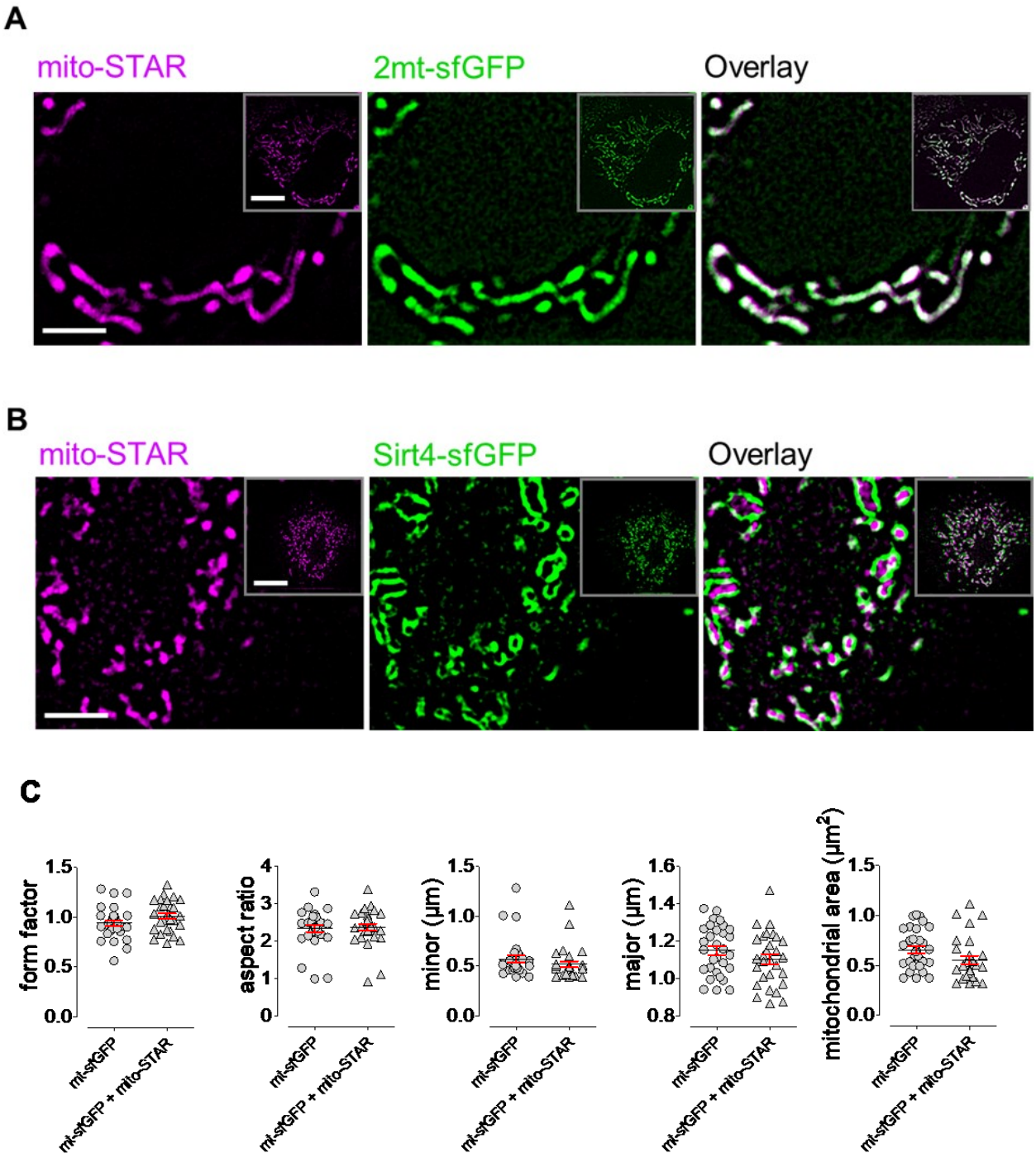

Figure 19. Analysis of the co-localization between mito-STAR and Sirt4-sfGFP and 2mt-sfGFP, respectively. (A) Representative images recorded with the SIM of HeLa cells expressing mito-STAR (magenta, left image) and 2mt-sfGFP (green, middle image). Image of the merged channels. Scale bar indicates 2.5µm. In the upper right corner of each image squares are showing the whole cell. Scale bar corresponds to 10 µm. **(B)** Same experimental approach as in **(A)**, but using Sirt4-sfGFP. Depicted experiments in **(A)** and **(B)** are representatives of 3 independent experiments, including 30 different cells.

(C) Calculation of different parameters for the analysis of the mitochondrial morphology. First diagram show values of the form factor. Second diagram represents the values of the calculated aspect ratios. Third and fourth diagram display values of the minor and major, respectively. Last diagram represents the values of the mitochondrial area. For all conditions, cells are shown in grey shapes, respectively. Data are illustrated as the mean ± SEM; n= 30 cells. For testing significance unpaired double sided t-test was applied. [Figure panels reproduced from Ramadani-Muja et al., Cells 2019.]

4.20. mito-STAR is suitable for the visualization of mitochondrial stress induced by oligomycin-A and antimycin-A1

In order to prove the suitability of mito-STAR to determine the subcellular distribution of Sirt4-sfCherry2$_{11}$ in living cells, we treated living HeLa cells, which expressed mito-STAR with oligomycin-A and antimycin-A1, known to depolarize the mitochondrial membrane potential (146) and induced thereby severe cell stress.

We imaged a dominant fluorescence signal arising from the nucleus in HeLa cells expressing mito-STAR, indicating the higher abundance of Sirt4-sfCherry2$_{11}$ in the nucleus upon mitochondrial stress, such as depolarization of the mitochondrial membrane potential **(Figure 20A)** (1).

Figure 20

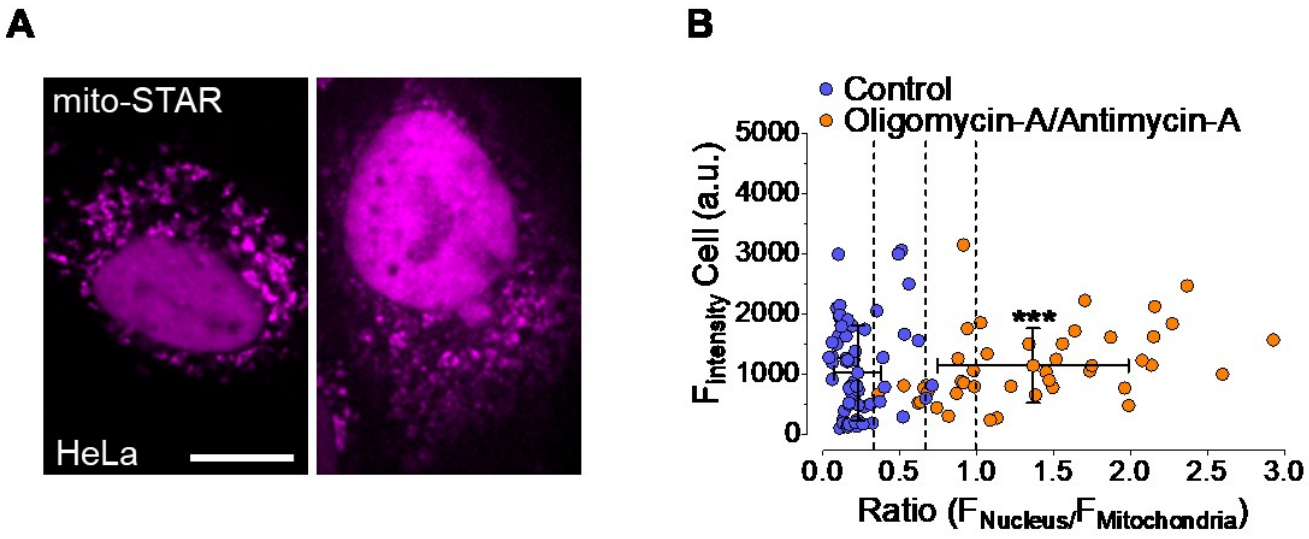

Figure 20. Application of the established split-sfCherry2 approach enables the visualization of the import of Sirt4-sfCherry2$_{11}$ into the lumen of mitochondria. (A) Two representative confocal images of HeLa cells expressing mito-STAR, which were treated with oligomycin-A and antimycin-A1. Scale bar corresponds to 10 µm. **(A)** Illustration of the ratio values of nuclear fluorescence to cytosolic fluorescence of HeLa cells expressing mito-STAR after treatment with oligomycin-A and antimycin-A1 against control condition. The calculated values were plotted against the whole cell fluorescence intensity. For each condition three independent experiments were done. Dots are shown as ratio values ± SD. N = 111 cells from 3 independent experiments (*** $p < 0.0001$, unpaired double-sided t-test). [Figure panels reproduced from Ramadani-Muja et al., Cells 2019.]

4.21. Development of mito-PRIMA, a dimerization-dependent FP based sensor to visualize defects in mitochondrial protein uptake with no need for optical resolution

Recapping all results so far it stands out that in almost all approaches we relied on sophisticated microscopes hence a high optical resolution. Therefore we wanted to offer a new class of sensors to study the mitochondrial protein import uptake, where there is no need for a high optical resolution.

As a result we came up with a new class of genetically encoded sensors, based on the dimerization-dependent FP-technology (ddFP) (141) in the green version, namely mito-PRIMA, which stands for **mito**chondrial **PR**otein **IM**port **A**nalyzer **(Figure 21A)**.

The idea behind the sensor is to fuse a dimeric tandem repeat of the mitochondrial targeting sequence of the COXVIII subunit (136) N-terminally to the non-fluorescent MonomerB (B) **(Figure 21A)**, which is efficiently imported into the lumen of mitochondria under conditions of an intact mitochondrial protein uptake **(Figure 21B)**. On the C-terminus of MonomerB we fused a nuclear localizing sequence (NLS) in a three times repeat (138) and end up eventually with 2mt-B-NLS **(Figure 21A)**. Due to cotranslational import of mitochondrial proteins however, the MTS is dominant over the NLS, meaning that under physiological conditions the NLS does not come into action **(Figure 21A)**. Under the same conditions the second part of the sensor, namely the green variant of the non-fluorescent MonomerA (GA), which harbors a green auto-fluorescence and is linked C-terminally to the established NLS in a three times repeat (GA-NLS), is transported to the nucleus **(Figure 21A and B)**. This means that under conditions of an intact mitochondrial protein import machinery we detect no fluorescence in the cell **(Figure 21B)**.

However, when the protein uptake machinery of mitochondria is somehow impaired, we know from previous experiments, that proteins fused to a mitochondrial targeting sequence accumulate in the cytosol and nucleus. Upon the abundance of 2mt-B-NLS in the cytosol, because of failed import, the NLS comes into play and is responsible for the transport and accumulation of 2mt-B-NLS into the nucleus **(Figure 21C)**. A green fluorescent signal would be detectable arising from the nucleus upon dimerization of MonomerA and MonomerB in the respective organelle as a direct indicator of defects in the mitochondrial protein import machinery **(Figure 21C)**.

Figure 21

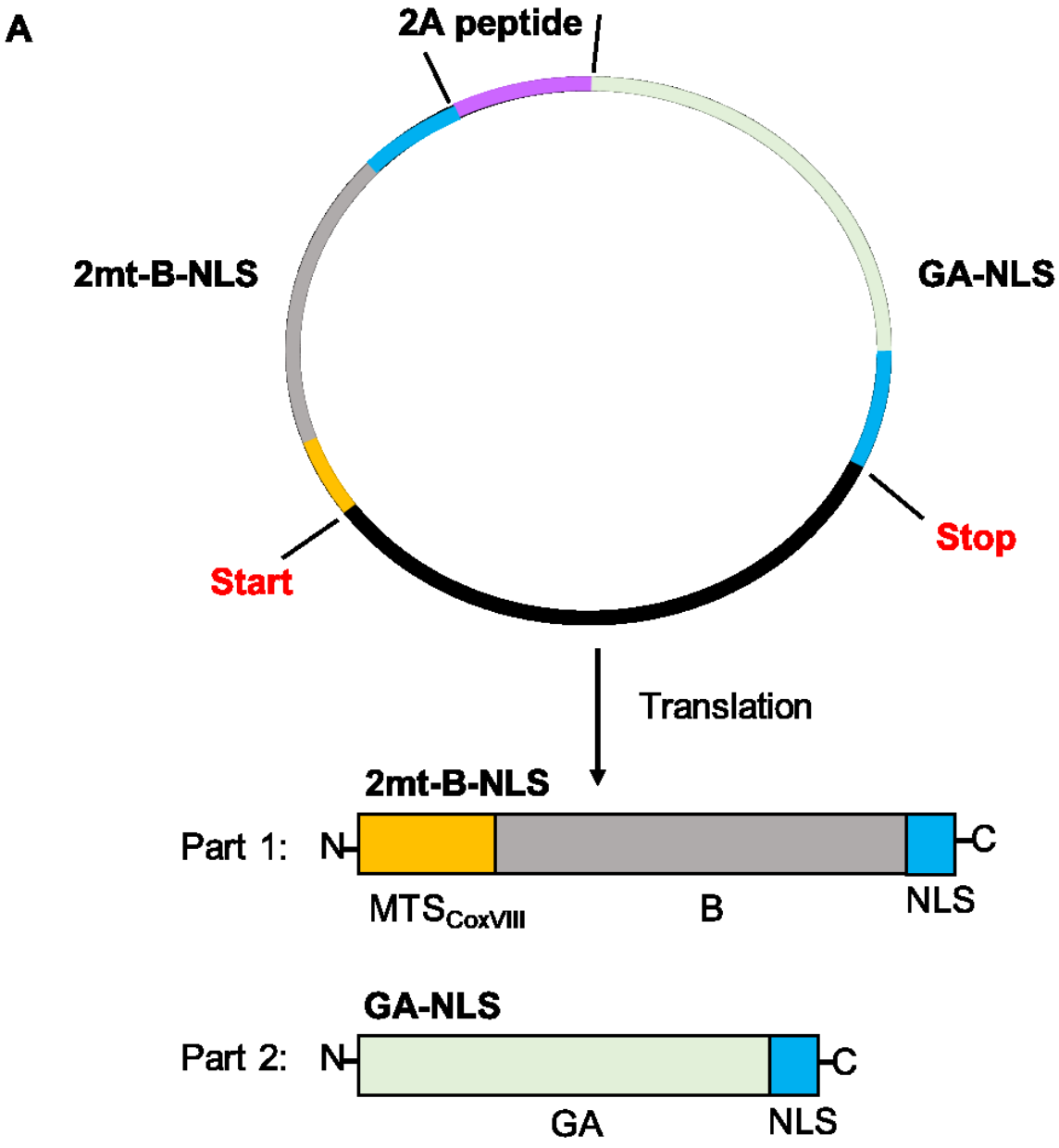

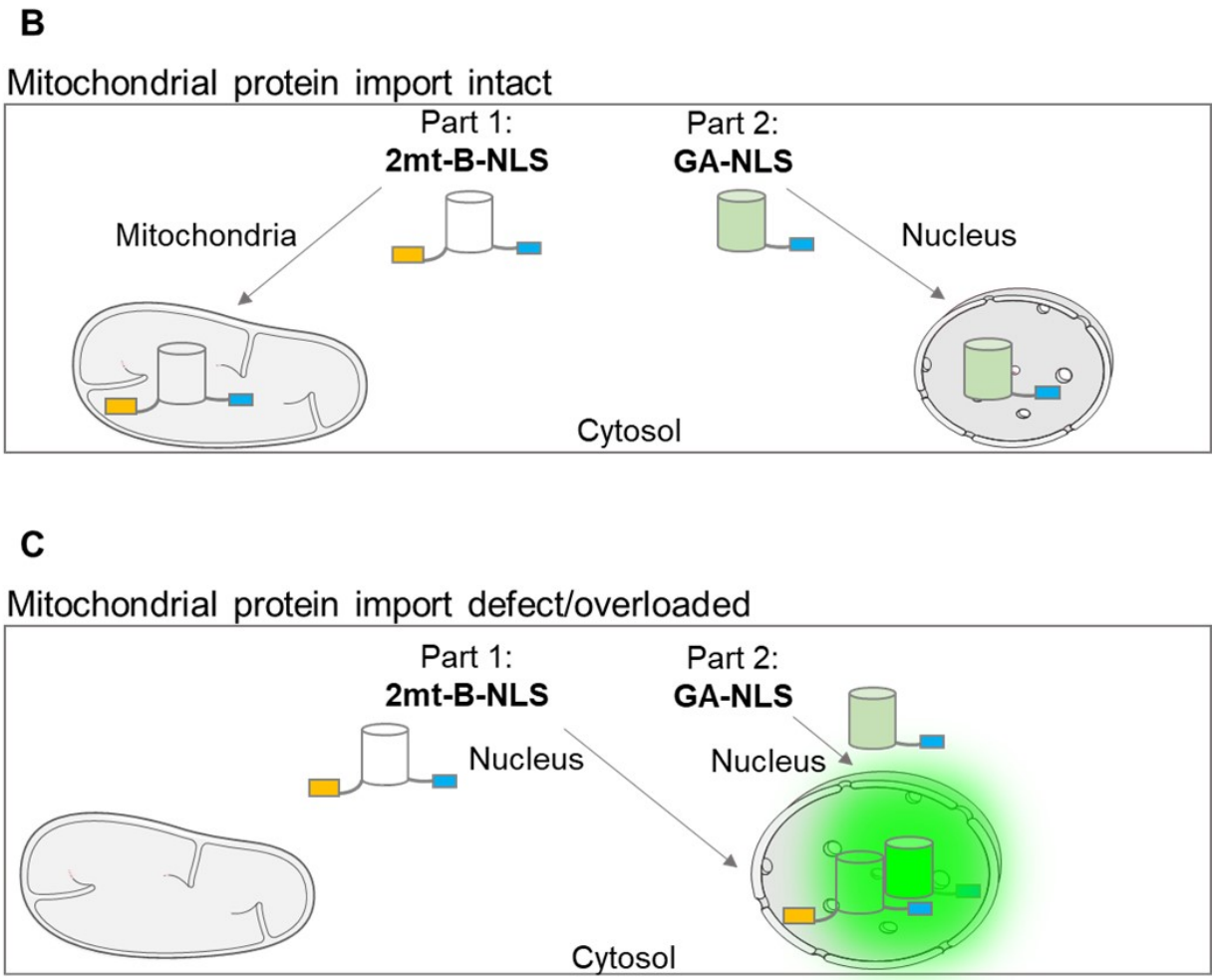

Figure 21. Design and Construction of the bipartite mito-RPIMA. (A) Overview of the plasmid encoding for mito-PRIMA, holding two parts (2mt-B-NLS and GA-NLS). A 2A peptide with self-cleavage activity is inserted between the two parts (purple). The sensor leads to two differentially targeted individual parts upon translation. Part 1 shows 2mt-B-NLS. Part 2 displays GA-NLS. **(B)** Scematic summary of the principle of mito-PRIMA in the cell under conditions of an intact mitochondrial protein import (MPI). 2mt-B-NLS upon import into mitochondria (displayed in grey) cannot dimerize with the complementary second part GA-NLS targeted to the nucleus (shown in light green because of the auto-fluorescence). **(C)** Scematic overview of the principle of mito-PRIMA in the cell under conditions of an defect or overloaded MPI. Upon failed import 2mt-B-NLS is transported into the nucleus, where the complementary GA-NLS is waiting to dimerize with part 1 of the sensor. Upon dimerization of the two parts a green fluorescent signal would be detectable in the cell.

4.22. mito-PRIMA lights up upon impaired mitochondrial protein import induced by depolarization of the mitochondrial membrane potential

Before testing the suitability of mito-PRIMA in HeLa cells we wanted to know which fluorescence signal intensities we have to expect, upon dimerization of both monomers in the nucleus. Therefore we co-expressed monomer A and monomer B fused to a NLS in a three times repeat, respectively, referred to as GA-NLS and B-NLS in HeLa cells.

Co-expression of GA-NLS and B-NLS in HeLa cells imaged on a confocal microscope resulted in a clear green fluorescence in the nucleus only, indicating the localization and successful dimerization of both monomers in the respective organelle **(Figure 22A, F and G)**. The expression level of HeLa cells co-transfected with GA-NLS and B-NLS showed a wide range, ranking from around 400 fluorescence intensity (arbitrary units) up to complete saturation of the imaging set-up **(Figure 22A, F and G)**.

In contrast to that expression of B-NLS in HeLa cells resulted in no fluorescence signal at all **(Figure 22B)** and when expressing GA-NLS in HeLa cells we detected in some cells a fluorescence signal **(Figure 22C, F and G)**, indicating the described auto-fluorescence of GA in the literature (141) (163), which can vary in its fluorescence intensity depending on the protein biosynthesis rate of the particular cell and/or on the amount of plasmids taken up by the cell.

Next, we expressed mito-PRIMA in HeLa cells and treated the cells with oligomycin-A and antimycin-A1. We detect a dominant fluorescence signal arising from the nucleus, comparable to that one of the condition, where we co-expressed GA-NLS and B-NLS, meaning that also under conditions of mitochondrial stress the expression level of mito-PRIMA was very heterogeneous **(Figure 22F and G)**. HeLa cells expressing mito-RPIMA under control conditions showed hardly any cell with a clear fluorescence signal coming from the nucleus **(Figure 22F and G)**. Yet, some cells depicted a nuclear fluorescence signal, which can be the auto-fluorescence of GA-NLS or might indicate failed import of 2mt-B-NLS into mitochondria, because of reasons we cannot say so far.

These results indicate the accumulation of 2mt-B-NLS in the nucleus, upon mistargeting induced by oligomycin-A and antimycin-A1 and hence the successful dimerization of 2mt-B-NLS with GA-NLS in the nucleus. Based on these observations we concluded, that mito-PRIMA is suitable to visualize failed import of mitochondrially targeted proteins.

Figure 22

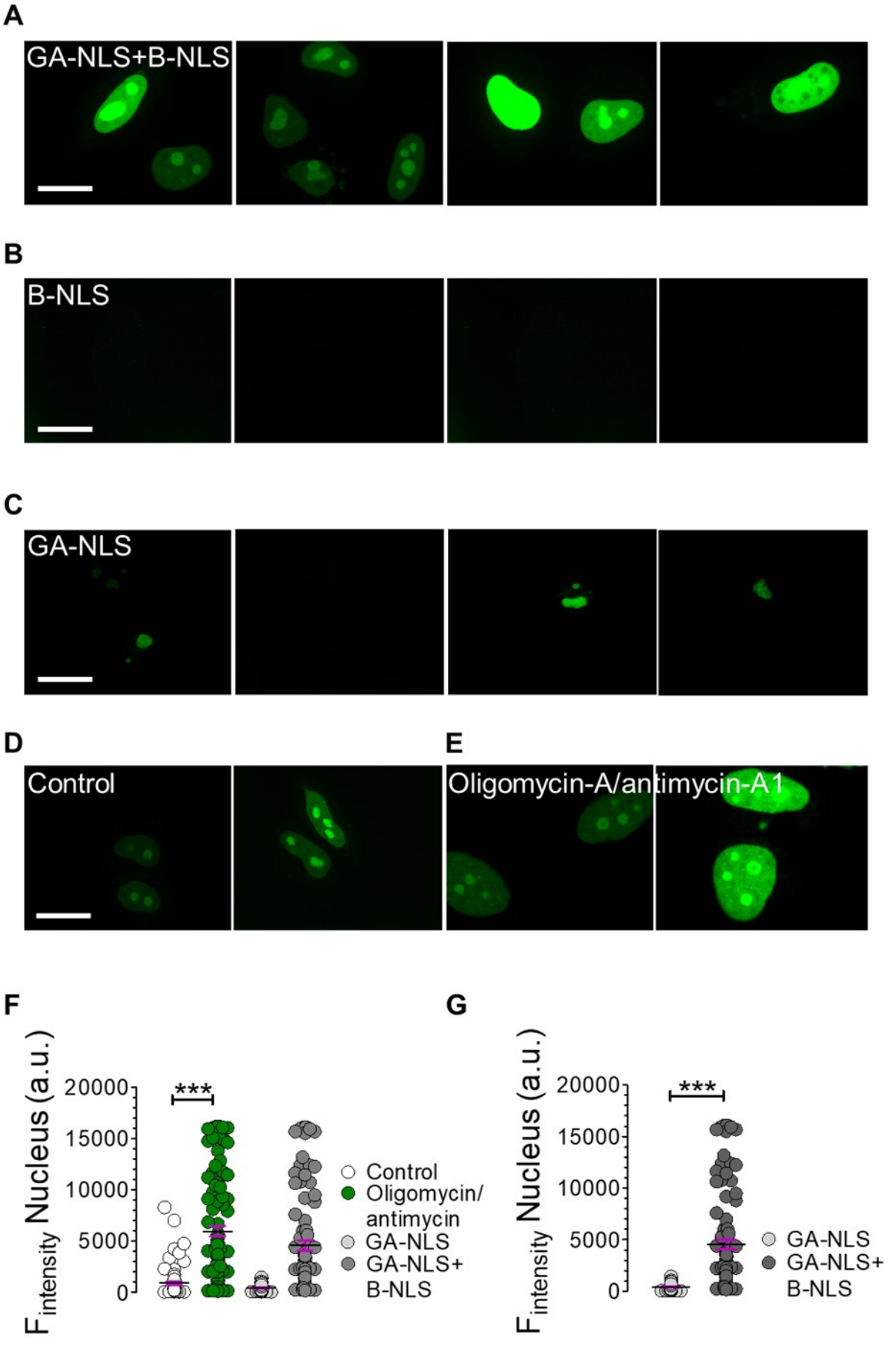
A
GA-NLS+B-NLS
B
B-NLS
C
GA-NLS
D
Control
E
Oligomycin-A/antimycin-A1
F
F intensity Nucleus (a.u.)
20000
15000
10000
5000
0
***
Control
Oligomycin/
antimycin
GA-NLS
GA-NLS+
B-NLS
G
F intensity Nucleus (a.u.)
20000
15000
10000
5000
0
***
GA-NLS
GA-NLS+
B-NLS

Figure 22. Application of mito-RPIMA in HeLa cells. (A) Four representative confocal images of HeLa cells co-expressing GA-NLS and B-NLS, showing heterogeneously green fluorescing nuclei. Scale bar indicates 10 µm. **(B)** Four recordings represented as confocal images of HeLa cells expressing B-NLS only, where no fluorescence can be seen. Scale bar corresponds to 10 µm. **(C)** Four representative confocal recordings displaying HeLa cells which expressed GA-NLS only. Slight auto-fluorescence is illustrated. Scale bar indicates 10 µm. **(D)** Two representative confocal images showing HeLa cells expressing mito-RPIMA under control conditions. Scale bar indicates 10 µm. (**E)** Identical experiment as in **(D)**, but cells are treated with oligomycin-A and antimycin-A1. (**F)** Illustration of the statistics of the average nuclear fluorescence intensities of each individual cell of 4 different conditions. Dots are shown as the mean ± SEM. N = 83 (control), n = 125 (oligomycin-A and antimycin-A1), n = 114 (GA-NLS), n = 104 (GA-NLS+B-NLS). Three independent experiments for each condition were performed. (*** $p < 0.0001$, unpaired double-sided t-test). (**G)** Same experimental approach, but showing GA-NLS+B-NLS compared to B-NLS only.

4.23. Stimulation of transcription triggered an overload of the mitochondrial protein import machinery in cancer cells

Based on the results we obtained from the approach with 2mt-sfGFP, where we demonstrated the high capacity of cancer cell mitochondria to import mitochondrially targeted proteins **(Figure 3)**, we were wondering whether we can unbalance the protein uptake machinery of mitochondria by stimulating the transcription and whether mito-PRIMA is able to capture these kind of events.

To find this out we aimed to apply mito-RPIMA, were a green fluorescent signal in the nucleus would be a direct indicator of mistargeted 2mt-B-NLS upon failed import into mitochondria, due to e. g. stimulation of transcription.

HeLa cells expressing mito-RPIMA treated with 5 µM suberanilohydroxamic acid (SAHA), a compound that is supposed to inhibit histone deacetylases and thereby stimulate transcription (164) displayed a strong nuclear fluorescence signal **(Figure 23A and C)**, indicating the mistargeting of 2mt-B-NLS and subsequent transport into the nucleus, followed by dimerization with GA-NLS. Still, we found a population of cells showing a clear nuclear fluorescence signal, which indicate failed import of 2mt-B-NLS into mitochondria in those particular cells, because of reasons we cannot predict exactly **(Figure 23B and C)**.

Figure 23

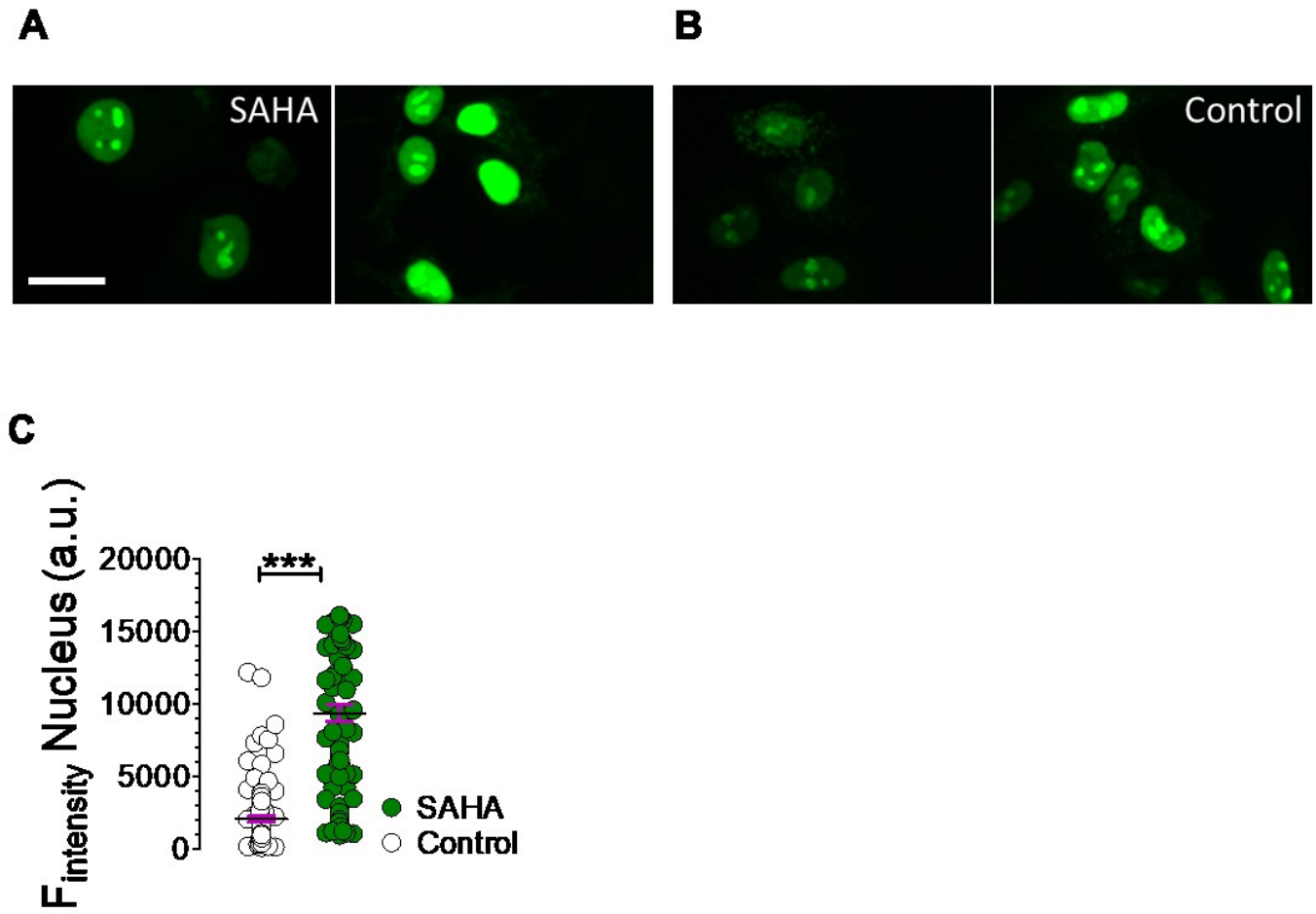

Figure 23. Visualization of the performance of mito-RPIMA treated with SAHA as a transcription inducer. (A) Two representative confocal images of HeLa cells expressing mito-RPIMA treated with SAHA. Scale bar indicates 10 µm. **(B)** Identical experiments, but showing the control condition. **(C)** Illustration of the statistics of the average nuclear fluorescence intensities of each individual cell of both conditions, SAHA and control. Dots are shown as the mean ± SEM. N = 111 (control), n = 92 (SAHA). Three independent experiments for both conditions were done. (*** $p < 0.0001$, unpaired double-sided t-test).

4.24. mito-PRIMA is suitable for the online visualization of impairments in the protein uptake machinery of mitochondria

Next we aimed to challenge the performance of mito-PRIMA by imaging HeLa cells expressing the sensor in living cells over the time for more than 14 hours in a row.

When we took a closer look at the online recordings we observed a sharp increase in fluorescence intensity over time compared to control condition, indicating the failed import of 2mt-B-NLS (Figure 24B). However, the starting point of the fluorescence increase differed from cell to cell in the treated condition ranking from 3 hours up to 11 hours **(Figure 24A, B and C)**, which might have various reasons, we cannot determine so far, such as: variations in the capacity of mitochondria to import proteins, different susceptibility of each HeLa cell to react to SAHA, cells might differ in the cell cycle or it depends upon the amount of plasmids a cell harbors, meaning the higher the amount of plasmids in the cell the more protein can be translated.

Apart from the aspect, that we do not know why each cell reacted at different times to treatment with SAHA, the recorded fluorescence increase with time is a direct measure of protein distribution outside of mitochondria, indicating an imbalance between protein synthesis and the capacity to import those proteins, resulting in failed import. Based on these recordings we reasoned that mito-PRIMA is highly suitable to visualize mitochondrial protein import defects in living cells over time.

Figure 24

A

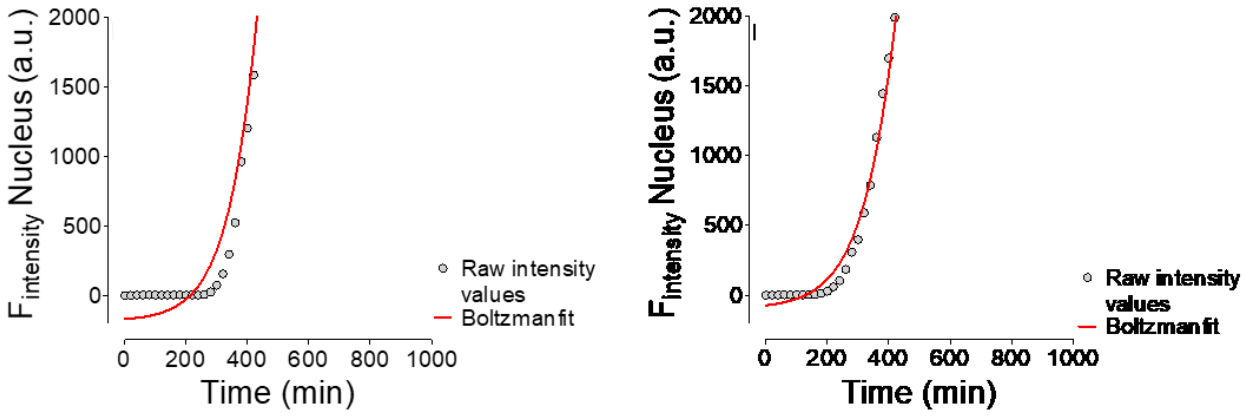

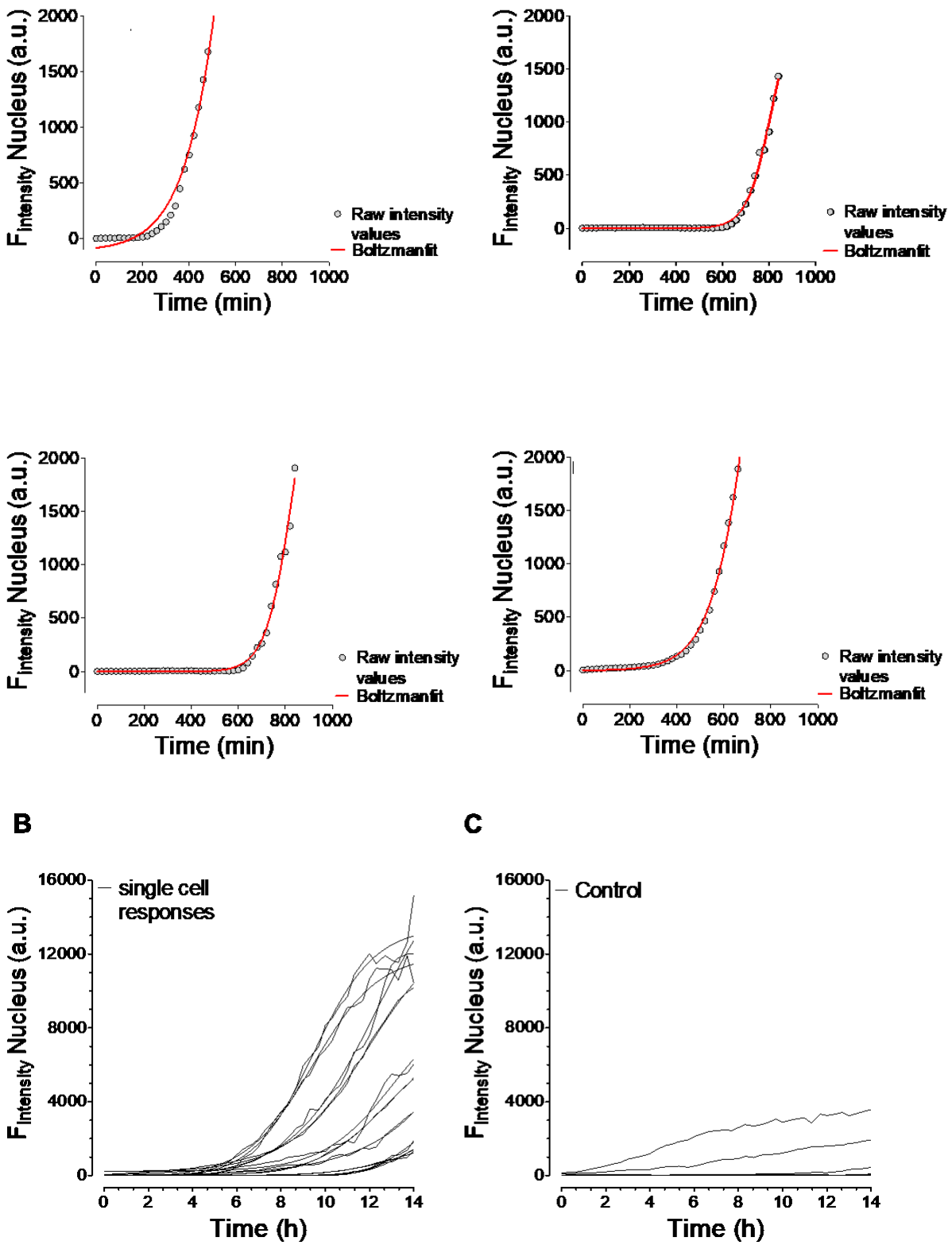

Figure 24. Long-term imaging of mito-RPIMA using the transcription inducer SAHA. (A) Curves of single HeLa cells, expressing mito-PRIMA upon cell treatment with SAHA shown as raw intensity values (grey dots) and overlaid by the calculated *Boltzmann fit* curve (red line). **(B)** Single cell responses of all HeLa cells treated with SAHA. N = 25 **(C)** Single cell responses of all HeLa cells of the control group. N = 12.

4.25. Combining online recordings of mito-PRIMA with 2mt-sfGFP emphasizes the high capacity of cancer cell mitochondria to import proteins efficiently

Application of mito-RPIMA to study mitochondrial protein import defects is not very well suitable if it is of interest to have additional information about e. g. the mitochondrial morphology. With mito-PRIMA one can only visualize, whether there is a defect in the import or not, because mitochondria are not visualized with this sensor approach.

Yet, we were curios whether the nuclear fluorescence signal of mito-PRIMA correlates to some extent with the approach of 2mt-sfGFP. To find that out, we performed a series of long-term (>16 h) time laps imaging experiments with 2mt-sfGFP in analogy to those experiments with mito-PRIMA **(Figure 25)**.

HeLa cells expressing 2mt-sfGFP treated with SAHA showed in most of the cells from the beginning on a drastic increase in the mitochondrial fluorescence intensity up to complete saturation of the signal, which was not the case in the control condition i.e. without cell treatment with SAHA **(Figure 25A)**. These findings demonstrate again the tremendous capacity of mitochondria in HeLa cells to efficiently import overexpressed proteins harboring an optimized MTS. In almost all cells treated with SAHA, where the mitochondrial fluorescence intensity reached a plateau the cytosolic fluorescence started to rise subsequently **(Figure 25A)**, indicating the accumulation of mitochondrially targeted proteins in the cytosol upon failed import into mitochondria. HeLa cells expressing 2mt-sfGFP in the control condition displayed no strong increase in the mitochondrial fluorescence intensity, which means that compared to cells treated with SAHA there is no stimulation of transcription/translation over time. Hence, the cytosolic fluorescence intensity also did not show any significant increase, indicating a rather constant and gradual import of 2mt-sfGFP into mitochondria under control conditions **(Figure 25B)**.

In line with the observations we made with mito-RPIMA, also in HeLa cells expressing 2mt-sfGFP and treated with SAHA, the starting point of the cytosolic fluorescence increase differed from cell to cell in the treated condition ranking from 3 hours up to 11 hours **(Figure 24 and 25)**.

Figure 25

A

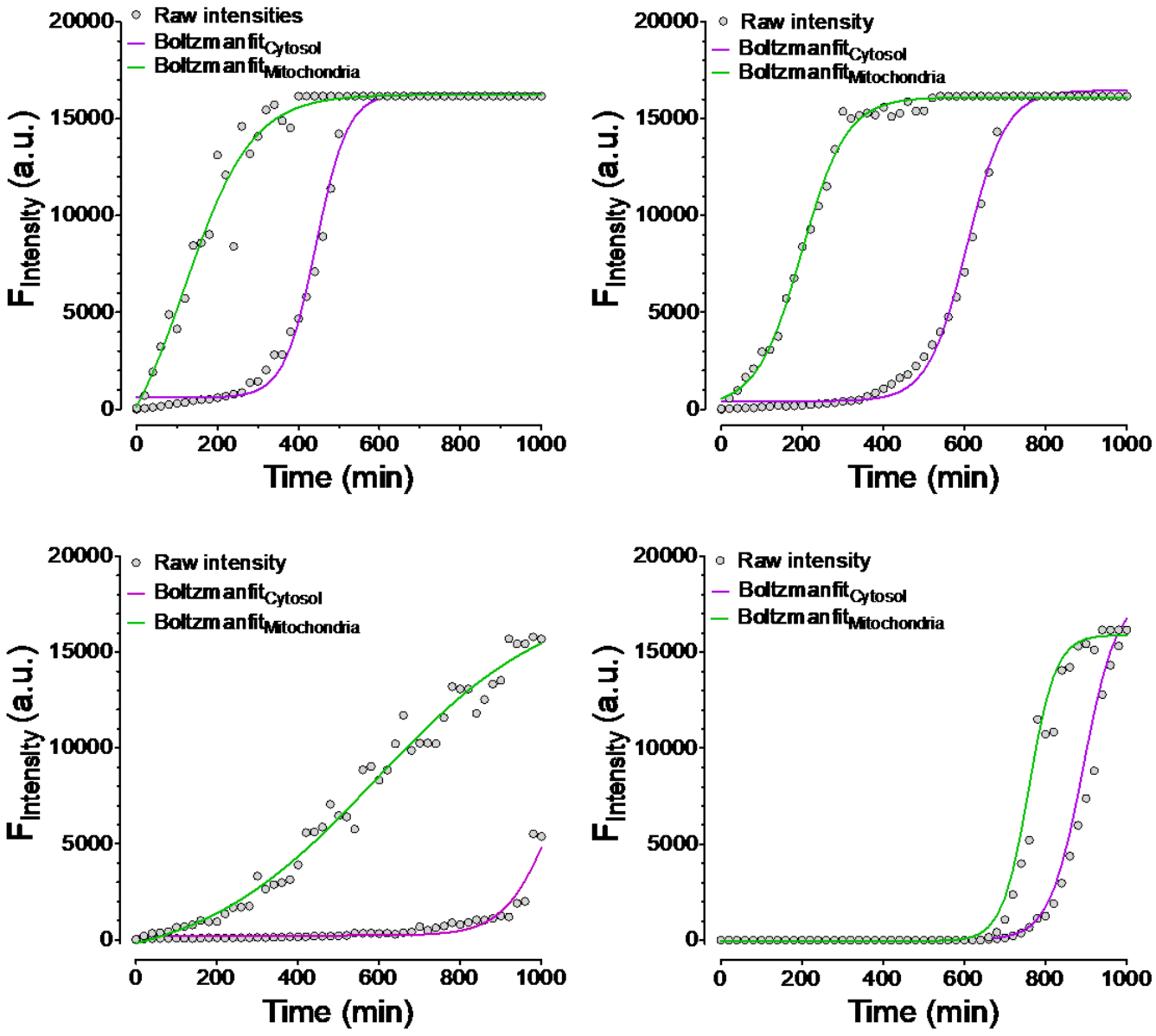
Raw intensities
Boltzmanfit Cytosol
Boltzmanfit Mitochondria
F Intensity (a.u.)
Time (min)
Raw intensity
Boltzmanfit Cytosol
Boltzmanfit Mitochondria
F Intensity (a.u.)
Time (min)
Raw intensity
Boltzmanfit Cytosol
Boltzmanfit Mitochondria
F Intensity (a.u.)
Time (min)
Raw intensity
Boltzmanfit Cytosol
Boltzmanfit Mitochondria
F Intensity (a.u.)
Time (min)

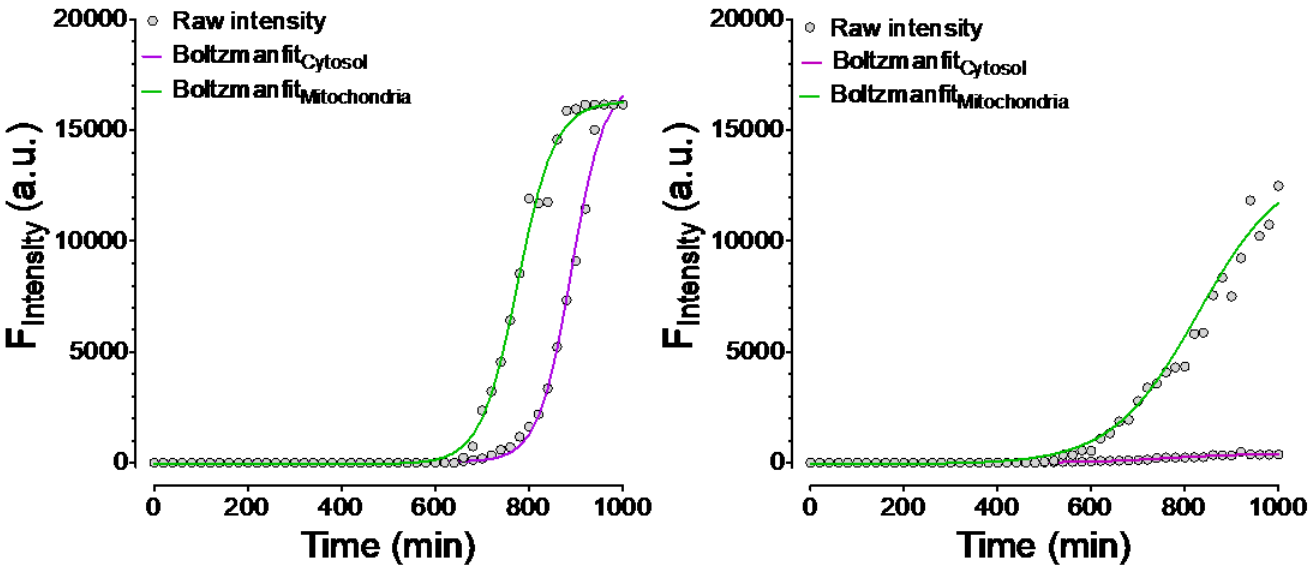
Raw intensity
Boltzmanfit$_{Cytosol}$
Boltzmanfit$_{Mitochondria}$
F$_{Intensity}$ (a.u.)
Time (min)

B

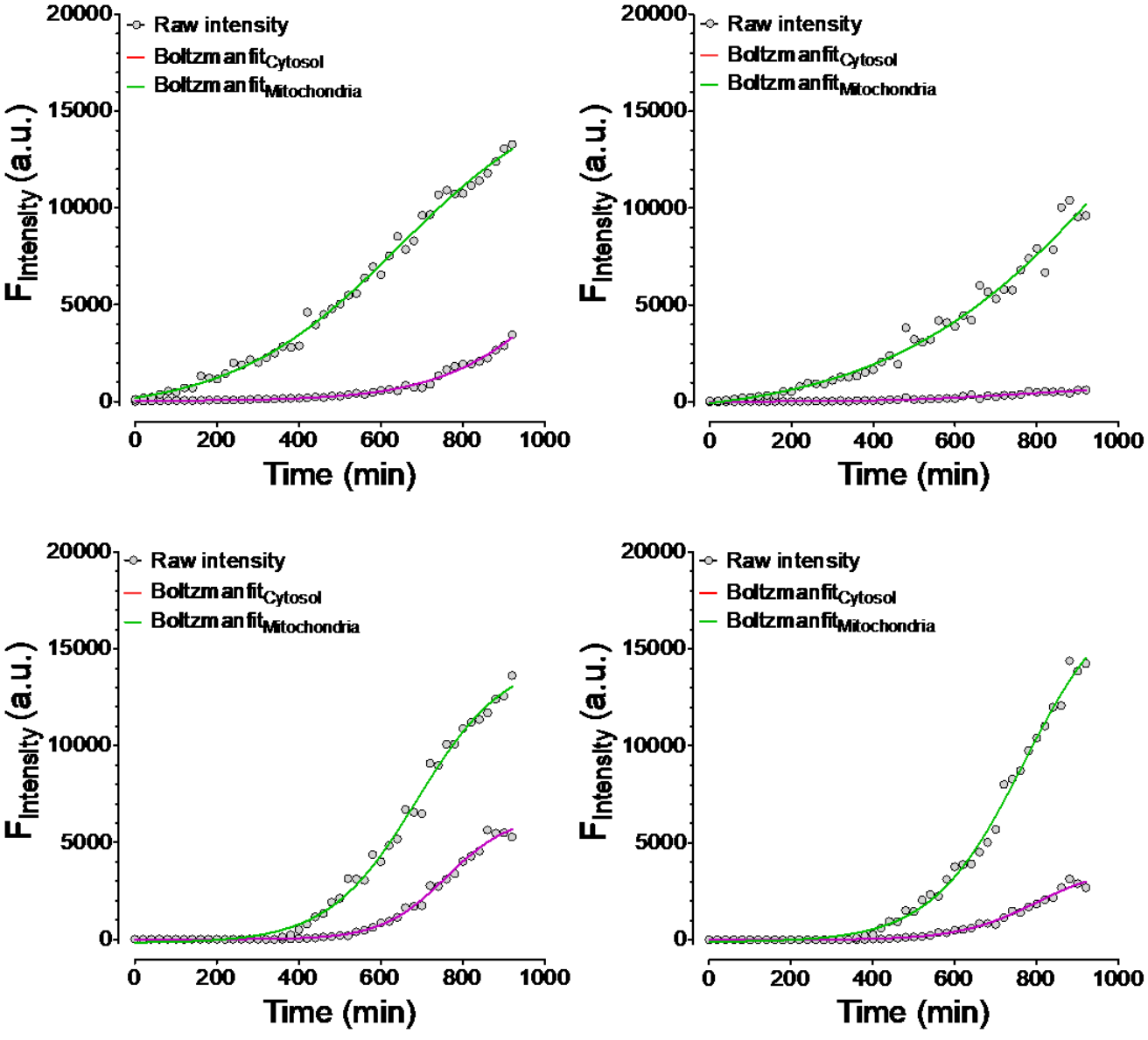
Raw intensity
Boltzmanfit$_{Cytosol}$
Boltzmanfit$_{Mitochondria}$
F$_{Intensity}$ (a.u.)
Time (min)

Figure 25. Performance of mito-RPIMA compared to 2mt-sfGFP for the visualization of mitochondrial protein import disturbances induced by a protein overload. (A) Curves of single HeLa cells, expressing 2mt-sfGFP upon cell treatment with SAHA shown as raw intensity values of mitochondria and the cytosol, respectively (grey dots). Both curves are overlain by the calculated *Boltzmann fit* curve (cytosolic course in purple, respectively; mitochondrial course in green, respectively). N = 6 (SAHA). **(A)** Identical experiment as in A, but showing the control group. N = 4 (control).

5. Discussion

In this study we aimed to come up with genetically encoded fluorescent protein- (FP) based tools, respective imaging protocols and image analysis for the determination of the efficiency of protein targeting to mitochondria and to visualize the activity and/or impairments in mitochondrial protein import in living cells. For that we exploited different FP-technologies, such as the full- (140), dimerization-dependent- (141) and self-complementation FP-technology (165) and developed thereby three classes of one-part, bipartite and tripartite fluorescent tools. Each class of these sensors has its strengths and weaknesses when it comes to their application in living cells.

5.1. Visualization of the activity and efficiency of protein targeting to mitochondria using 2mt-sfGFP

In the first attempt we tested 2mt-sfGFP, and exploited the power of the super-folder green fluorescent protein (sfGFP) to quantify mitochondrial protein import and defects thereof in cancer cells. The reason, why we aimed using this specific FP lies in its fast folding and maturation behaviour, meaning that sfGFP becomes fluorescent within several minutes upon its biosynthesis, because it harbors a very fast maturation kinetic (144). This features of sfGFP was very precious for us, since we were able to image the acute subcellular distribution of the probe was almost upon its nascent synthesis by the cells of interest. Picking sfGFP enabled not only localisation analysis of the respective probe as endpoint-readout, but also the dynamic visualization of the protein of interest. In order to visualize the efficiency of protein targeting to mitochondria, we decided to fuse the sfGFP to an established mitcohondrial targeting sequence (MTS), namely to that one of the COXVIII subunit (136), which has been frequently used to target FPs into mitochondria. The MTS of the COXVIII subunit depicts a classic N-terminal MTS, meaning that this probe targets into mitochondria based on the presequence mitochondrial protein import pathway (166). As indicated by 2mt-sfGFP, we fused sfGFP to a dimeric tandem repeat of the MTS, because the balance between the number of repeat and the rest of the length of the translated protein seemed to be essential for the correct and efficient targeting to mitochondria (136) (145). As demonstrated by others repeats of MTSs significantly can improve targeting efficiency of respective FP fusion constructs (136). More MTSs most likely increase the probability of the formation of stable and effective interactions between the nascent peptide and the TOM and TIM machinery (99). We and others speculate that MTSs once formed at ribosomes recruit the whole ribosome to the surface of mitochondria (167) (168) for a co-translational import of proteins into mitochondria.

Based on our results and experiences with mitochondria targeted constructs we hypothesis that the import efficiency of proteins with an N-terminal MTS into mitochondria depends on the MTS itself and the remaining sequence as well as the size of the whole protein. E.g. the cameleons, genetically encoded Ca^{2+} probes containing two FPs for Förster resonance energy transfer (FRET), need at least two to four MTSs from the COXVIII subunit for an efficient mitochondrial targeting (136). These findings might indicate that different MTSs allow manipulating the sensitivity of mt-FP fusion constructs to sense different levels of mitochondrial targeting efficiencies or deficiencies. Notably, for several studies similar FP-based constructs with similar MTSs have been used to prove the mitochondrial localization, the mitochondrial targeting efficiency or how interventions can influence the targeting of the respective probe to mitochondria. However, we noticed that in most cases such as in (169) (170) only some representative images are shown with missing systematic strategies and statics. Therefore we felt more and more the need of the establishment of a systematic approach to quantify mitochondrial protein import with the help of simply mitochondria targeted FPs. As a result we scrutinized the subcellular distribution of 2mt-sfGFP which enabled not only the qualitative, but also the quantitative determination of mitochondrial targeting efficiency in living HeLa and INS-1 cells. The aspect, which makes our approach ingenious is that we are not detecting only the fluorescence signal which arises from mitochondria, we also capture the fluorescence signal coming from the cytosol and/or nucleus, which represents the mistargeting of the respective fluorescent probe. By taking that into account, we incorporated the subcellular distribution of 2mt-sfGFP in our analysis approach and were thereby able to successfully generate and establish assessing of MPI under different conditions. In this context we showed that high plasmid DNA concentrations coding for the mitochondria targeted fluorescent construct increase the number of cells with clear mistargeting of the probe. Our explanation for this is that rather than triggering some stress for mitochondria the rate of construct synthesis within cells becomes higher than the capacity of mitochondria to import them under these conditions. With other words if more copies of plasmids are within cells higher levels of the construct are translated within the same time – thus if we measure the fluorescence increase of 2mt-sfGFP in the cytosol as an indicator of impaired mitochondrial protein import the slope of fluorescence intensity increase is higher, if more copies of the plasmids are within the cell. Accordingly, this approach can also be used to measure the rate of transcription and translation i.e. the protein biosynthesis of 2mt-sfGFP, by performing online experiments overtime in living cells. With the approach of 2mt-sfGFP we also found out, that depolarization of mitochondria leads to severe mistargeting of 2mt-sfGFP, as expected. Notably, seCFP-OMP25, a FP fused to a targeting peptide for the outer mitochondrial membrane, did not show any significant accumulation of fluorescence within the cytosol upon cell treatment with oligomycin-A and antimycin-A1 overnight, indicating that depolarization of mitochondria does not affect the targeting efficiency

to the outer membrane of the organelle. These findings also demonstrate that the FP does not leak from mitochondria upon treatment with oligomycin-A and antimycin-A1. However, Sirt4-sfGFP and n4mt-sfGFP, which are trapped to the outer mitochondrial membrane showed a clear mistargeting outside of mitochondria upon depolarization of the mitochondrial membrane potential.

Following the fluorescence changes over time, the reason for a cytosolic accumulation of fluorescence of the 2mt-sfGFP construct is not due to relocation of already mitochondria targeted proteins, but indeed the resynthesis of 2mt-sfGFP that cannot be transported into mitochondria anymore, due to complete depolarization of mitochondria upon cell treatment with oligomycin-A and antimycin-A1. Fusion of a MTS to sfGFP offers the possibility to expand the tool box of sensors in such a way, that different mitochondrial targeting sequences (160) (158) (159), with probably different efficiencies for mitochondrial targeting can be fused to sfGFP, generating thereby sensors with various import sensitivities. We also think that this approach, meaning fusion of different mitochondrial import sequences fused to fast maturing FPs, can be used to assess the relative strengths of different MTS. We also noticed, that the approach with the 2mt-sfGPF acts as a dual sensor, meaning that in addition to that we can determine the targeting efficiency to mitochondria we also have the read-out about the proteinbiosynthesis rate, especially when we perform online experiments in living cells.

5.2. Investigating the subcellular distribution of mitochondrial Sirtuin4 using a construct, based on bimolecular fluorescence self-complementation

Based on the so far established approach with 2mt-sfGFP we aimed to apply this method in an extended edition to a mitochondrial protein and ended up with the visualization of the subcellular distribution of Sirtuin4 (Sirt4), which is a mitochondria targeted sirtuin isoform (153). The investigation of the subcellular localization of Sirt4 is highly relevant since mitochondrial sirtuins, such as Sirtuin3 (Sirt3), Sirt4 and Sirtuin5 (Sirt5) control essential cellular processes related to stress (171). We fused Sirt4 to sfGFP (Sirt4-sfGFP) and could thereby visualize and quantify the subcellular distribution of Sirt4-sfGFP under different conditions in living cells (1). Having a closer look at Sirt4-sfGFP unveiled trapping of Sirt4-sfGFP to the outer mitochondrial membrane, possibly due to slow mitochondrial protein import kinetics of Sirt4. Therefore it seems necessary to test other FP variants with different folding kinetics and find out, whether the rapid folding of sfGFP prevents the complete import of Sirt4-sfGFP into the lumen of mitochondria. Indeed, fusion of slower maturing FPs improved the targeting efficiency of Sirt4

into mitochondria. Another side-effect of fusing sfGFP to Sirt4 was the induction of mitcohondrial swelling. To overcome these effects we decided to apply another FP-technology and confirm the localization of Sirt4 to the mitochondrial matrix, namely the self-complementation split-FP technology (161). Thus, we generated another fusion construct, where we linked Sirt4 to a 17 amino acid non-fluorescent short peptide, representing one part ($sfCherry2_{11}$) of sfCherry2, which upon self-complementation with the non-fluorescent mitochondrially targeted rest of the non-fluorescent complementary second part ($sfCherry2_{1-10}$) of sfCherry2 generates red fluorescence (161) (1).

Most studies discuss and demonstrate the localization of Sirt4 in the mitochondrial matrix, due to its classic N-terminal targeting sequence (153) , however Zeng et al. claim, that under certain conditions Sirt4 can be also found in the nucleus (156). Some mitochondrial proteins can localize to the nucleus upon mitochondrial stress in the frame of the mitochondrial unfolded protein response (mtUPR), such as ATF5 (131) or Sirt3 (172) hence we thought that this might also be the case for Sirt4. Taking this into consideration we thought that it makes sense to expand the approach. Adding to this probe further well approved targeting strategies we generated mito-STAR to study the quantitative distribution of Sirt4 between mitochondria and the nucleus using high – and super resolution microscopy techniques (1). Indeed, expressing mito-STAR improve the targeting efficiency of Sirt4-$sfCherry2_{11}$ compared to Sirt4-sfGFP, but still many cells harbored in addition to the mitochondrial fluorescence a clear nuclear fluorescence, indicating the abundance of Sirt4-$sfCherry2_{11}$ in the nucleus under physiological conditions. Under conditions of mitochondrial stress Sirt4-$sfCherry2_{11}$ drastically accumulated in the nucleus. Based on these results we hypothesize the involvement of Sirt4 to the retrograde mitochondria-to-nucleus signaling. Furthermore we think that this approach is expandable to other mitochondrial proteins and hence is applicable to screen various compounds that might influence the mitochondrial protein import, such as stendomycin, a compound that might directly inhibit the TIM machinery (170).

5.3. Dimerization-dependent FP based sensors to assess impairments in the mitochondrial protein import machinery with no need for optical resolution

In this study, we also aimed to construct, develop and establish genetically encoded sensors which do not rely on sophisticated microscopes and do not require the cytosolic accumulation of a respective probe, as a quantitative and qualitative readout for the severity of the mistargeting. To fulfill these needs we came up with mito-PRIMA, which is a bipartite sensor based on the dimerization-dependent FP-technology (141) (163). We exploited the established MTS of the COXVIII subunit (136) in a dimeric tandem repeat and fused it to one of the non-fluorescent pairs of the ddFP-pair. On the other hand we utilized the established nuclear localizing sequence in a three times repeat (138), linked to the second auto-fluorescent pair of the ddFP-pair and combined these two parts by a self-cleavage peptide (137) in order to achieve equal amount of both parts within a cell.

By applying the dually targeted bipartite probe, which is non-fluorescent and located to the mitochondria under conditions of an efficient mitochondrial protein uptake machinery we managed to generate a green fluorescence signal coming from the nucleus upon mistargeting of mitochondrially targeted proteins due to failed import. This means that as soon as we detect a fluorescence signal it indicates that the protein import machinery of mitochondria is somehow impaired. The sensor mito-PRIMA proved highly suitable for the detection of impairments in the mitochondrial protein uptake machinery, since treatment and online imaging of HeLa cells treated with SAHA, a transcription inducer led to a fluorescence signal coming from the nucleus, which was constantly increasing with time. However, due to the fact that under conditions of an intact mitochondrial protein import the ddFP pairs are spatially separated from each other hence the sensor gives no fluorescence signal it was very challenging to detect those cells. We therefore aimed to expand the bipartite probe by an additional part, namely a red reporter FP. This would make the experimental approach much easier and by that we would have a sort of sensor, which provides information about the proteinbiosynthesis rate within a particular cell. As discussed above, it is essential to balance the ratio between the repeats of a MTS to the rest of the protein to guarantee an efficient targeting of the respective protein to mitochondria. We designed mito-PRIMA using two repeats of the COXVIII subunit. However, the rest of the protein, which has to be translated is much bigger, compared to 2mt-sfGFP for example. Our data might indicate that mito-PRIMA is not as efficient in its targeting capacity as 2mt-sfGFP is. Meaning that with mito-PRIMA we generated a tool, which is very sensitive to mitochondrial protein import imbalances. In this case, by fusing various repeats of MTSs to mito-PRIMA we can generate additional probes with different sensitivities to

mitochondrial stress. Another aspect to consider is the fact that mito-RPIMA gives no fluorescence signals from mitochondria, meaning that by expressing mito-PRIMA in living cells mitochondria are not visible. On the one hand this approach is straight forward if only defects of the import machinery of mitochondria should be assessed. On the other hand the lack of any information of the morphology of mitochondria can be a clear disadvantage of this tool. Nevertheless, mito-PRIMA seems to be an attractive reporter for high throughput measurements to screen a series of compounds, which influence the mitochondrial import. Additional experiments in the near future will prove how efficient MPI can be investigated applying mito-PRIMAs in cell populations on conventional fluorescence plate readers and/or FACS devices.

5.4. Application of the novel mitochondrial protein import sensors in the field of neuroscience

Both, Parkinson´s disease and Huntington´s disease are associated with alterations within specific regions in the brain, such as the loss of neurons in the substantia nigra in the case of Parkinson´s disease and the loss of neurons in the striatum, in the case of Huntington´s disease (173). These neurodegenerative disorders are very often related to protein aggregate accumulation and mitochondrial malfunction (174). Especially, defects in the mitochondrial protein import induced by misfolded proteins can contribute to the formation of neurodegenerative alterations, such as Parkinson´s disease and Huntington´s disease (169) (175).

So far, only few methods are available that allow the visualization of the mitochondrial protein import using fluorescence microscopy and genetically encoded probes (162) (176) (177). However, due to the lack of consistent systematics arose by the usage of these currently available approaches, we were eager to offer FP-based tools, which overcome this limitation.

In order to probe the novel mitochondrial protein import sensors, we plan to utilize the developed and established protocols and image analysis to reveal important new insights in the formation and progression of neurodegenerative disorders related to defects in the mitochondrial protein uptake machinery. We feel, that the application of the novel sensors will lead to new understandings making the identification of new pharmacological targets in e. g. Parkinson´s disease and Huntington´s disease possible.

6. References

1. Ramadani-Muja J, Gottschalk B, Pfeil K, Burgstaller S, Rauter T, Bischof H, et al. Visualization of Sirtuin 4 Distribution between Mitochondria and the Nucleus, Based on Bimolecular Fluorescence Self-Complementation. Cells. 2019 Dec 6;8(12):1583.

2. Cabral F, Solioz M, Rudin Y, Schatz G, Clavilier L, Slonimski PP. Identification of the structural gene for yeast cytochrome c oxidase subunit II on mitochondrial DNA. J Biol Chem. 1978 Jan 10;253(1):297–304.

3. Beasley EM, Wachter C, Schatz G. Putting energy into mitochondrial protein import. Curr Opin Cell Biol. 1992 Aug;4(4):646–51.

4. Hurt EC, Schatz G. A cytosolic protein contains a cryptic mitochondrial targeting signal. Nature. 1987 Feb;325(6104):499–503.

5. Omura T. Mitochondria-targeting sequence, a multi-role sorting sequence recognized at all steps of protein import into mitochondria. J Biochem (Tokyo). 1998;123(6):1010–6.

6. Anderson S, Bankier AT, Barrell BG, de Bruijn MHL, Coulson AR, Drouin J, et al. Sequence and organization of the human mitochondrial genome. Nature. 1981 Apr;290(5806):457–65.

7. Dolezal P. Evolution of the Molecular Machines for Protein Import into Mitochondria. Science. 2006 Jul 21;313(5785):314–8.

8. Taylor SW, Fahy E, Zhang B, Glenn GM, Warnock DE, Wiley S, et al. Characterization of the human heart mitochondrial proteome. Nat Biotechnol. 2003 Mar;21(3):281–6.

9. Baker KP, Schaniel A, Vestweber D, Schatz G. A yeast mitochondrial outer membrane protein essential for protein import and cell viability. Nature. 1990 Dec;348(6302):605–9.

10. Wasilewski M, Chojnacka K, Chacinska A. Protein trafficking at the crossroads to mitochondria. Biochim Biophys Acta BBA - Mol Cell Res. 2017 Jan;1864(1):125–37.

11. Endo T, Yamano K. Multiple pathways for mitochondrial protein traffic. Biol Chem [Internet]. 2009 Aug 1 [cited 2020 Jan 30];390(8). Available from: http://www.degruyter.com/view/j/bchm.2009.390.issue-8/bc.2009.087/bc.2009.087.xml

12. Wiedemann N, Pfanner N. Mitochondrial Machineries for Protein Import and Assembly. Annu Rev Biochem. 2017;86:685–714.

13. Neupert W. SnapShot: Mitochondrial Architecture. Cell. 2012 Apr;149(3):722-722.e1.

14. Grevel A, Pfanner N, Becker T. Coupling of import and assembly pathways in mitochondrial protein biogenesis. Biol Chem. 2019 Dec 18;401(1):117–29.

15. Gebert N, Ryan MT, Pfanner N, Wiedemann N, Stojanovski D. Mitochondrial protein import machineries and lipids: A functional connection. Biochim Biophys Acta BBA - Biomembr. 2011 Mar;1808(3):1002–11.

16. Quirós PM, Mottis A, Auwerx J. Mitonuclear communication in homeostasis and stress. Nat Rev Mol Cell Biol. 2016 Apr;17(4):213–26.

17. Harbauer AB, Zahedi RP, Sickmann A, Pfanner N, Meisinger C. The Protein Import Machinery of Mitochondria—A Regulatory Hub in Metabolism, Stress, and Disease. Cell Metab. 2014 Mar;19(3):357–72.

18. Spinelli JB, Haigis MC. The multifaceted contributions of mitochondria to cellular metabolism. Nat Cell Biol. 2018 Jul;20(7):745–54.

19. Hackenbrock CR. ULTRASTRUCTURAL BASES FOR METABOLICALLY LINKED MECHANICAL ACTIVITY IN MITOCHONDRIA. J Cell Biol. 1966 Aug 1;30(2):269–97.

20. Frey TG, Mannella CA. The internal structure of mitochondria. Trends Biochem Sci. 2000 Jul;25(7):319–24.

21. Comte J, Maĭsterrena B, Gautheron DC. Lipid composition and protein profiles of outer and inner membranes from pig heart mitochondria. Comparison with microsomes. Biochim Biophys Acta BBA - Biomembr. 1976 Jan;419(2):271–84.

22. Bayrhuber M, Meins T, Habeck M, Becker S, Giller K, Villinger S, et al. Structure of the human voltage-dependent anion channel. Proc Natl Acad Sci. 2008 Oct 7;105(40):15370–5.

23. Forte M, Blachly-Dyson E. VDAC Channels. IUBMB Life Int Union Biochem Mol Biol Life. 2001 Sep 1;52(3–5):113–8.

24. Mannella CA. The 'ins' and 'outs' of mitochondrial membrane channels. Trends Biochem Sci. 1992 Aug;17(8):315–20.

25. Shoshan-Barmatz V, De Pinto V, Zweckstetter M, Raviv Z, Keinan N, Arbel N. VDAC, a multi-functional mitochondrial protein regulating cell life and death. Mol Aspects Med. 2010 Jun;31(3):227–85.

26. Kühlbrandt W. Structure and function of mitochondrial membrane protein complexes. BMC Biol. 2015 Dec;13(1):89.

27. Vogel F, Bornhövd C, Neupert W, Reichert AS. Dynamic subcompartmentalization of the mitochondrial inner membrane. J Cell Biol. 2006 Oct 23;175(2):237–47.

28. Gottschalk B, Klec C, Leitinger G, Bernhart E, Rost R, Bischof H, et al. MICU1 controls cristae junction and spatially anchors mitochondrial Ca2+ uniporter complex. Nat Commun. 2019;10(1):3732.

29. Brdiczka D. Contact sites between mitochondrial envelope membranes. Structure and function in energy- and protein-transfer. Biochim Biophys Acta BBA - Rev Biomembr. 1991 Nov;1071(3):291–312.

30. Jacob WA, Bakker A, Hertsens RC, Biermans W. Mitochondrial matrix granules: Their behavior during changing metabolic situations and their relationship to contact sites between inner and outer mitochondrial membranes. Microsc Res Tech. 1994 Mar 1;27(4):307–18.

31. van der Klei IJ, Veenhuis M, Neupert W. A morphological view on mitochondrial protein targeting. Microsc Res Tech. 1994 Mar 1;27(4):284–93.

32. Mannella CA, Pfeiffer DR, Bradshaw PC, Moraru II, Slepchenko B, Loew LM, et al. Topology of the Mitochondrial Inner Membrane: Dynamics and Bioenergetic Implications. IUBMB Life Int Union Biochem Mol Biol Life. 2001 Sep 1;52(3–5):93–100.

33. Mesecke N, Terziyska N, Kozany C, Baumann F, Neupert W, Hell K, et al. A Disulfide Relay System in the Intermembrane Space of Mitochondria that Mediates Protein Import. Cell. 2005 Jul;121(7):1059–69.

34. Olichon A, Baricault L, Gas N, Guillou E, Valette A, Belenguer P, et al. Loss of OPA1 Perturbates the Mitochondrial Inner Membrane Structure and Integrity, Leading to Cytochrome *c* Release and Apoptosis. J Biol Chem. 2003 Mar 7;278(10):7743–6.

35. Sjöstrand FS. Electron Microscopy of Mitochondria and Cytoplasmic Double Membranes: Ultra-Structure of Rod-shaped Mitochondria. Nature. 1953 Jan;171(4340):30–1.

36. Palade GE. AN ELECTRON MICROSCOPE STUDY OF THE MITOCHONDRIAL STRUCTURE. J Histochem Cytochem. 1953 Jul;1(4):188–211.

37. Perkins GA, Frey TG. Recent structural insight into mitochondria gained by microscopy. Micron. 2000 Feb;31(1):97–111.

38. Davies KM, Anselmi C, Wittig I, Faraldo-Gomez JD, Kuhlbrandt W. Structure of the yeast F1Fo-ATP synthase dimer and its role in shaping the mitochondrial cristae. Proc Natl Acad Sci. 2012 Aug 21;109(34):13602–7.

39. Cogliati S, Enriquez JA, Scorrano L. Mitochondrial Cristae: Where Beauty Meets Functionality. Trends Biochem Sci. 2016 Mar;41(3):261–73.

40. Model K, Prinz T, Ruiz T, Radermacher M, Krimmer T, Kühlbrandt W, et al. Protein translocase of the outer mitochondrial membrane: role of import receptors in the structural organization of the TOM complex. J Mol Biol. 2002 Feb;316(3):657–66.

41. Schatz G, Dobberstein B. Common Principles of Protein Translocation Across Membranes. Science. 1996 Mar 15;271(5255):1519–26.

42. Brix J, Rüdiger S, Bukau B, Schneider-Mergener J, Pfanner N. Distribution of Binding Sequences for the Mitochondrial Import Receptors Tom20, Tom22, and Tom70 in a Presequence-carrying Preprotein and a Non-cleavable Preprotein. J Biol Chem. 1999 Jun 4;274(23):16522–30.

43. Ahting U, Thun C, Hegerl R, Typke D, Nargang FE, Neupert W, et al. The Tom Core Complex. J Cell Biol. 1999 Nov 29;147(5):959–68.

44. Hill K, Model K, Ryan MT, Dietmeier K, Martin F, Wagner R, et al. Tom40 forms the hydrophilic channel of the mitochondrial import pore for preproteins. Nature. 1998 Oct;395(6701):516–21.

45. Dietmeier K, Hönlinger A, Bömer U, Dekker PJT, Eckerskorn C, Lottspeich F, et al. Tom5 functionally links mitochondrial preprotein receptors to the general import pore. Nature. 1997 Jul;388(6638):195–200.

46. Model K, Meisinger C, Prinz T, Wiedemann N, Truscott KN, Pfanner N, et al. [No title found]. Nat Struct Biol. 2001 Apr 1;8(4):361–70.

47. Wiedemann N, Kozjak V, Chacinska A, Schönfisch B, Rospert S, Ryan MT, et al. Machinery for protein sorting and assembly in the mitochondrial outer membrane. Nature. 2003 Jul;424(6948):565–71.

48. Becker T, Pfannschmidt S, Guiard B, Stojanovski D, Milenkovic D, Kutik S, et al. Biogenesis of the Mitochondrial TOM Complex: Mim1 PROMOTES INSERTION AND

ASSEMBLY OF SIGNAL-ANCHORED RECEPTORS. J Biol Chem. 2008 Jan 4;283(1):120–7.

49. Hulett JM, Lueder F, Chan NC, Perry AJ, Wolynec P, Likić VA, et al. The Transmembrane Segment of Tom20 Is Recognized by Mim1 for Docking to the Mitochondrial TOM Complex. J Mol Biol. 2008 Feb;376(3):694–704.

50. Pfanner N, Craig EA, Meijer M. The protein import machine of the mitochondrial inner membrane. Trends Biochem Sci. 1994 Sep;19(9):368–72.

51. Ryan KR, Jensen RE. Protein translocation across mitochondrial membranes: What a long, strange trip it is. Cell. 1995 Nov;83(4):517–9.

52. Tokatlidis K, Junne T, Moes S, Schatz G, Glick BS. Translocation arrest of an intramitochondrial sorting signal next to Tim11 at the inner-membrane import site. Nature. 1996 Dec;384(6609):585–8.

53. Sirrenberg C, Bauer MF, Guiard B, Neupert W, Brunner M. Import of carrier proteins into the mitochondrial inner membrane mediated by Tim22. Nature. 1996 Dec;384(6609):582–5.

54. Koehler CM. Import of Mitochondrial Carriers Mediated by Essential Proteins of the Intermembrane Space. Science. 1998 Jan 16;279(5349):369–73.

55. Berthold J, Bauer MF, Schneider H-C, Klaus C, Dietmeier K, Neupert W, et al. The MIM complex mediates preprotein translocationacross the mitochondrial inner membrane and couples it to the mt-Hsp70/ATP driving system. Cell. 1995 Jun;81(7):1085–93.

56. Dekker PJT. The Tim core complex defines the number of mitochondrial translocation contact sites and can hold arrested preproteins in the absence of matrix Hsp70-Tim44. EMBO J. 1997 Sep 1;16(17):5408–19.

57. Sirrenberg C, Endres M, Fölsch H, Stuart RA, Neupert W, Brunner M. Carrier protein import into mitochondria mediated by the intermembrane proteins Tim10/Mrs11 and Tim12/Mrs5. Nature. 1998 Feb;391(6670):912–5.

58. Hell K, Herrmann JM, Pratje E, Neupert W, Stuart RA. Oxa1p, an essential component of the N-tail protein export machinery in mitochondria. Proc Natl Acad Sci. 1998 Mar 3;95(5):2250–5.

59. Hell K, Herrmann J, Pratje E, Neupert W, Stuart RA. Oxa1p mediates the export of the N- and C-termini of pCoxII from the mitochondrial matrix to the intermembrane space. FEBS Lett. 1997 Dec 1;418(3):367–70.

60. Glick BS, Brandt A, Cunningham K, Müller S, Hallberg RL, Schatz G. Cytochromes c1 and b2 are sorted to the intermembrane space of yeast mitochondria by a stop-transfer mechanism. Cell. 1992 May;69(5):809–22.

61. Ieva R, Schrempp SG, Opaliński Ł, Wollweber F, Höß P, Heißwolf AK, et al. Mgr2 Functions as Lateral Gatekeeper for Preprotein Sorting in the Mitochondrial Inner Membrane. Mol Cell. 2014 Dec;56(5):641–52.

62. Walker JE, Lutter R, Dupuis A, Runswick MJ. Identification of the subunits of F1F0-ATPase from bovine heart mitochondria. Biochemistry. 1991 Jun;30(22):5369–78.

63. Harmon HJ, Hall JD, Crane FL. Structure of mitochondrial cristae membranes. Biochim Biophys Acta BBA - Rev Biomembr. 1974 Sep;344(2):119–55.

64. Pfanner N. Mitochondrial import: Crossing the aqueous intermembrane space. Curr Biol. 1998 Apr;8(8):R262–5.

65. Truscott KN, Wiedemann N, Rehling P, Muller H, Meisinger C, Pfanner N, et al. Mitochondrial Import of the ADP/ATP Carrier: the Essential TIM Complex of the Intermembrane Space Is Required for Precursor Release from the TOM Complex. Mol Cell Biol. 2002 Nov 15;22(22):7780–9.

66. van Wilpe S, Ryan MT, Hill K, Maarse AC, Meisinger C, Brix J, et al. Tom22 is a multifunctional organizer of the mitochondrial preprotein translocase. Nature. 1999 Sep;401(6752):485–9.

67. Chacinska A, Lind M, Frazier AE, Dudek J, Meisinger C, Geissler A, et al. Mitochondrial Presequence Translocase: Switching between TOM Tethering and Motor Recruitment Involves Tim21 and Tim17. Cell. 2005 Mar;120(6):817–29.

68. Chacinska A, Pfannschmidt S, Wiedemann N, Kozjak V, Sanjuán Szklarz LK, Schulze-Specking A, et al. Essential role of Mia40 in import and assembly of mitochondrial intermembrane space proteins. EMBO J. 2004 Sep 29;23(19):3735–46.

69. Mordas A, Tokatlidis K. The MIA Pathway: A Key Regulator of Mitochondrial Oxidative Protein Folding and Biogenesis. Acc Chem Res. 2015 Aug 18;48(8):2191–9.

70. Di Fonzo A, Ronchi D, Lodi T, Fassone E, Tigano M, Lamperti C, et al. The Mitochondrial Disulfide Relay System Protein GFER Is Mutated in Autosomal-Recessive Myopathy with Cataract and Combined Respiratory-Chain Deficiency. Am J Hum Genet. 2009 May;84(5):594–604.

71. Srere PA. The infrastructure of the mitochondrial matrix. Trends Biochem Sci. 1980 May;5(5):120–1.

72. Hackenbrock CR. Chemical and physical fixation of isolated mitochondria in low-energy and high-energy states. Proc Natl Acad Sci. 1968 Oct 1;61(2):598–605.

73. Pfanner N, Wiedemann N, Meisinger C, Lithgow T. Assembling the mitochondrial outer membrane. Nat Struct Mol Biol. 2004 Nov;11(11):1044–8.

74. Lill R. Function and biogenesis of iron–sulphur proteins. Nature. 2009 Aug;460(7257):831–8.

75. Lill R, Srinivasan V, Mühlenhoff U. The role of mitochondria in cytosolic-nuclear iron–sulfur protein biogenesis and in cellular iron regulation. Curr Opin Microbiol. 2014 Dec;22:111–9.

76. McBride HM, Neuspiel M, Wasiak S. Mitochondria: More Than Just a Powerhouse. Curr Biol. 2006 Jul;16(14):R551–60.

77. Kitakawa M, Isono K. The mitochondrial ribosomes. Biochimie. 1991 Jun;73(6):813–25.

78. Bauer MF, Hofmann S, Neupert W, Brunner M. Protein translocation into mitochondria: the role of TIM complexes. Trends Cell Biol. 2000 Jan;10(1):25–31.

79. Hawlitschek G, Schneider H, Schmidt B, Tropschug M, Hartl F-U, Neupert W. Mitochondrial protein import: Identification of processing peptidase and of PEP, a processing enhancing protein. Cell. 1988 Jun;53(5):795–806.

80. Ungermann C, Neupert W, Cyr D. The role of Hsp70 in conferring unidirectionality on protein translocation into mitochondria. Science. 1994 Nov 18;266(5188):1250–3.

81. Vögtle F-N, Wortelkamp S, Zahedi RP, Becker D, Leidhold C, Gevaert K, et al. Global Analysis of the Mitochondrial N-Proteome Identifies a Processing Peptidase Critical for Protein Stability. Cell. 2009 Oct;139(2):428–39.

82. Vögtle F-N, Prinz C, Kellermann J, Lottspeich F, Pfanner N, Meisinger C. Mitochondrial protein turnover: role of the precursor intermediate peptidase Oct1 in protein stabilization. Glick B, editor. Mol Biol Cell. 2011 Jul;22(13):2135–43.

83. Dyall SD. Ancient Invasions: From Endosymbionts to Organelles. Science. 2004 Apr 9;304(5668):253–7.

84. Gray MW. Mitochondrial Evolution. Science. 1999 Mar 5;283(5407):1476–81.

85. Reinders J, Zahedi RP, Pfanner N, Meisinger C, Sickmann A. Toward the Complete Yeast Mitochondrial Proteome: Multidimensional Separation Techniques for Mitochondrial Proteomics. J Proteome Res. 2006 Jul;5(7):1543–54.

86. Pagliarini DJ, Calvo SE, Chang B, Sheth SA, Vafai SB, Ong S-E, et al. A Mitochondrial Protein Compendium Elucidates Complex I Disease Biology. Cell. 2008 Jul;134(1):112–23.

87. Pfanner N, Meijer M. Mitochondrial biogenesis: The Tom and Tim machine. Curr Biol. 1997;7(2):R100–3.

88. Mayer A, Nargang FE, Neupert W, Lill R. MOM22 is a receptor for mitochondrial targeting sequences and cooperates with MOM19. EMBO J. 1995 Sep 1;14(17):4204–11.

89. von Heijne G. Mitochondrial targeting sequences may form amphiphilic helices. EMBO J. 1986 Jun;5(6):1335–42.

90. Pfanner N. Protein sorting: Recognizing mitochondrial presequences. Curr Biol. 2000 Jun;10(11):R412–5.

91. Roise D, Theiler F, Horvath SJ, Tomich JM, Richards JH, Allison DS, et al. Amphiphilicity is essential for mitochondrial presequence function. EMBO J. 1988 Mar;7(3):649–53.

92. Roise D, Schatz G. Mitochondrial presequences. J Biol Chem. 1988 Apr 5;263(10):4509–11.

93. Söllner T, Griffiths G, Pfaller R, Pfanner N, Neupert W. MOM19, an import receptor for mitochondrial precursor proteins. Cell. 1989 Dec 22;59(6):1061–70.

94. Abe Y, Shodai T, Muto T, Mihara K, Torii H, Nishikawa S, et al. Structural Basis of Presequence Recognition by the Mitochondrial Protein Import Receptor Tom20. Cell. 2000 Mar;100(5):551–60.

95. Schatz G. Just follow the acid chain. Nature. 1997 Jul;388(6638):121–2.

96. Voos W, Martin H, Krimmer T, Pfanner N. Mechanisms of protein translocation into mitochondria. Biochim Biophys Acta BBA - Rev Biomembr. 1999 Nov;1422(3):235–54.

97. Brix J, Dietmeier K, Pfanner N. Differential Recognition of Preproteins by the Purified Cytosolic Domains of the Mitochondrial Import Receptors Tom20, Tom22, and Tom70. J Biol Chem. 1997 Aug 15;272(33):20730–5.

98. Lithgow T, Glick BS, Schatz G. The protein import receptor of mitochondria. Trends Biochem Sci. 1995 Mar;20(3):98–101.

99. Backes S, Hess S, Boos F, Woellhaf MW, Gödel S, Jung M, et al. Tom70 enhances mitochondrial preprotein import efficiency by binding to internal targeting sequences. J Cell Biol. 2018 Apr 2;217(4):1369–82.

100. Geissler A, Krimmer T, Bömer U, Guiard B, Rassow J, Pfanner N. Membrane Potential-Driven Protein Import into Mitochondria: The Sorting Sequence of Cytochrome b2 Modulates the Δψ-Dependence of Translocation of the Matrix-targeting Sequence. Mol Biol Cell. 2000;11(11):3977–91.

101. Ryan KR, Leung RS, Jensen RE. Characterization of the Mitochondrial Inner Membrane Translocase Complex: the Tim23p Hydrophobic Domain Interacts with Tim17p but Not with Other Tim23p Molecules. Mol Cell Biol. 1998 Jan 1;18(1):178–87.

102. Schatz G. The Protein Import System of Mitochondria. J Biol Chem. 1996 Dec 13;271(50):31763–6.

103. Ishihara N, Mihara K. Identification of the Protein Import Components of the Rat Mitochondrial Inner Membrane, rTIM17, rTIM23, and rTIM44. J Biochem (Tokyo). 1998 Apr 1;123(4):722–32.

104. Banerjee R, Gladkova C, Mapa K, Witte G, Mokranjac D. Protein translocation channel of mitochondrial inner membrane and matrix-exposed import motor communicate via two-domain coupling protein. eLife. 2015 Dec 29;4:e11897.

105. Horst M. Sequential action of two hsp70 complexes during protein import into mitochondria. EMBO J. 1997 Apr 15;16(8):1842–9.

106. De Los Rios P, Ben-Zvi A, Slutsky O, Azem A, Goloubinoff P. Hsp70 chaperones accelerate protein translocation and the unfolding of stable protein aggregates by entropic pulling. Proc Natl Acad Sci. 2006 Apr 18;103(16):6166–71.

107. Mossmann D, Meisinger C, Vögtle F-N. Processing of mitochondrial presequences. Biochim Biophys Acta BBA - Gene Regul Mech. 2012 Sep;1819(9–10):1098–106.

108. Naoé M, Ohwa Y, Ishikawa D, Ohshima C, Nishikawa S, Yamamoto H, et al. Identification of Tim40 That Mediates Protein Sorting to the Mitochondrial Intermembrane Space. J Biol Chem. 2004 Nov 12;279(46):47815–21.

109. Wenz L-S, Ellenrieder L, Qiu J, Bohnert M, Zufall N, van der Laan M, et al. Sam37 is crucial for formation of the mitochondrial TOM–SAM supercomplex, thereby promoting β-barrel biogenesis. J Cell Biol. 2015 Sep 28;210(7):1047–54.

110. Newmeyer DD, Ferguson-Miller S. Mitochondria. Cell. 2003 Feb;112(4):481–90.

111. Thayer WS, Ohnishi T, Rubin E. Characterization of iron-sulfur clusters in rat liver submitochondrial particles by electron paramagnetic resonance spectroscopy. Alterations

produced by chronic ethanol consumption. Biochim Biophys Acta BBA - Bioenerg. 1980 Jun;591(1):22–36.

112. Kennedy EP, Lehninger AL. The products of oxidation of fatty acids by isolated rat liver mitochondria. J Biol Chem. 1950 Jul;185(1):275–85.

113. West AP, Khoury-Hanold W, Staron M, Tal MC, Pineda CM, Lang SM, et al. Mitochondrial DNA stress primes the antiviral innate immune response. Nature. 2015 Apr;520(7548):553–7.

114. Youle RJ, Narendra DP. Mechanisms of mitophagy. Nat Rev Mol Cell Biol. 2011 Jan;12(1):9–14.

115. Yogev O, Pines O. Dual targeting of mitochondrial proteins: Mechanism, regulation and function. Biochim Biophys Acta BBA - Biomembr. 2011 Mar;1808(3):1012–20.

116. Haynes CM, Ron D. The mitochondrial UPR - protecting organelle protein homeostasis. J Cell Sci. 2010 Nov 15;123(22):3849–55.

117. Topf U, Wrobel L, Chacinska A. Chatty Mitochondria: Keeping Balance in Cellular Protein Homeostasis. Trends Cell Biol. 2016 Aug;26(8):577–86.

118. Nargund AM, Pellegrino MW, Fiorese CJ, Baker BM, Haynes CM. Mitochondrial import efficiency of ATFS-1 regulates mitochondrial UPR activation. Science. 2012;337(6094):587–90.

119. Haynes CM, Yang Y, Blais SP, Neubert TA, Ron D. The Matrix Peptide Exporter HAF-1 Signals a Mitochondrial UPR by Activating the Transcription Factor ZC376.7 in C. elegans. Mol Cell. 2010 Feb;37(4):529–40.

120. Weidberg H, Amon A. MitoCPR—A surveillance pathway that protects mitochondria in response to protein import stress. Science. 2018 Apr 13;360(6385):eaan4146.

121. Shpilka T, Haynes CM. The mitochondrial UPR: mechanisms, physiological functions and implications in ageing. Nat Rev Mol Cell Biol. 2018;19(2):109–20.

122. Naresh NU, Haynes CM. Signaling and Regulation of the Mitochondrial Unfolded Protein Response. Cold Spring Harb Perspect Biol. 2019 Jun;11(6):a033944.

123. Martinus RD, Garth GP, Webster TL, Cartwright P, Naylor DJ, Høj PB, et al. Selective Induction of Mitochondrial Chaperones in Response to Loss of the Mitochondrial Genome. Eur J Biochem. 1996 Aug;240(1):98–103.

124. Zhao Q. A mitochondrial specific stress response in mammalian cells. EMBO J. 2002 Sep 2;21(17):4411–9.

125. Yoneda T. Compartment-specific perturbation of protein handling activates genes encoding mitochondrial chaperones. J Cell Sci. 2004 Aug 15;117(18):4055–66.

126. Houtkooper RH, Mouchiroud L, Ryu D, Moullan N, Katsyuba E, Knott G, et al. Mitonuclear protein imbalance as a conserved longevity mechanism. Nature. 2013 May;497(7450):451–7.

127. Runkel ED, Liu S, Baumeister R, Schulze E. Surveillance-Activated Defenses Block the ROS–Induced Mitochondrial Unfolded Protein Response. Mango SE, editor. PLoS Genet. 2013 Mar 14;9(3):e1003346.

128. Jafari G, Wasko BM, Tonge A, Schurman N, Dong C, Li Z, et al. Tether mutations that restore function and suppress pleiotropic phenotypes of the *C. elegans isp-1(qm150)* Rieske iron–sulfur protein. Proc Natl Acad Sci. 2015 Nov 10;112(45):E6148–57.

129. Touvier T, De Palma C, Rigamonti E, Scagliola A, Incerti E, Mazelin L, et al. Muscle-specific Drp1 overexpression impairs skeletal muscle growth via translational attenuation. Cell Death Dis. 2015 Feb;6(2):e1663–e1663.

130. Rauthan M, Ranji P, Aguilera Pradenas N, Pitot C, Pilon M. The mitochondrial unfolded protein response activator ATFS-1 protects cells from inhibition of the mevalonate pathway. Proc Natl Acad Sci. 2013 Apr 9;110(15):5981–6.

131. Fiorese CJ, Schulz AM, Lin Y-F, Rosin N, Pellegrino MW, Haynes CM. The Transcription Factor ATF5 Mediates a Mammalian Mitochondrial UPR. Curr Biol CB. 2016;26(15):2037–43.

132. Wrobel L, Topf U, Bragoszewski P, Wiese S, Sztolsztener ME, Oeljeklaus S, et al. Mistargeted mitochondrial proteins activate a proteostatic response in the cytosol. Nature. 2015 Aug;524(7566):485–8.

133. Callegari S, Dennerlein S. Sensing the Stress: A Role for the UPRmt and UPRam in the Quality Control of Mitochondria. Front Cell Dev Biol. 2018;6:31.

134. Young L. Role of the ABC Transporter Mdl1 in Peptide Export from Mitochondria. Science. 2001 Mar 16;291(5511):2135–8.

135. Haynes CM, Petrova K, Benedetti C, Yang Y, Ron D. ClpP Mediates Activation of a Mitochondrial Unfolded Protein Response in C. elegans. Dev Cell. 2007 Oct;13(4):467–80.

136. Palmer AE, Giacomello M, Kortemme T, Hires SA, Lev-Ram V, Baker D, et al. Ca2+ indicators based on computationally redesigned calmodulin-peptide pairs. Chem Biol. 2006;13(5):521–30.

137. Wang Y, Wang F, Wang R, Zhao P, Xia Q. 2A self-cleaving peptide-based multi-gene expression system in the silkworm Bombyx mori. Sci Rep. 2015 Dec;5(1):16273.

138. Kalderon D, Roberts BL, Richardson WD, Smith AE. A short amino acid sequence able to specify nuclear location. Cell. 1984;39(3):499–509.

139. Cabantous S, Terwilliger TC, Waldo GS. Protein tagging and detection with engineered self-assembling fragments of green fluorescent protein. Nat Biotechnol. 2005 Jan;23(1):102–7.

140. Snapp E. Design and Use of Fluorescent Fusion Proteins in Cell Biology. Curr Protoc Cell Biol. 2005 Jun;27(1):21.4.1-21.4.13.

141. Alford SC, Abdelfattah AS, Ding Y, Campbell RE. A Fluorogenic Red Fluorescent Protein Heterodimer. Chem Biol. 2012 Mar;19(3):353–60.

142. Biasini M, Bienert S, Waterhouse A, Arnold K, Studer G, Schmidt T, et al. SWISS-MODEL: modelling protein tertiary and quaternary structure using evolutionary information. Nucleic Acids Res. 2014 Jul 1;42(W1):W252–8.

143. Jackson SE, Craggs TD, Huang J. Understanding the folding of GFP using biophysical techniques. Expert Rev Proteomics. 2006;3(5):545–59.

144. Balleza E, Kim JM, Cluzel P. Systematic characterization of maturation time of fluorescent proteins in living cells. Nat Methods. 2018 Jan;15(1):47–51.

145. Fukasawa Y, Tsuji J, Fu S-C, Tomii K, Horton P, Imai K. MitoFates: Improved Prediction of Mitochondrial Targeting Sequences and Their Cleavage Sites. Mol Cell Proteomics. 2015 Apr;14(4):1113–26.

146. Kalbáčová M, Vrbacký M, Drahota Z, Mělková Z. Comparison of the effect of mitochondrial inhibitors on mitochondrial membrane potential in two different cell lines using flow cytometry and spectrofluorometry: Flow Cytometry and Spectrofluorometry in Detection of $\Delta\Psi_m$. Cytometry A. 2003 Apr;52A(2):110–6.

147. van der Laan M, Wiedemann N, Mick DU, Guiard B, Rehling P, Pfanner N. A Role for Tim21 in Membrane-Potential-Dependent Preprotein Sorting in Mitochondria. Curr Biol. 2006 Nov;16(22):2271–6.

148. Shariff K, Ghosal S, Matouschek A. The Force Exerted by the Membrane Potential during Protein Import into the Mitochondrial Matrix. Biophys J. 2004 Jun;86(6):3647–52.

149. Horie C, Suzuki H, Sakaguchi M, Mihara K. Characterization of signal that directs C-tail-anchored proteins to mammalian mitochondrial outer membrane. Mol Biol Cell. 2002;13(5):1615–25.

150. Haigis MC, Mostoslavsky R, Haigis KM, Fahie K, Christodoulou DC, Murphy AJ, et al. SIRT4 inhibits glutamate dehydrogenase and opposes the effects of calorie restriction in pancreatic beta cells. Cell. 2006;126(5):941–54.

151. Iwahara T, Bonasio R, Narendra V, Reinberg D. SIRT3 Functions in the Nucleus in the Control of Stress-Related Gene Expression. Mol Cell Biol. 2012;32(24):5022–34.

152. Anderson KA, Huynh FK, Fisher-Wellman K, Stuart JD, Peterson BS, Douros JD, et al. SIRT4 Is a Lysine Deacylase that Controls Leucine Metabolism and Insulin Secretion. Cell Metab. 2017;25(4):838-855.e15.

153. Michishita E, Park JY, Burneskis JM, Barrett JC, Horikawa I. Evolutionarily conserved and nonconserved cellular localizations and functions of human SIRT proteins. Mol Biol Cell. 2005;16(10):4623–35.

154. Kunze M, Berger J. The similarity between N-terminal targeting signals for protein import into different organelles and its evolutionary relevance. Front Physiol. 2015;6.

155. Jeong SM, Xiao C, Finley LWS, Lahusen T, Souza AL, Pierce K, et al. SIRT4 has tumor-suppressive activity and regulates the cellular metabolic response to DNA damage by inhibiting mitochondrial glutamine metabolism. Cancer Cell. 2013;23(4):450–63.

156. Zeng J, Jiang M, Wu X, Diao F, Qiu D, Hou X, et al. SIRT4 is essential for metabolic control and meiotic structure during mouse oocyte maturation. Aging Cell. 2018;17(4):e12789.

157. Martin RM, Ter-Avetisyan G, Herce HD, Ludwig AK, Lättig-Tünnemann G, Cardoso MC. Principles of protein targeting to the nucleolus. Nucleus. 2015 Jul 4;6(4):314–25.

158. Rosso L, Marques AC, Reichert AS, Kaessmann H. Mitochondrial Targeting Adaptation of the Hominoid-Specific Glutamate Dehydrogenase Driven by Positive Darwinian Selection. Przeworski M, editor. PLoS Genet. 2008 Aug 8;4(8):e1000150.

159. Takakubo F, Cartwright P, Hoogenraad N, Thorburn DR, Collins F, Lithgow T, et al. An amino acid substitution in the pyruvate dehydrogenase E1 alpha gene, affecting mitochondrial import of the precursor protein. Am J Hum Genet. 1995 Oct;57(4):772–80.

160. Horwich AL, Kalousek F, Fenton WA, Furtak K, Pollock RA, Rosenberg LE. The ornithine transcarbamylase leader peptide directs mitochondrial import through both its midportion structure and net positive charge. J Cell Biol. 1987 Aug 1;105(2):669–77.

161. Feng S, Sekine S, Pessino V, Li H, Leonetti MD, Huang B. Improved split fluorescent proteins for endogenous protein labeling. Nat Commun. 2017;8(1):370.

162. Ruan L, Zhou C, Jin E, Kucharavy A, Zhang Y, Wen Z, et al. Cytosolic proteostasis through importing of misfolded proteins into mitochondria. Nature. 2017;543(7645):443–6.

163. Ding Y, Li J, Enterina JR, Shen Y, Zhang I, Tewson PH, et al. Ratiometric biosensors based on dimerization-dependent fluorescent protein exchange. Nat Methods. 2015 Mar;12(3):195–8.

164. Elsharkawi I, Sandeep D, El-Serafi A. Investigating the role of the histone deacetylases-inhibitor suberanilohydroxamic acid in the differentiation of stem cells into insulin secreting cells. Hamdan Med J. 2019;12(1):10.

165. Kamiyama D, Sekine S, Barsi-Rhyne B, Hu J, Chen B, Gilbert LA, et al. Versatile protein tagging in cells with split fluorescent protein. Nat Commun. 2016 Apr;7(1):11046.

166. Schleiff E, Turnbull JL. Characterization of the N-Terminal Targeting Signal Binding Domain of the Mitochondrial Outer Membrane Receptor, Tom20 †. Biochemistry. 1998 Sep;37(38):13052–8.

167. Mukhopadhyay A, Ni L, Weiner H. A co-translational model to explain the in vivo import of proteins into HeLa cell mitochondria. Biochem J. 2004 Aug 15;382(1):385–92.

168. Verner K. Co-translational protein import into mitochondria: an alternative view. Trends Biochem Sci. 1993 Oct;18(10):366–71.

169. Yano H, Baranov SV, Baranova OV, Kim J, Pan Y, Yablonska S, et al. Inhibition of mitochondrial protein import by mutant huntingtin. Nat Neurosci. 2014;17(6):822–31.

170. Filipuzzi I, Steffen J, Germain M, Goepfert L, Conti MA, Potting C, et al. Stendomycin selectively inhibits TIM23-dependent mitochondrial protein import. Nat Chem Biol. 2017;13(12):1239–44.

171. Merksamer PI, Liu Y, He W, Hirschey MD, Chen D, Verdin E. The sirtuins, oxidative stress and aging: an emerging link. Aging. 2013;5(3):144–50.

172. Papa L, Germain D. SirT3 Regulates the Mitochondrial Unfolded Protein Response. Mol Cell Biol. 2014 Feb 15;34(4):699–710.

173. Franco-Iborra S, Cuadros T, Parent A, Romero-Gimenez J, Vila M, Perier C. Defective mitochondrial protein import contributes to complex I-induced mitochondrial dysfunction and neurodegeneration in Parkinson's disease. Cell Death Dis. 2018 Nov;9(11):1122.

174. Liu W, Duan X, Fang X, Shang W, Tong C. Mitochondrial protein import regulates cytosolic protein homeostasis and neuronal integrity. Autophagy. 2018 Aug 3;14(8):1293–309.

175. Journal of Parkinson's disease & Alzheimer's disease. J Park Dis Alzheimers Dis [Internet]. 2014 [cited 2020 Feb 5];1(1). Available from: http://www.avensonline.org/fulltextarticles/jpa-2376-922x-01-0003.html

176. Calì T, Ottolini D, Soriano ME, Brini M. A new split-GFP-based probe reveals DJ-1 translocation into the mitochondrial matrix to sustain ATP synthesis upon nutrient deprivation. Hum Mol Genet. 2015 Feb 15;24(4):1045–60.

177. Kashiwagi S, Fujioka Y, Satoh AO, Yoshida A, Fujioka M, Nepal P, et al. Folding latency of fluorescent proteins affects the mitochondrial localization of fusion proteins [Internet]. Cell Biology; 2019 Sep [cited 2020 Feb 5]. Available from: http://biorxiv.org/lookup/doi/10.1101/768432